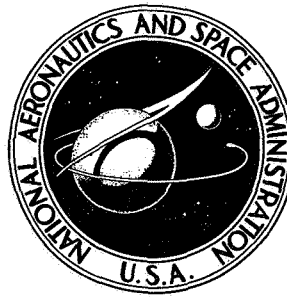


NASA TECHNICAL NOTE



N73-26926
NASA TN D-7303

NASA TN D-7303

CASE FILE
COPY

BUCKLING TESTS OF TWO 4.6-METER-DIAMETER,
MAGNESIUM RING-STIFFENED CONICAL SHELLS
LOADED UNDER EXTERNAL PRESSURE

by James Kent Anderson and Randall C. Davis

Langley Research Center

Hampton, Va. 23665

1. Report No. NASA TN D-7303		2. Government Accession No.		3. Recipient's Catalog No.	
4. Title and Subtitle BUCKLING TESTS OF TWO 4.6-METER-DIAMETER, MAGNESIUM RING-STIFFENED CONICAL SHELLS LOADED UNDER EXTERNAL PRESSURE				5. Report Date July 1973	
				6. Performing Organization Code	
7. Author(s) James Kent Anderson and Randall C. Davis				8. Performing Organization Report No. L-8835	
9. Performing Organization Name and Address NASA Langley Research Center Hampton, Va. 23665				10. Work Unit No. 501-22-01-02	
				11. Contract or Grant No.	
12. Sponsoring Agency Name and Address National Aeronautics and Space Administration Washington, D.C. 20546				13. Type of Report and Period Covered Technical Note	
				14. Sponsoring Agency Code	
15. Supplementary Notes					
16. Abstract <p>Two ring-stiffened magnesium conical shells with a 120° apex angle and a 4.6-meter diameter were loaded to failure by a uniform external pressure. The cones differed from one another only in the number of internal stiffening rings. Test specimen details, test procedure, and test results are discussed. Both buckling and prebuckling data are compared with appropriate theoretical predictions. Measured strains in skin and rings agreed well with theoretical predictions. Extensive imperfection measurements were made and reported on both cones in the "as fabricated" condition.</p>					
17. Key Words (Suggested by Author(s)) Shells Magnesium Buckle Test Cones Imperfections Ring stiffened				18. Distribution Statement Unclassified - Unlimited	
19. Security Classif. (of this report) Unclassified		20. Security Classif. (of this page) Unclassified		21. No. of Pages 66	
				22. Price* \$3.00	

BUCKLING TESTS OF TWO 4.6-METER-DIAMETER, MAGNESIUM
RING-STIFFENED CONICAL SHELLS LOADED
UNDER EXTERNAL PRESSURE

By James Kent Anderson and Randall C. Davis
Langley Research Center

SUMMARY

Two ring-stiffened magnesium conical shells with a 120° apex angle and a 4.6-meter diameter were loaded to failure by a uniform external pressure. The cones differed from one another only in the number of internal stiffening rings. Test specimen details, test procedure, and test results are discussed. Both buckling and prebuckling data are compared with appropriate theoretical predictions. Measured strains in skin and rings agreed well with theoretical predictions. Extensive imperfection measurements were made and reported on both cones in the "as fabricated" condition.

INTRODUCTION

Results of structural tests on two large magnesium conical shells are presented and compared with contemporary theoretical predictions. The size, mass, and configuration of these shells are such as to be applicable to space missions where large, lightweight, blunt-shaped structures are needed for deceleration in a thin atmosphere, such as that of the planet Mars.

The test specimens are truncated conical shell structures which have an apex angle of 120° and a base diameter of 4.6 meters. The overall shape and loading of the cones are shown in figure 1. The base edge (large-diameter end) and the truncated edge (small-diameter end) are supported by relatively stiff tubular rings, and the wall of the cone is stiffened by smaller tubular rings. The cones are loaded by a uniform external pressure, with the load being supported or reacted at the ring at the truncated end. The two cones differ only in the number of internal stiffening rings. Little test information is available on this type of structure under this loading.

This paper describes the geometry and fabrication of the specimens, the test setup, and test procedure and discusses the test results and compares these results with theoretical predictions. Test results include the prebuckling strain distributions in the shell wall and the cone buckling phenomenon. To characterize the buckling behavior, this paper

reports the collapse external pressure load, apparent shape of the buckling mode, deflection of the base edge at buckling, and the pressure-strain history in an area of maximum wall deflection. Also included in this paper is an extensive initial imperfection survey of the surface of each cone. These measurements are given in appendix A. Appendix B discusses in some detail the analyses to which the test data in this report were compared.

SYMBOLS

The units used for physical quantities defined in this paper are given in the International System of Units (SI). Correlation between this system of units and U.S. Customary Units is given in reference 1.

n	number of circumferential buckling waves
p_{cr}	critical buckling pressure, N/m^2
p_{ult}	collapse pressure, N/m^2
R	radius, m
s	meridional coordinate with origin at base ring, m
s_L	meridional length between attachment of base ring and payload ring, m
x	axial coordinate, m
y	radial coordinate, m
z	normal coordinate, m
ϵ_{s0}	outside surface meridional strain
ϵ_{si}	inside surface meridional strain
$\epsilon_{\theta 0}$	outside surface circumferential strain
$\epsilon_{\theta i}$	inside surface circumferential strain
$\epsilon_{\theta r}$	circumferential strain in inner stiffening rings

TEST SPECIMENS

The two test specimens are essentially identical except for the number of small internal stiffening rings. Cone 1 has 31 of these rings and cone 2 has 25 of these rings. A general overall view of the test cones is shown in figure 2. Construction details with nominal dimensions are shown in figure 3. Actual measured dimensions are given in table 1.

Each cone is formed from 12 panels which are fastened together at butt joints with doubler strips, both inside and outside; the panels and strips are fastened together by both rivets and a room-temperature-curing structural adhesive, with the rivets being the primary fastening system. The shell wall is reinforced on the outside surface at both the small and the large end by doubler strips, which are both riveted and bonded to the wall.

The 4.5-meter-diameter tubular ring (base ring) having a section with a 15.2-cm outside diameter (O.D.) is fastened to the shell wall by rivets. The base ring is fabricated from three equal-length segments fastened together by the use of riveted coupling sleeves. A structural membrane, which is used as a pressure seal in the test setup, is attached to the cone at the base ring and is held in place by rivets and an adhesive at the junction of the base ring and shell wall.

The 2.0-meter-diameter tubular ring (termed the payload ring if the structure is to be used as a decelerator in a space mission) having a section with a 6.4-cm outside diameter is fabricated from two equal-length segments fastened to each other and to the shell wall in the same manner as the base ring. The tubular rings with 1.9-cm outside diameter which are used to stiffen the wall are fabricated from as few segments as practical and fastened together with rivets and coupling sleeves. These joints are staggered about the cone with respect to adjacent ring joints. Rivets are used to attach these rings to the wall.

All the tubes were extruded from ZK60A magnesium alloy and were heat treated to the T5 condition before delivery to the NASA Langley Research Center. The skin was fabricated from rolled AZ31B magnesium alloy and delivered in the H24, or hard-rolled, condition.

Preliminary stress analysis of the cones indicated that the shell wall at the small-diameter end would be subjected to excessive circumferential tensile stresses if the cones were loaded to the expected test pressures. The inverted inner cone shown in figure 3 was riveted to the payload ring to alleviate this condition by restraining the rotation of the ring under load. A reanalysis showed that circumferential tensile stresses were reduced when the ring rotation was constrained. This inner cone was fabricated from 7075-T6 aluminum alloy.

An extensive imperfection survey was made of the shell in an "as fabricated" and no-load condition. Measurements were made along meridional lines every 5° around the circumference with the use of a straightedge and with the base ring and payload ring as end reference points. Normal departures of the conical surface from a straight line were measured with an electrical device and autographically recorded on a continuous plotter. The measurements are presented in appendix A and show that both cones were of very good quality and adhered closely to the prescribed geometry. These cones were fabricated by the Langley Research Center Fabrication Division.

TEST PROCEDURE

Each cone was instrumented with 146 strain gages to provide a comprehensive strain survey for evaluation of cone response to applied external surface pressure. In addition, the base ring on each cone was instrumented to measure vertical and horizontal displacements during loading.

A schematic view of the test setup is shown in figure 4. The inner steel conical test fixture, the test cone, and a membranelike skirt at the base ring form an airtight chamber. By pumping a partial vacuum in this chamber, a uniform external pressure is exerted on the test cone, which is reacted at the bottom of the payload ring by the flat machined surface at the top of the conical test fixture. The membranelike skirt which seals the chamber is intended to provide minimal restraint to the shell during loading by restricting the loading from the membrane to a small meridional load applied tangentially to the inside surface of the shell. Loading pressure was controlled by manually operated valves, and the resulting pressure-strain response for selected gages was monitored on two oscilloscopes. Test data were recorded automatically with the use of the Langley central digital data recording facility. Figure 5 is a photograph of the major components of the test setup without the test cone.

Two types of tests were conducted on each cone, one to determine the prebuckling strain distribution in the test cones as a function of pressure and the other to determine buckling pressure, buckling mode, base-ring displacements, and strain at buckling. The prebuckling strain distribution tests were made with pressures up to 13.8 kN/m^2 (0.136 atmosphere), which was considerably less than the predicted buckling pressure. For these tests, three of the 12 panels, 120° apart, were extensively instrumented with strain gages, the number of gages being limited by the number that could be recorded in one test. For the buckling tests, strain gages were located at points of expected maximum buckling deflections to record the skin and ring strains and thus indicate the buckling mode. One panel on each of the cones was also instrumented with a sufficient number of strain gages to indicate the circumferential strain profile at buckling. The horizontal and vertical displacements of the base ring were also measured during the

buckling tests; for this purpose, displacement transducers were placed at two locations, 180° apart, on the base ring.

Photographs were taken after each cone had been loaded to failure. Then each cone was cut into three parts and micrometer measurements were taken of the structural components. The results of these measurements are given in table 1.

TEST RESULTS

Two different sets of tests were conducted on each cone, one to determine the pre-buckling strain distribution and the other to obtain information on the buckling of the cones.

Prebuckling Strain Distribution Tests

A comparison of the measured and predicted prebuckling strain distributions is presented in figures 6 to 9. Two computer programs, BOSOR 2 and SALORS, were used to compute the theoretical strain values. These programs are discussed briefly in appendix B.

In figures 6 and 7 outside and inside surface circumferential skin strains are plotted against the dimensionless meridional distance s/s_L , where s/s_L is measured in such a way that the base ring is at $s/s_L = 0$ and the payload ring is at $s/s_L = 1.0$. Test strain measurements were taken from three panels on each cone, each panel being 120° apart. The location of these panels and their imperfection measurements are given in appendix A.

Theoretical and measured strains in the internal stiffening rings of cones 1 and 2 are compared in figures 8(a) and (b), respectively. Test results revealed that the base rings were subjected to light compressive strains in the circumferential direction. The payload rings, on the other hand, were relatively highly strained at the 13.8 kN/m² pre-buckling pressure loading; tensile strains of approximately 0.0012 were measured as a result of the bending produced by the payload ring rotation.

Outside surface prebuckling strains in the meridional direction along a meridional line are shown in figures 9(a) and (b) for cones 1 and 2, respectively. The theoretical curve for the meridional strains predicted by using SALORS has a number of discontinuities which occur at ring attachment points. These discontinuities reflect the rapid change in strain which occurs across ring attachment points. The meridional strains predicted by using BOSOR 2 represent the average of the strains caused by the discrete rings; thus discontinuities are not evident on the curve. Only the theoretical meridional strains on the inside surface of the skins for cones 1 and 2 are shown in figures 10(a) and (b), respectively, since data collection limitations precluded the placing of strain gages on these inner surfaces.

Buckling Tests

The buckling character of both cones 1 and 2 was almost identical, with failure accompanied by a "snap" type noise and the simultaneous appearance of several large buckles (general instability) about the circumference of each cone. Just prior to collapse, strain measurements in the region of expected maximum buckling displacements began to show strain reversal or nonlinearity, which indicated that the wall in this area had begun to bend. The maximum pressure at collapse for cone 1 was 23.10 kN/m^2 , and the apparent buckling mode contained six circumferential waves. The appearance of the external surface showed very little evidence of failure after pressure load had been removed. Inspection of the interior of the cone revealed that there were three meridional lines around the cone where the internal rings had been crippled. The three lines were spaced about a wave length apart. Figure 11 shows the external surface of cone 1 after buckling and while still under pressure loading. The horizontal or radial displacement of the base ring at buckling was only a few thousandths of a centimeter inward; however, the vertical displacement was between 0.74 and 1.04 cm downward.

The maximum pressure at collapse for cone 2 was 22.06 kN/m^2 , and the apparent buckling mode also contained six circumferential waves. The appearance of this cone after removal of pressure was similar to that of the first one. Figure 12 shows the exterior surface of cone 2 after buckling and while still under pressure loading. Figure 13(b) shows an overall view of the interior of cone 2 after removal from the test setup, and figure 13(a) shows a closeup view of the crippled rings. The base ring experienced only slight inward displacement at buckling, while the vertical displacement was between 0.66 and 0.91 cm downward.

Test procedure for the buckling test called for all 12 panels of each cone to be instrumented with a sufficient number of strain gages to determine wall bending and to anticipate the onset of buckling. These gages were placed midway between panel seams and at the meridional station in the vicinity of maximum deflection. Inspection of the test data showed that panel 9 of cone 1 exhibited the most wall bending during the buckling tests; strain-gage data from this area are shown in figure 14(a). The back-to-back strain gages located on the skin (gages 1 and 2 and gages 4 and 5) indicated that the compressive strain became smaller as the pressure loading approached the collapse level, while the strain gage located on the stiffening ring (gage 3) indicated an increase in compressive strain. Thus, these strain data show that the wall is bending in this area and producing a convex outward curvature. For cone 2, the most wall bending occurred in panel 1. (See fig. 14(b).)

One panel on each cone was instrumented with a sufficient number of strain gages to indicate the strain profile at buckling. Figures 15 and 16 present the outside and inside circumferential strain profile at buckling for each cone and also at several lower

pressures for trend comparison. Test data are plotted at discrete points as shown; however, a continuous curve is faired through these points to indicate the approximate strain levels at points where data were not taken.

Theoretical buckling predictions from BOSOR 2 and SALORS are given in table 2 along with the test values.

Discussion of Test Results

After failure, each cone maintained the ability to carry some pressure loading although at a lower level than the collapse pressure. Each cone buckled into an apparent general instability mode of six circumferential waves although both buckling computer programs (BOSOR 2 and SALORS) predicted buckling modes of seven waves. Fabrication details of the test cones may be responsible for the difference in the theoretically predicted mode and apparent test mode because of the closeness of the buckling pressures for the buckling modes of six and seven waves, as discussed in appendix B. The cone was built from 12 panels and buckled into six circumferential waves, and the interior rings crippled at or very near panel joints.

Good agreement between test and theory was obtained for the meridional strains except in the vicinity of the payload ring of cone 1. Here there was large scatter of the test points; the lack of agreement in this region might be due to some shell imperfections although examination of the imperfection plots given in appendix A do not indicate any large geometric imperfections.

Theoretical predictions of buckling pressures usually are higher than actual test results. The BOSOR 2 analysis predicts a buckling pressure that must be reduced by about 19 percent for each cone for agreement with test results. The SALORS analysis predicts a buckling pressure that must be reduced by approximately 18 and 12 percent for cones 1 and 2, respectively.

The tests also verified that the base rings were sufficiently stiff to prevent inextensional shell buckling. This problem had been studied earlier by Cohen (ref. 2).

CONCLUDING REMARKS

The test results from an investigation to determine the buckling phenomenon and structural response caused by applied uniform external pressure on two magnesium, ring-stiffened conical shells, with dimensions applicable to space missions involving structural decelerators, have been presented. Insight was also gained as to the practical fabrication of such large shells, in that results of imperfection measurements performed on these cones indicate that similar shells with like proportions can be built to close tolerances.

Test results were compared with two contemporary sophisticated shell-of-revolution analyses. The prebuckling test strains for both the skin and the rings agreed very well with those predicted by the two shell analysis programs, BOSOR 2 and SALORS. Both cones buckled into a general instability buckling mode with six circumferential waves. Both analysis programs predicted a buckling mode of seven waves for each cone, compared with the six waves in the tests; however, construction details of the cones may be responsible for this discrepancy. The BOSOR 2 and SALORS analyses predicted a critical buckling pressure that should be reduced by about 20 percent for adequate agreement with the tests.

Langley Research Center,
National Aeronautics and Space Administration,
Hampton, Va., May 25, 1973.

APPENDIX A

SHELL SURFACE IMPERFECTION MEASUREMENTS

The conical shell surfaces of both cones were measured extensively to determine the geometric imperfections present in an "as fabricated" and no-load condition. The distances from a straight meridian to the surface of the cones were established along meridional lines between the shell doublers located at each end of the cones. Measurements were taken every 5° around the circumference starting at the seam between panels 12 and 1 and proceeding counterclockwise. Figure 17 shows locations on the panels where imperfection measurements were made and shows meridional locations where strain gages were installed for the prebuckling tests and for the buckling tests.

Figure 18 presents the imperfection measurements for all 12 panels of cone 1, and figure 19 presents those for cone 2. Each panel is numbered for reference in the test and figures.

APPENDIX B

PREBUCKLING AND BUCKLING ANALYSES FOR TEST CONES

Two computer programs, SALORS and BOSOR 2, were used to analyze the cones reported in the text. A discussion and comparison of these programs are given in reference 3. Both systems employ finite-difference procedures; however, BOSOR 2 applies the difference approximations to the energy expression, whereas the SALORS program applies the difference approximations to the differential equations. In these analyses, Young's modulus for the magnesium alloys was taken to be 44.8 kN/m^2 and Poisson's ratio to be 0.35.

The SALORS program (Structural Analysis of Layered Orthotropic Ring-Stiffened Shells of Revolution) is described in detail in reference 4. The theoretical predictions given in the text are based on the analytical model of the cones shown in figure 20(a). This model is formed from two conical segments, the magnesium cone and the aluminum inverted inner cone. There is one major construction difference between the analytical model and the test cone, that is, the inverted inner cone is not attached to the payload ring in the analytical model but instead is considered to be attached to the edge of the magnesium cone. The program describes the ring properties at one discrete point and thus could not reflect the fact that the payload ring is connected to two conical segments. The external pressure loading was considered to be live (load remains normal to the deformed surface). A nonlinear analysis was used to compute the prebuckling strain distributions, whereas a linear prebuckling stress state was used in the stability analysis.

The BOSOR (Buckling Of Shells Of Revolution) program is described in detail in reference 5. The analytical model is given in figure 20(b). BOSOR 2 treats the attachment of the inverted inner cone to the payload ring in a different fashion than does SALORS. The program has the capability of treating segments of shells that are not continuous by maintaining adjacent segment edges a fixed distance apart during loading. External pressure loading was not considered to be live. Prebuckling strains were computed by using a nonlinear analysis for both the prebuckling strain distributions and the buckling analysis.

Figure 21 is a plot of the buckling pressure as a function of buckling mode number as computed by BOSOR 2 for its analytical model. The closeness in the buckling pressures for the buckling modes of 6 and 7 is apparent, thus lending credibility to the assumption that the construction details of the test cones may have affected the buckling modes.

REFERENCES

1. Anon.: Metric Practice Guide. E 380-72, Amer. Soc. Testing Mater., June 1972.
2. Cohen, Gerald A.: The Effect of Edge Constraint on the Buckling of Sandwich and Ring-Stiffened 120 Degree Conical Shells Subjected to External Pressure. NASA CR-795, 1967.
3. Anderson, M. S.; Fulton, R. E.; Heard, W. L., Jr.; and Waltz, J. E.: Stress, Buckling, and Vibration Analysis of Shells of Revolution. Computers & Structures, vol. 1, nos. 1/2, Aug. 1971, pp. 157-192.
4. Heard, Walter L., Jr.; Anderson, Melvin S.; and Chen, Ming M.: Computer Program for Structural Analysis of Layered Orthotropic Ring-Stiffened Shells of Revolution (SALORS) - Linear Stress Analysis Option. NASA TN D-7179, 1973.
5. Bushnell, David: Buckling and Vibration of Segmented, Ring-Stiffened Shells of Revolution - User's Manual for BOSOR 2. LMSC 6-78-68-40 (Contract N00014-67-C-0256), Lockheed Missiles & Space Co., Sept. 1968.

TABLE 1.- MEASURED CONE DIMENSIONS

Cone	Thickness of skin of wall, cm	Inner stiffening ring		Wall thickness of payload ring, cm	Wall thickness of base ring, cm
		Outside diameter, cm	Wall thickness, cm		
1	0.130	1.906	0.069	0.323	0.398
2	0.133	1.916	0.072	0.323	0.398

TABLE 2.- BUCKLING RESULTS FROM TESTS AND THEORY

Cone	BOSOR 2		SALORS		Test	
	P_{cr} , kN/m ²	n	P_{cr} , kN/m ²	n	P_{ult} , kN/m ²	n
1	28.70	7	28.17	7	23.10	6
2	27.20	7	25.12	7	22.06	6

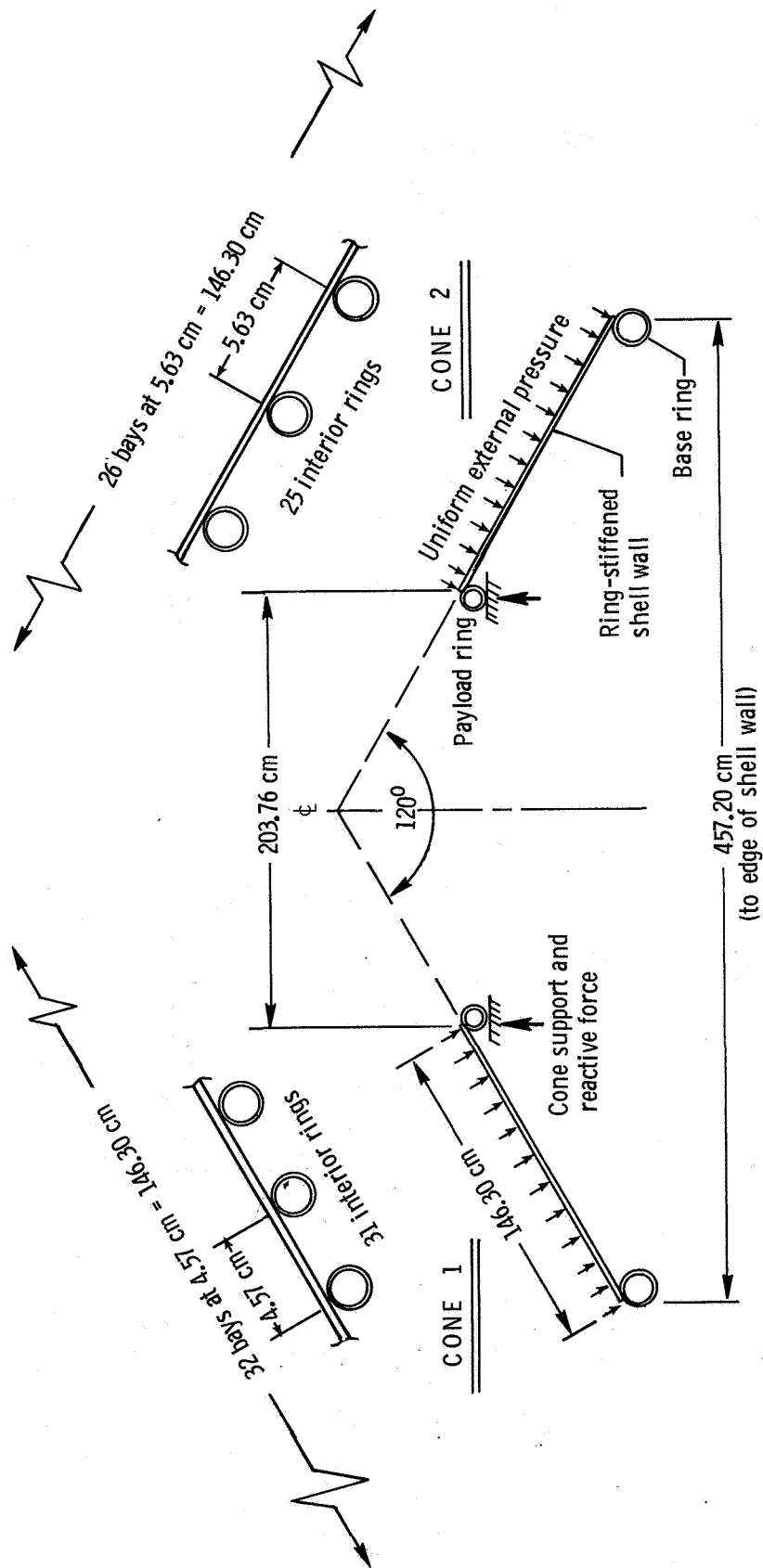
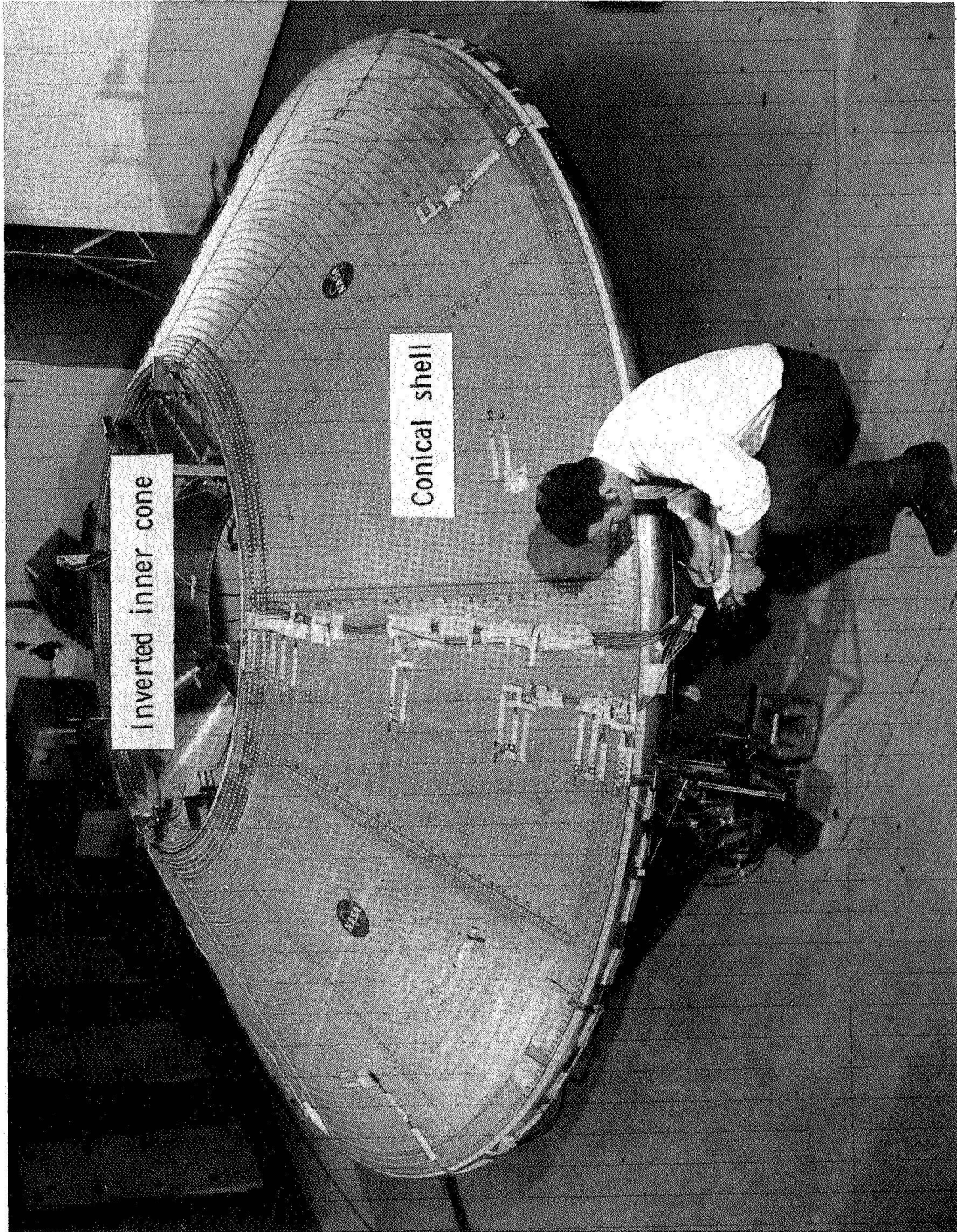


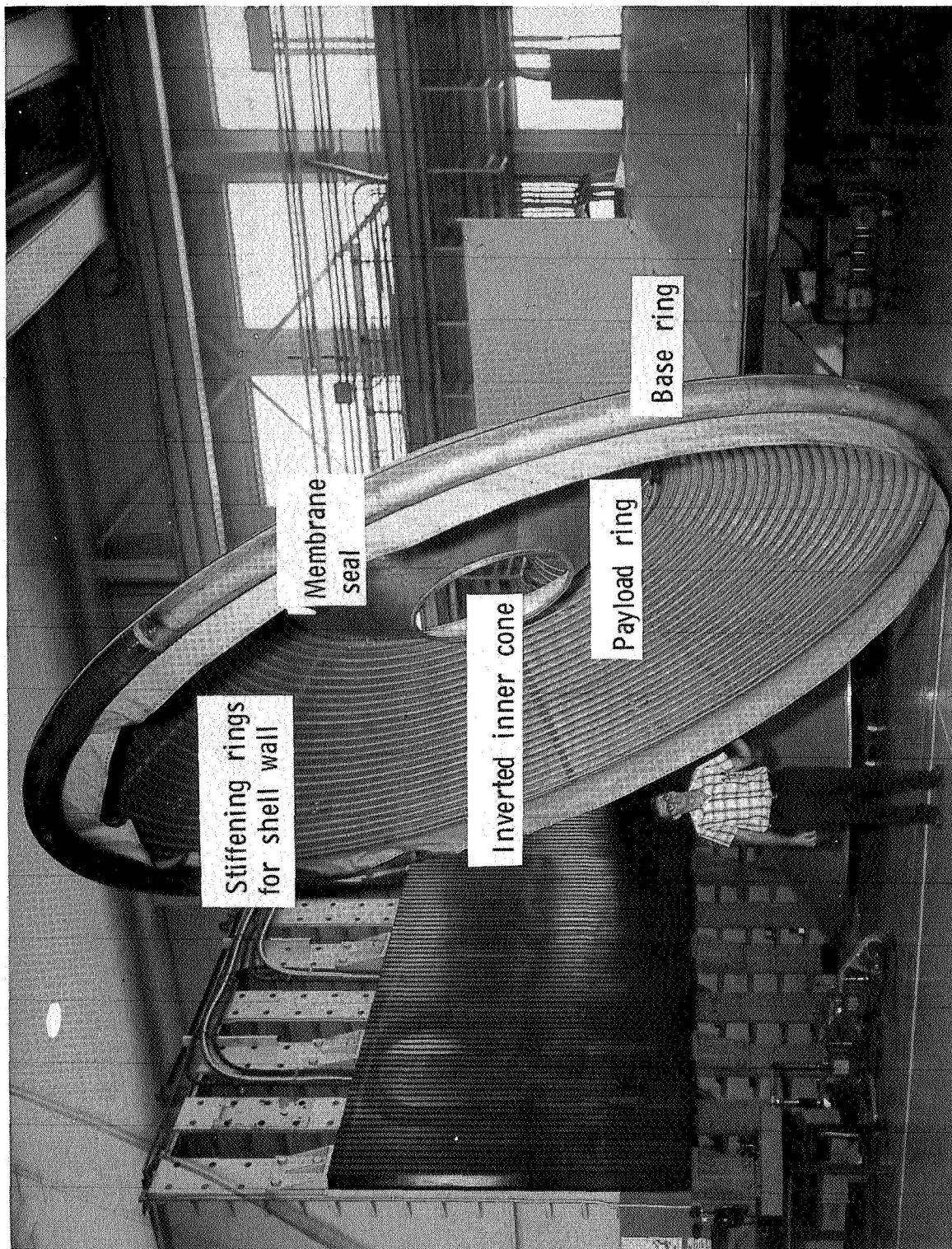
Figure 1.- Cross section of test cones showing overall shape and design test loading.



L-69-2854.1

(a) Exterior of cone 1.

Figure 2.- Overall view of cones.



L-69-4623.1

(b) Interior of cone 2.

Figure 2.- Concluded.

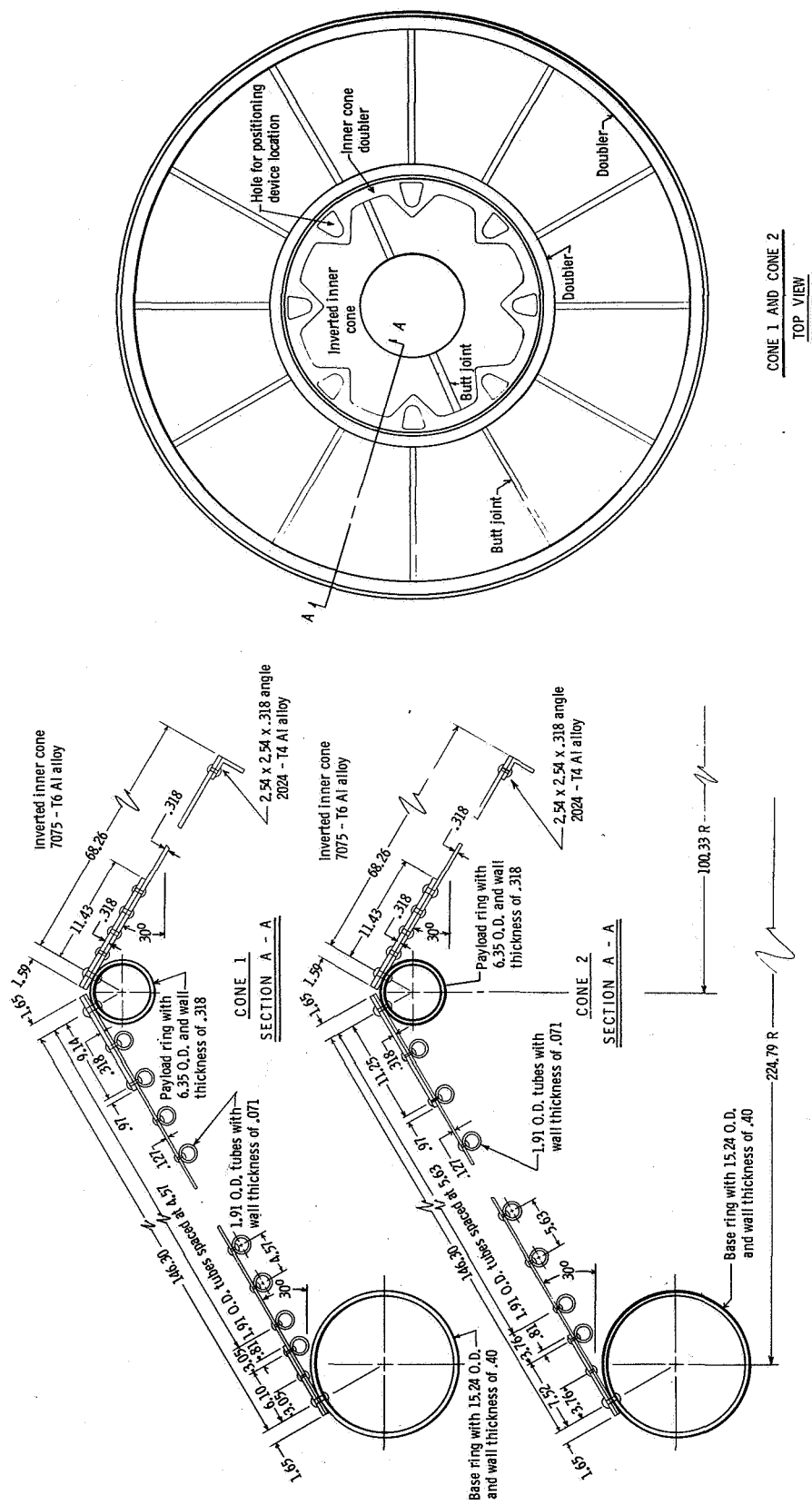


Figure 3.- Construction details. (All dimensions are given in centimeters.)

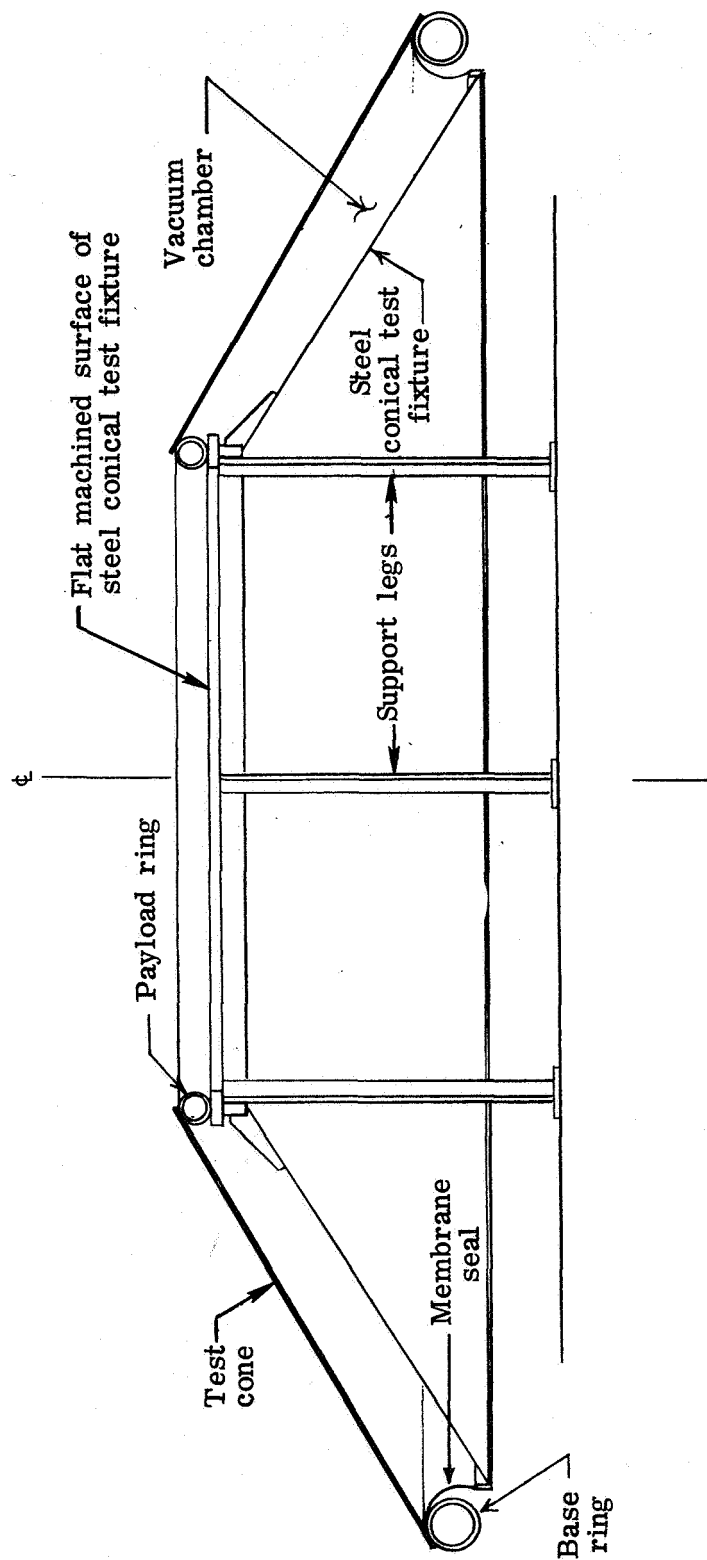


Figure 4.- Schematic view of test setup (inverted inner cone not shown).

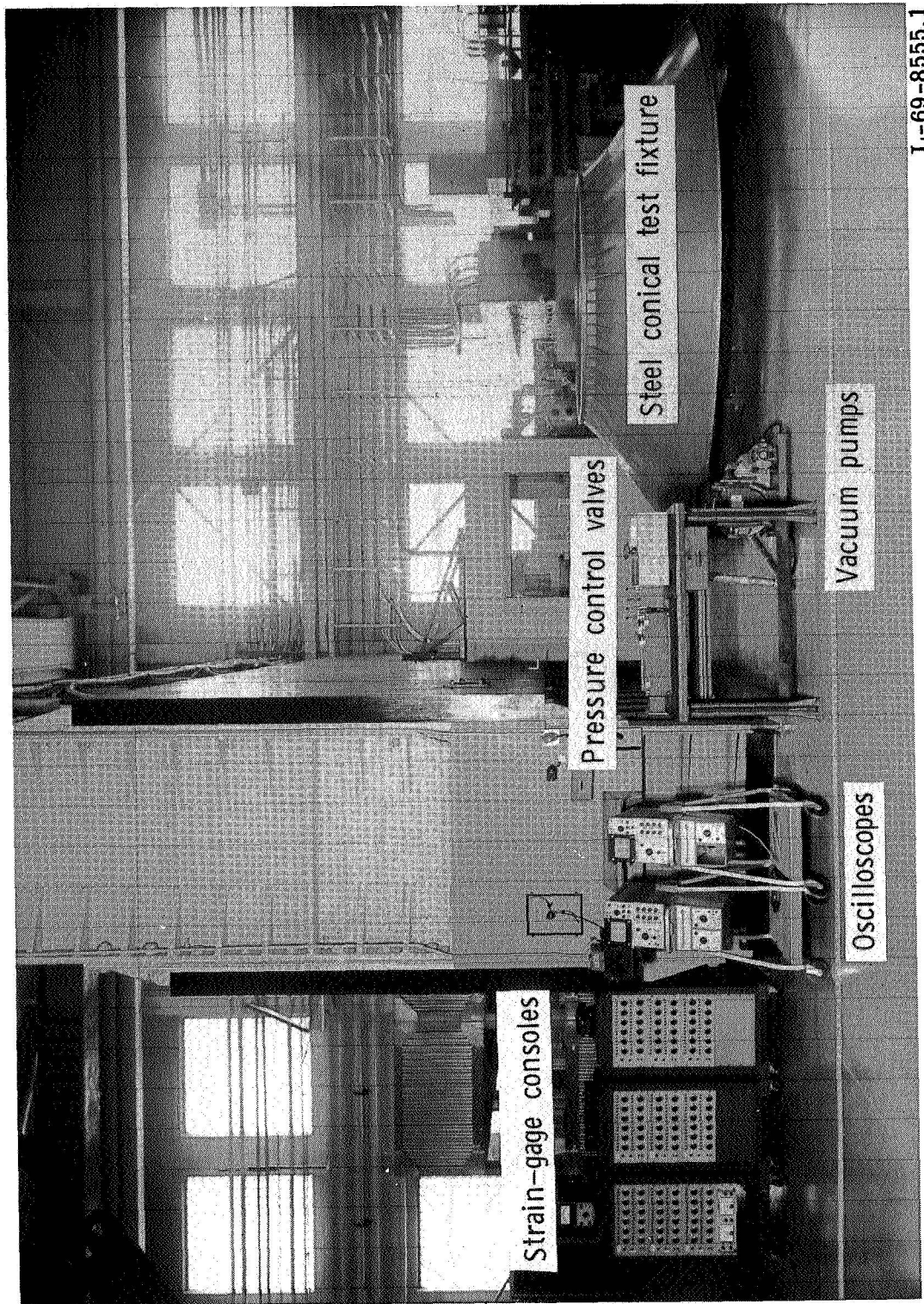
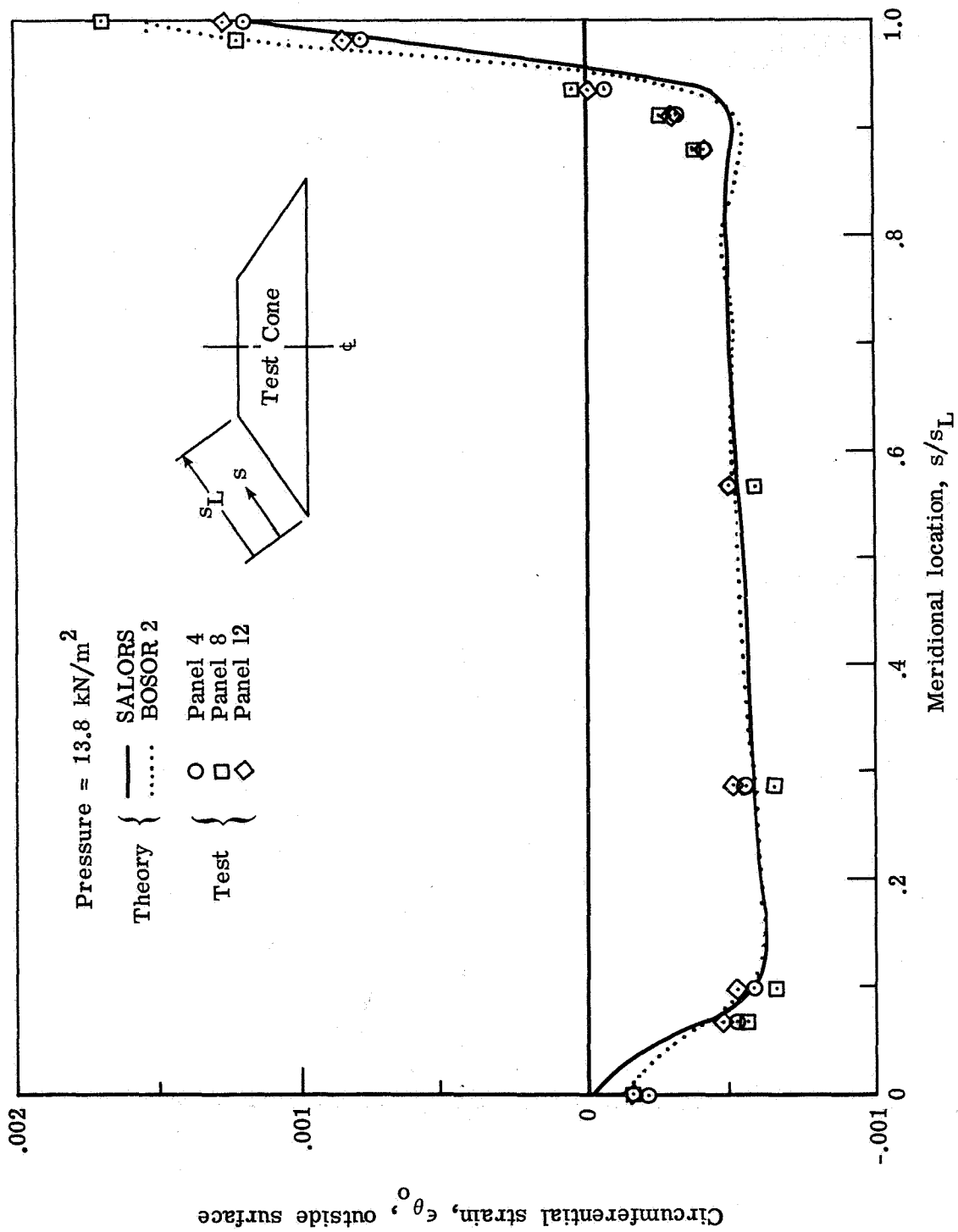
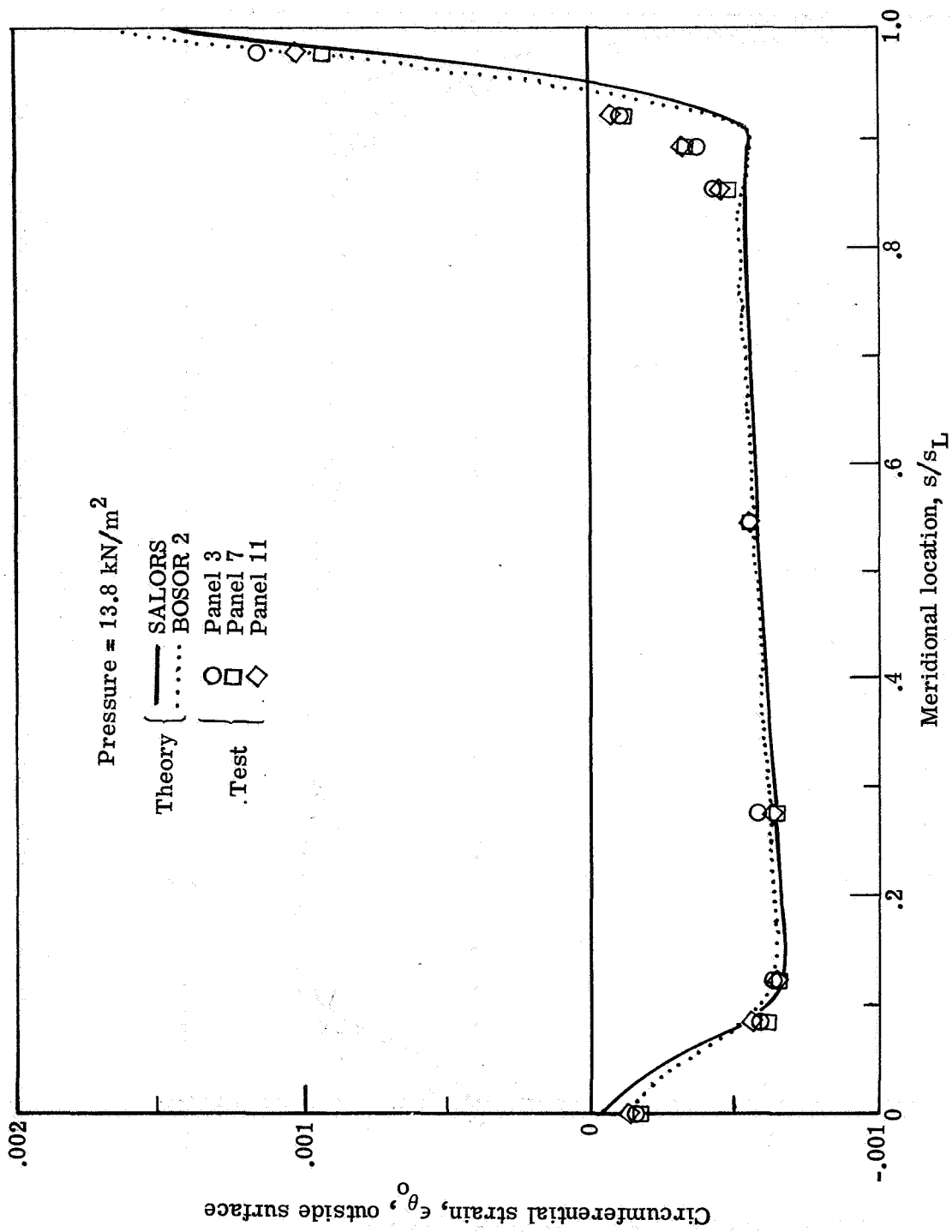


Figure 5. - Test setup components excluding test cones.



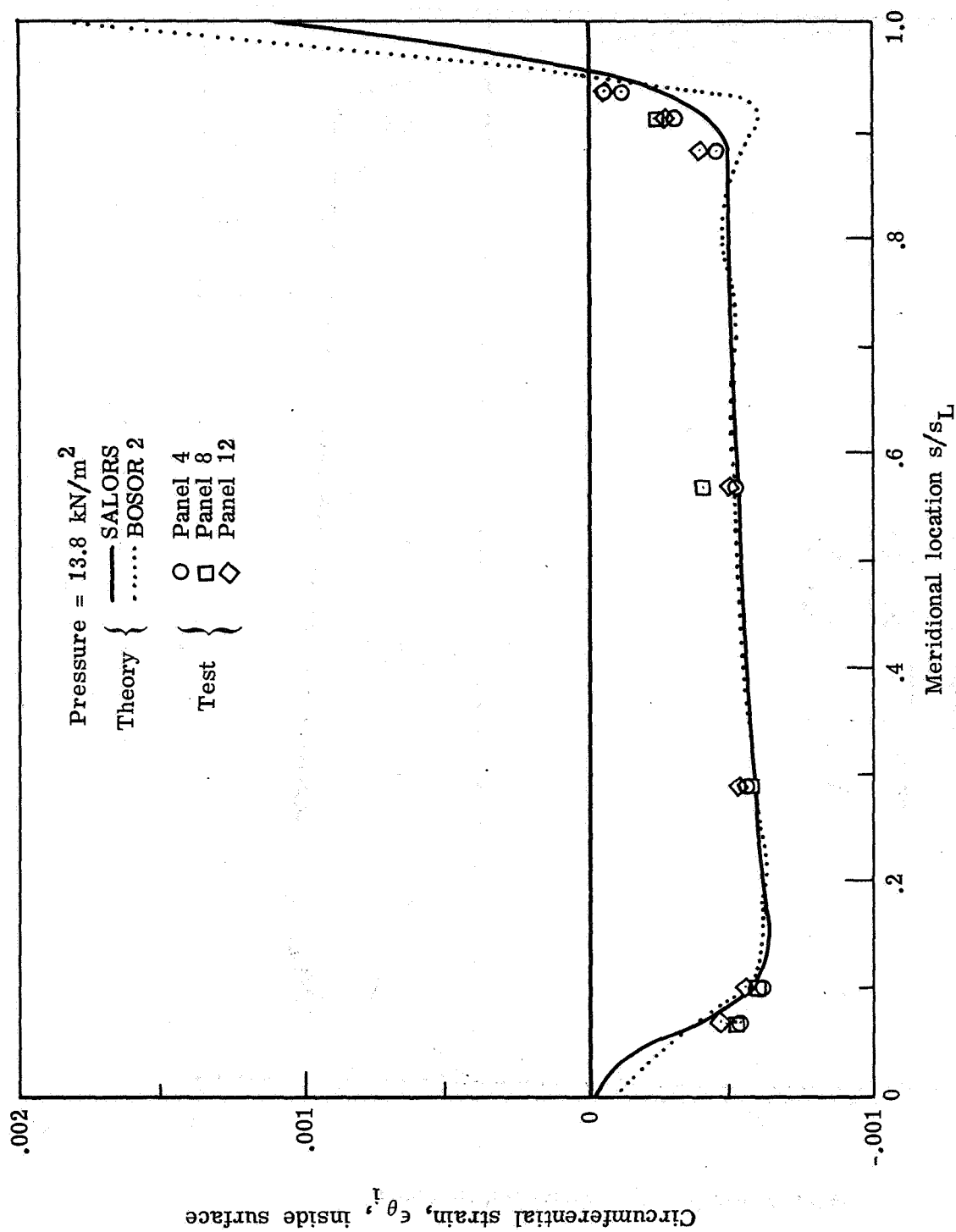
(a) Cone 1.

Figure 6.- Comparison of test and theoretical circumferential strains on outside surface.



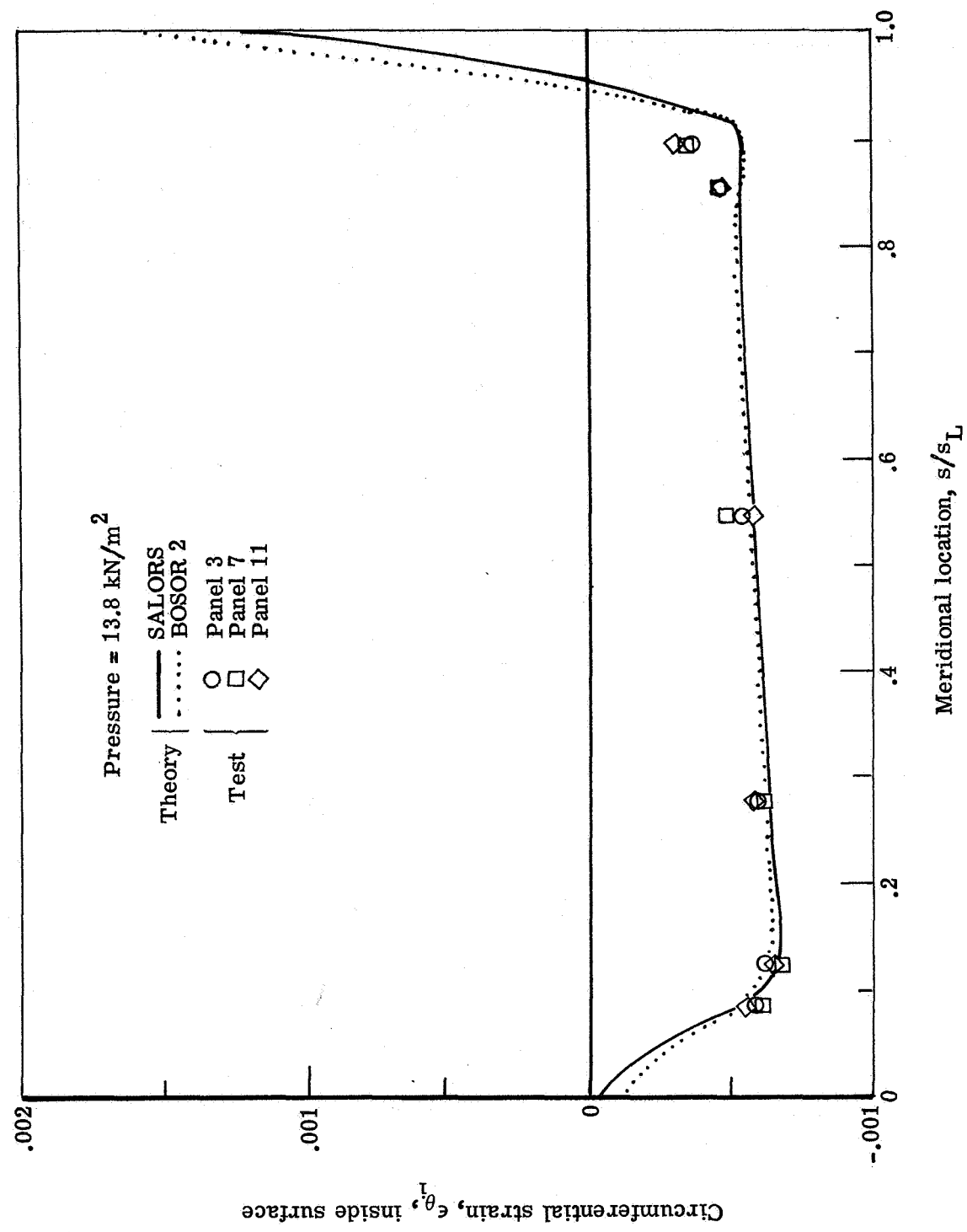
(b) Cone 2.

Figure 6.- Concluded.



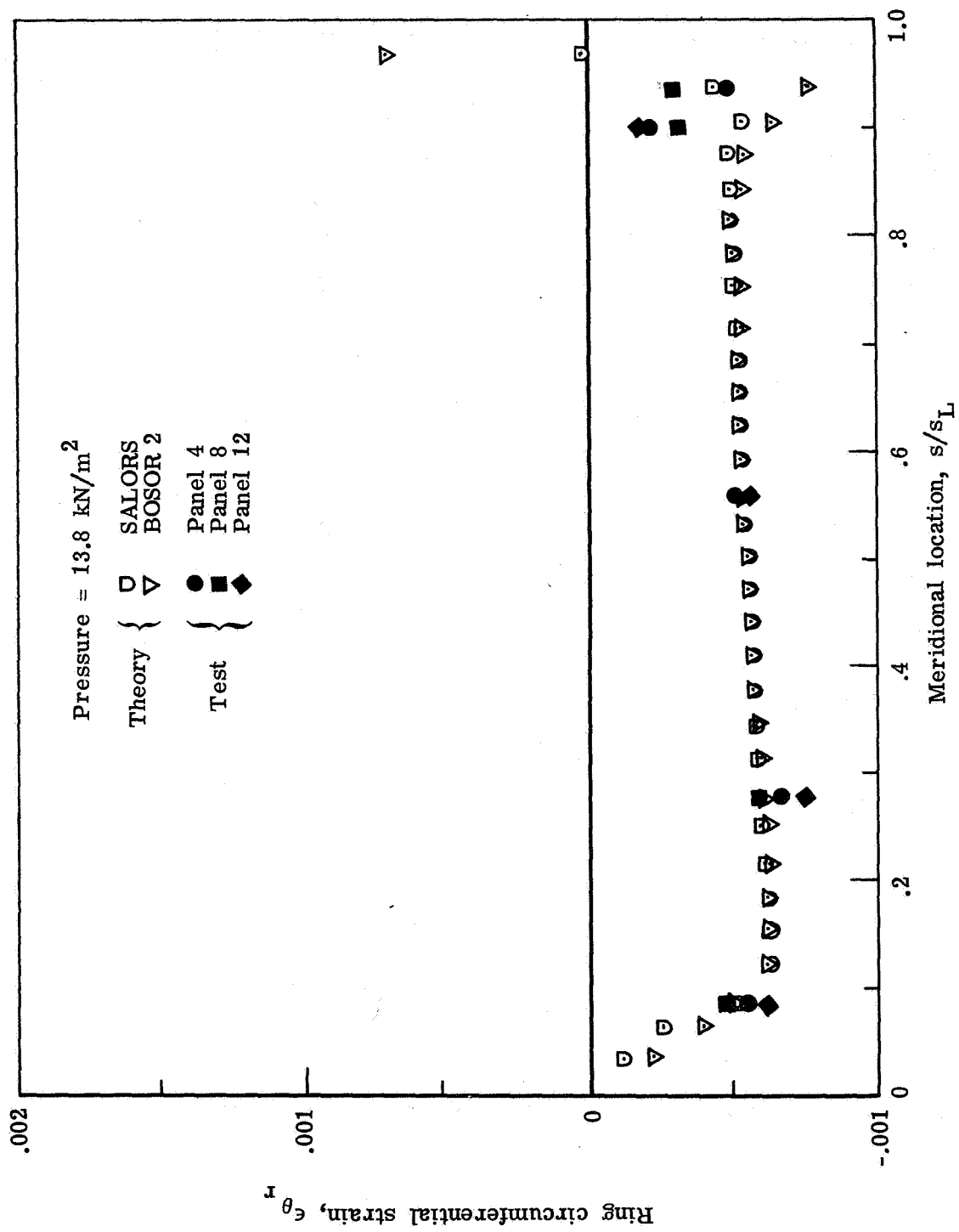
(a) Cone 1.

Figure 7.- Comparison of test and theoretical circumferential strains on inside surface.



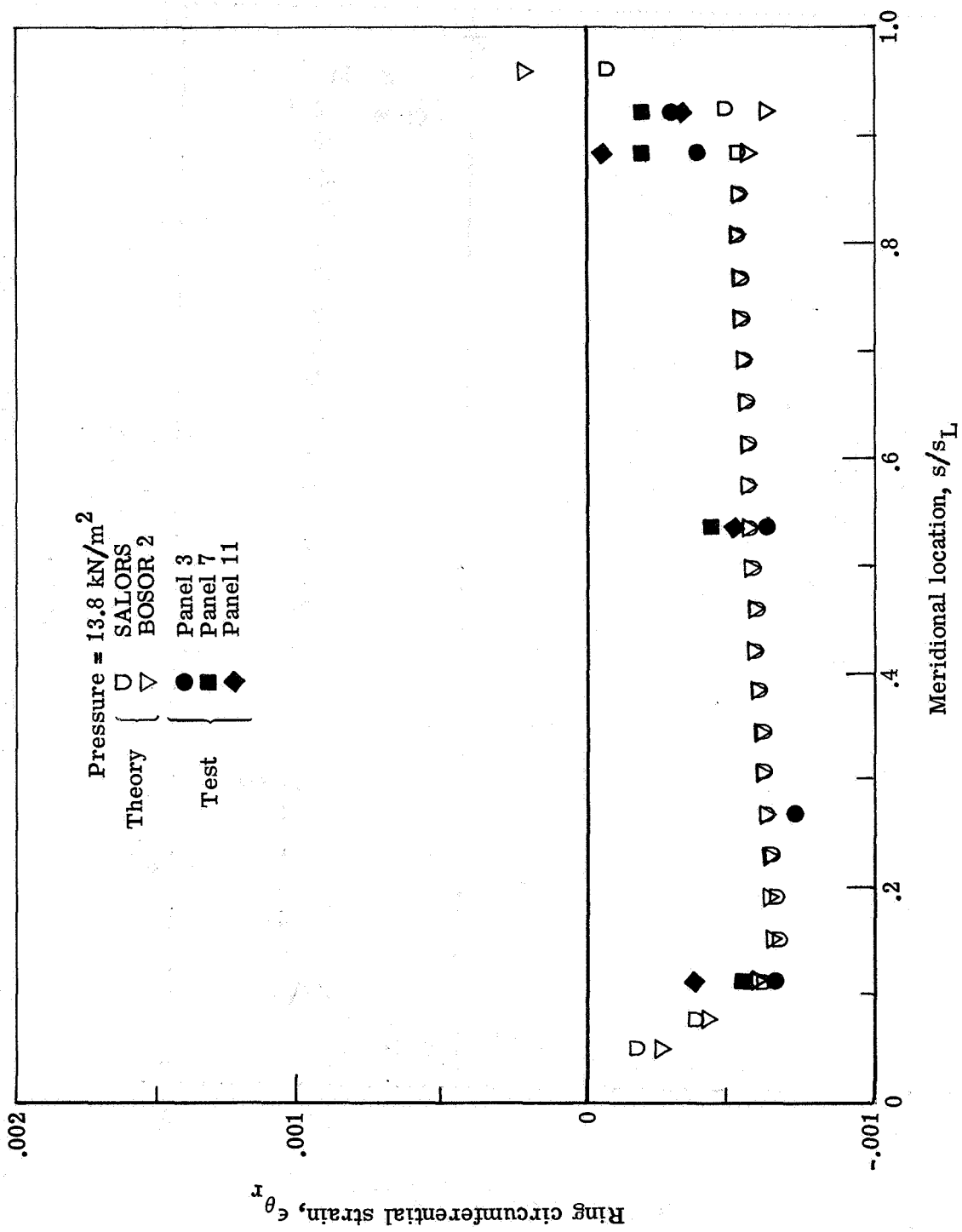
(b) Cone 2.

Figure 7.- Concluded.



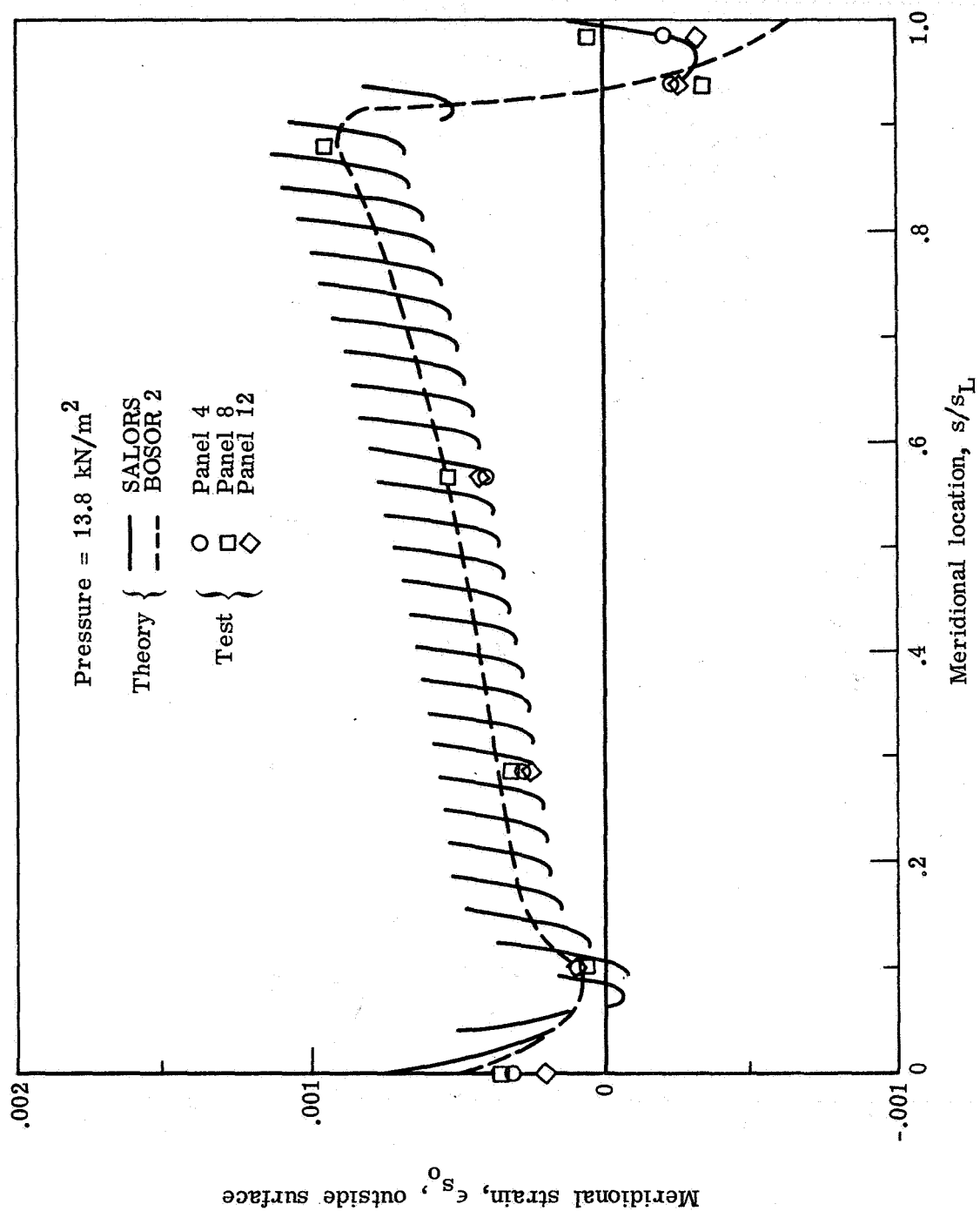
(a) Cone 1.

Figure 8.- Comparison of test and theoretical circumferential strains in shell stiffening rings.



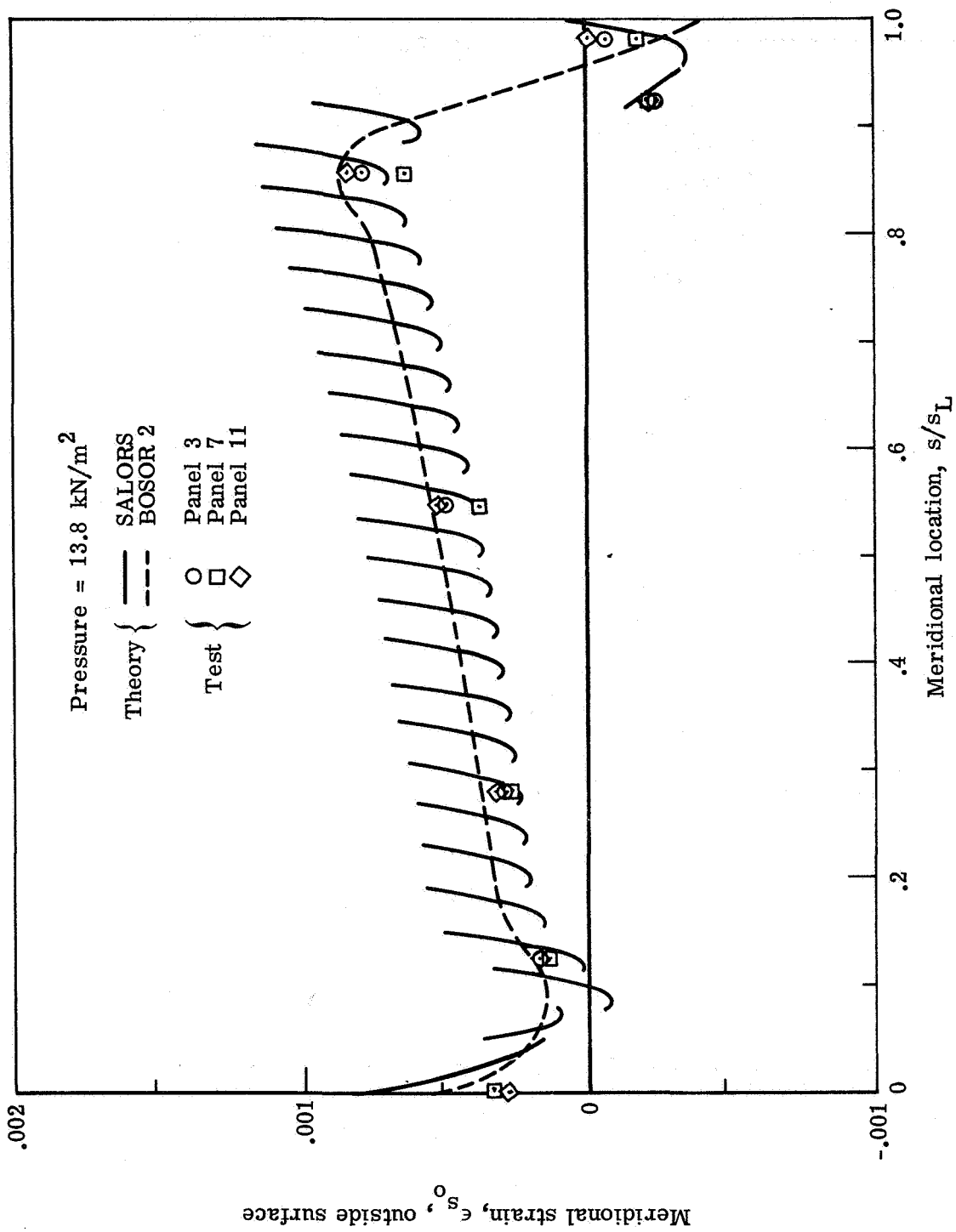
(b) Cone 2.

Figure 8.- Concluded.



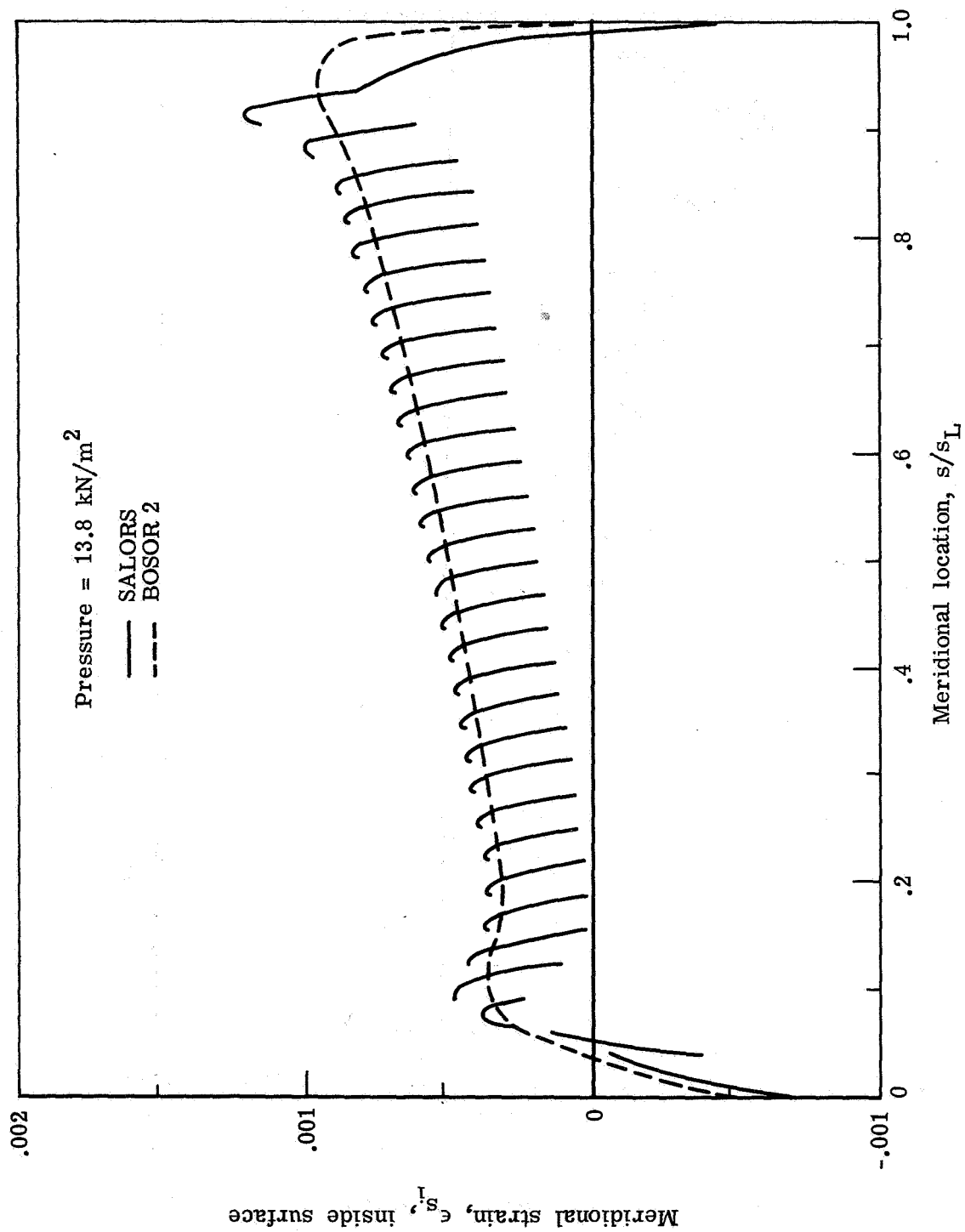
(a) Cone 1.

Figure 9.- Comparison of test and theoretical meridional strains on outside surface.



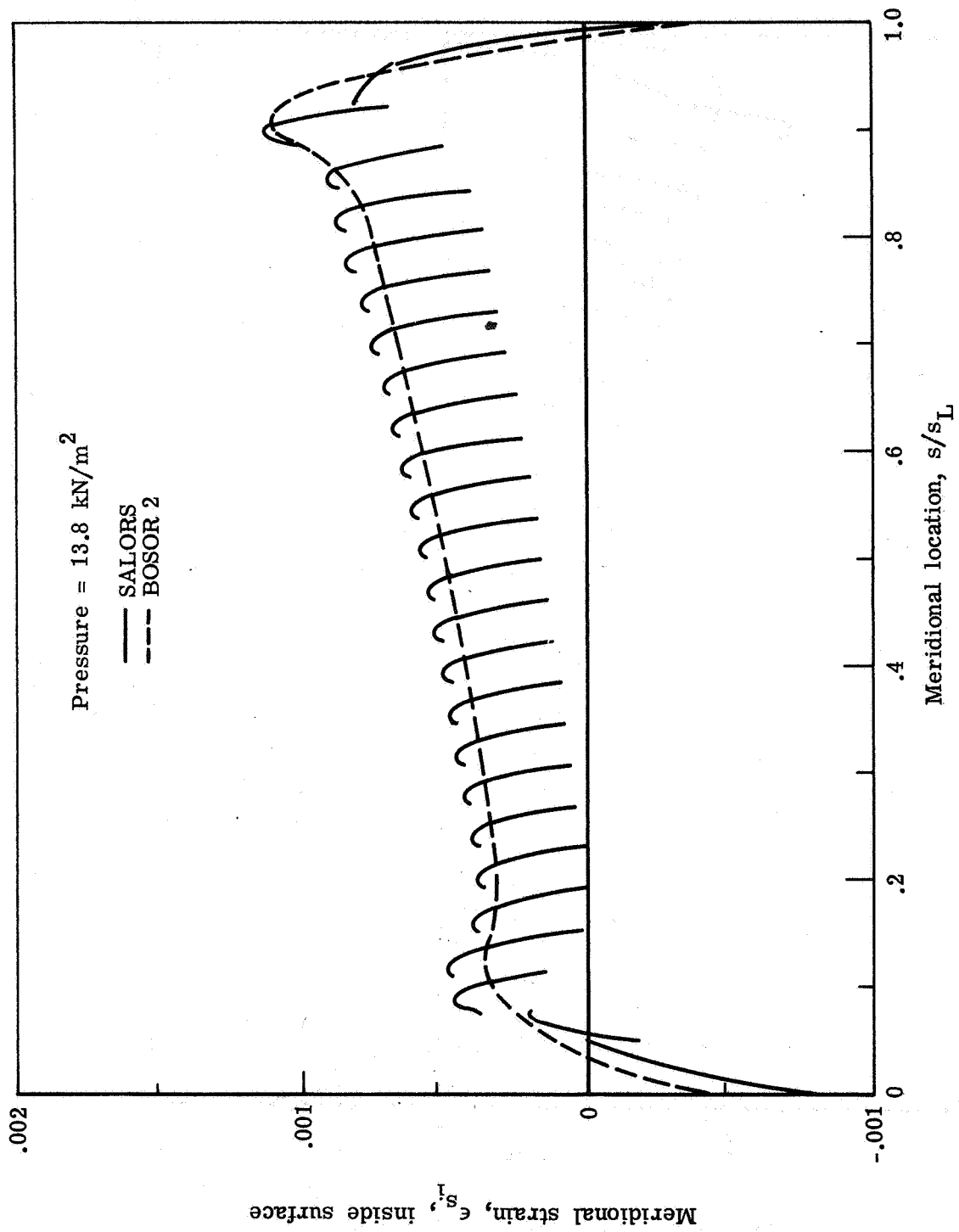
(b) Cone 2.

Figure 9.- Concluded.



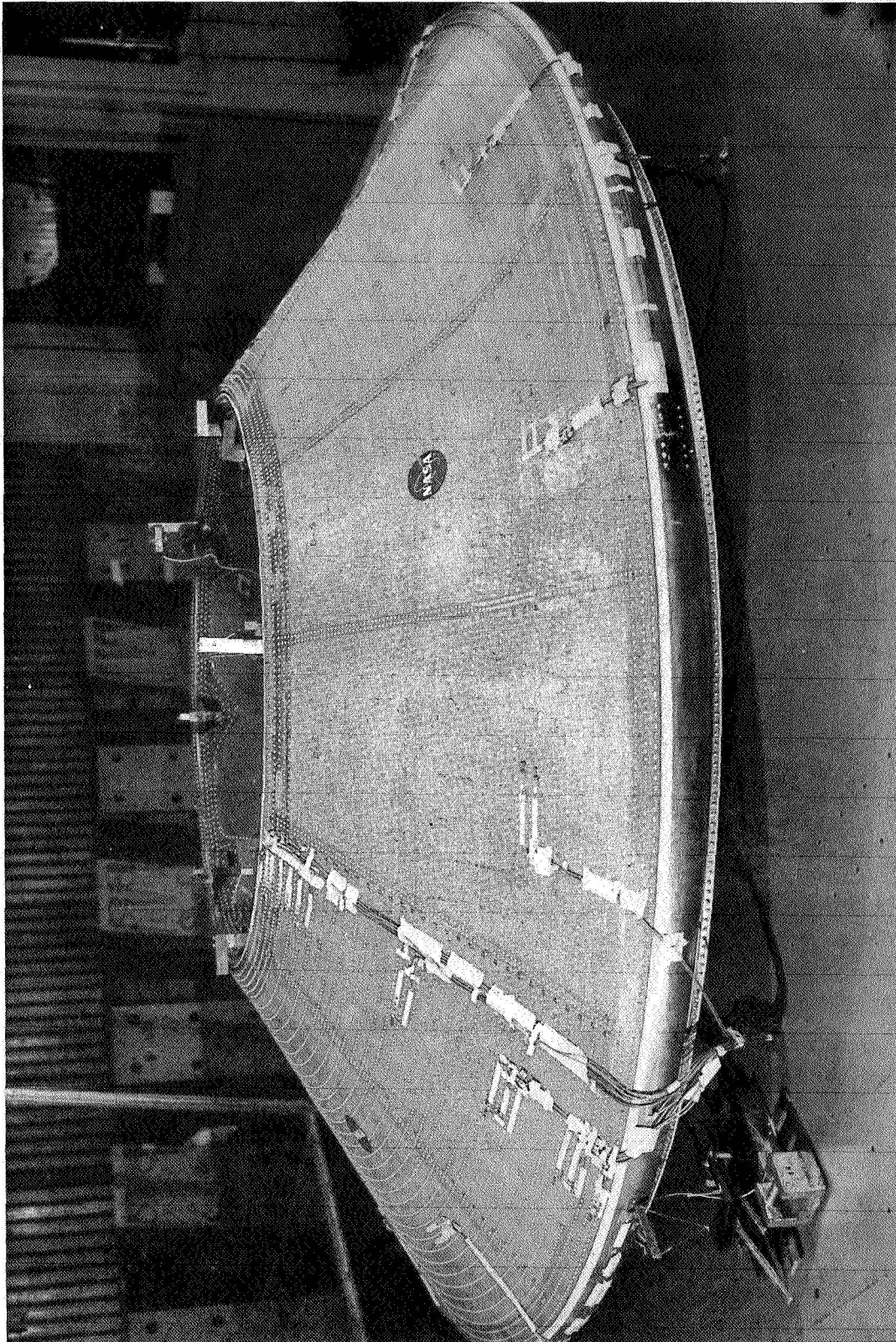
(a) Cone 1.

Figure 10.- Theoretical meridional strains on inside surface.



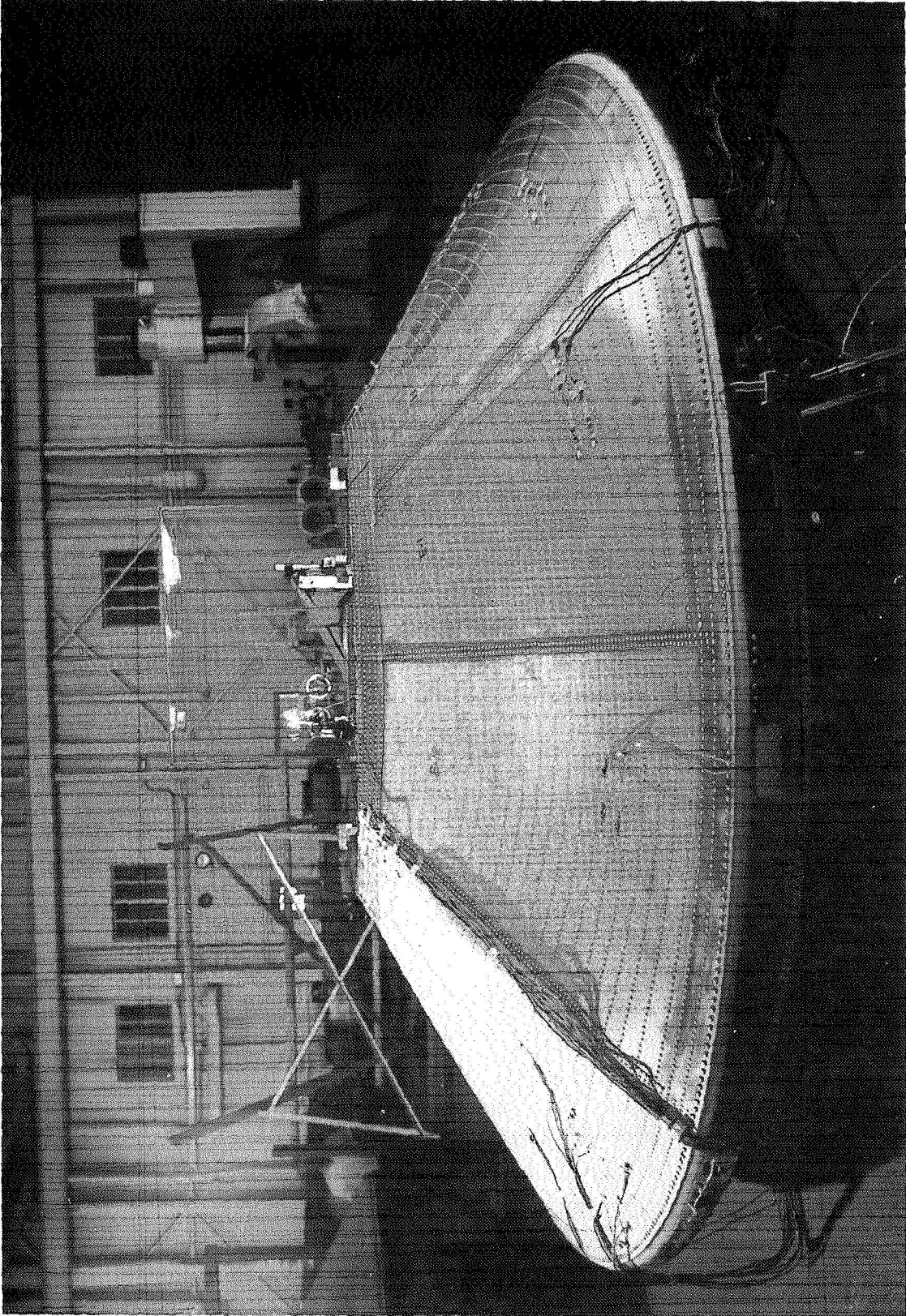
(b) Cone 2.

Figure 10.- Concluded.



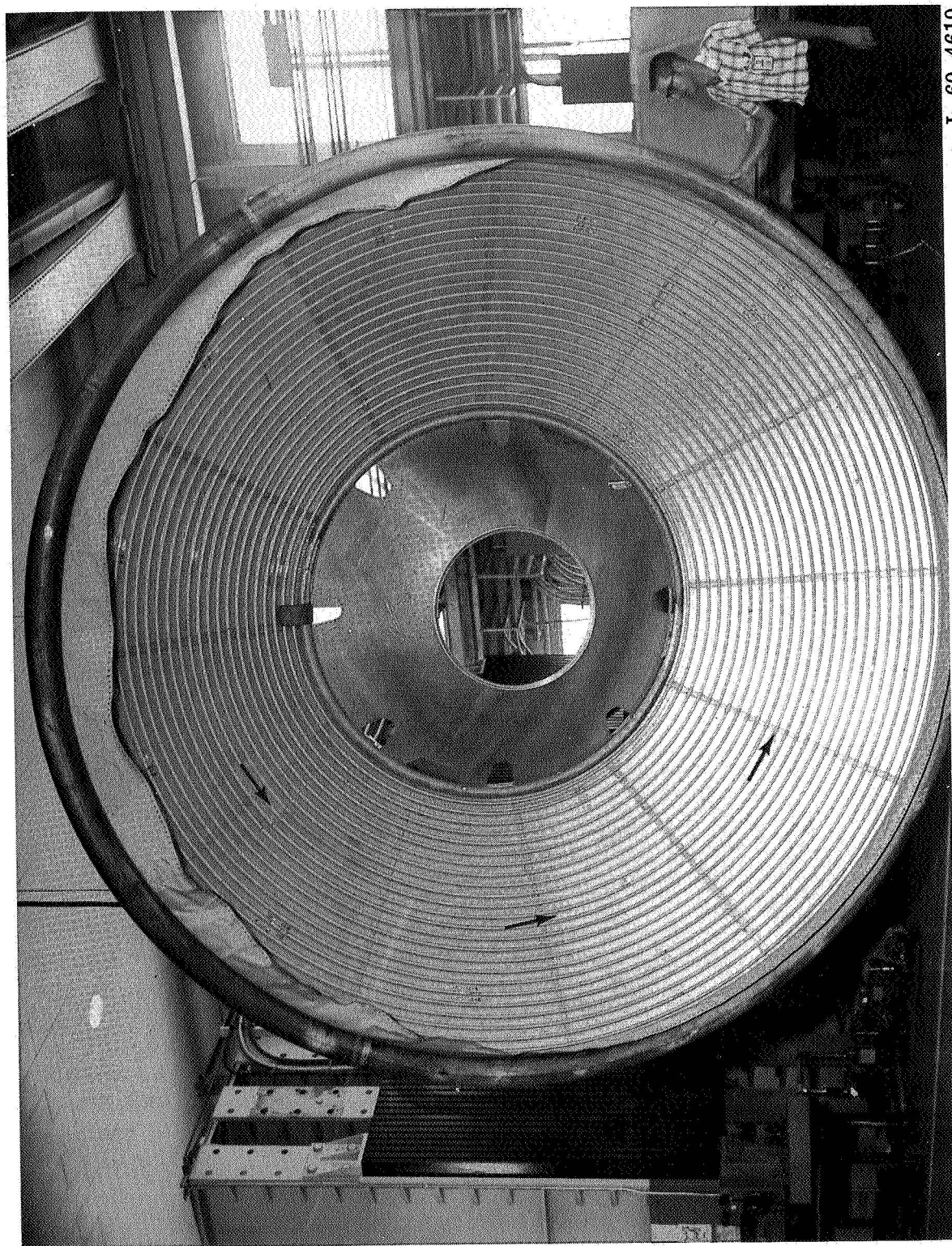
L-69-2877

Figure 11.- Outside surface of cone 1 after buckling and while still under pressure loading.



L-69-4243

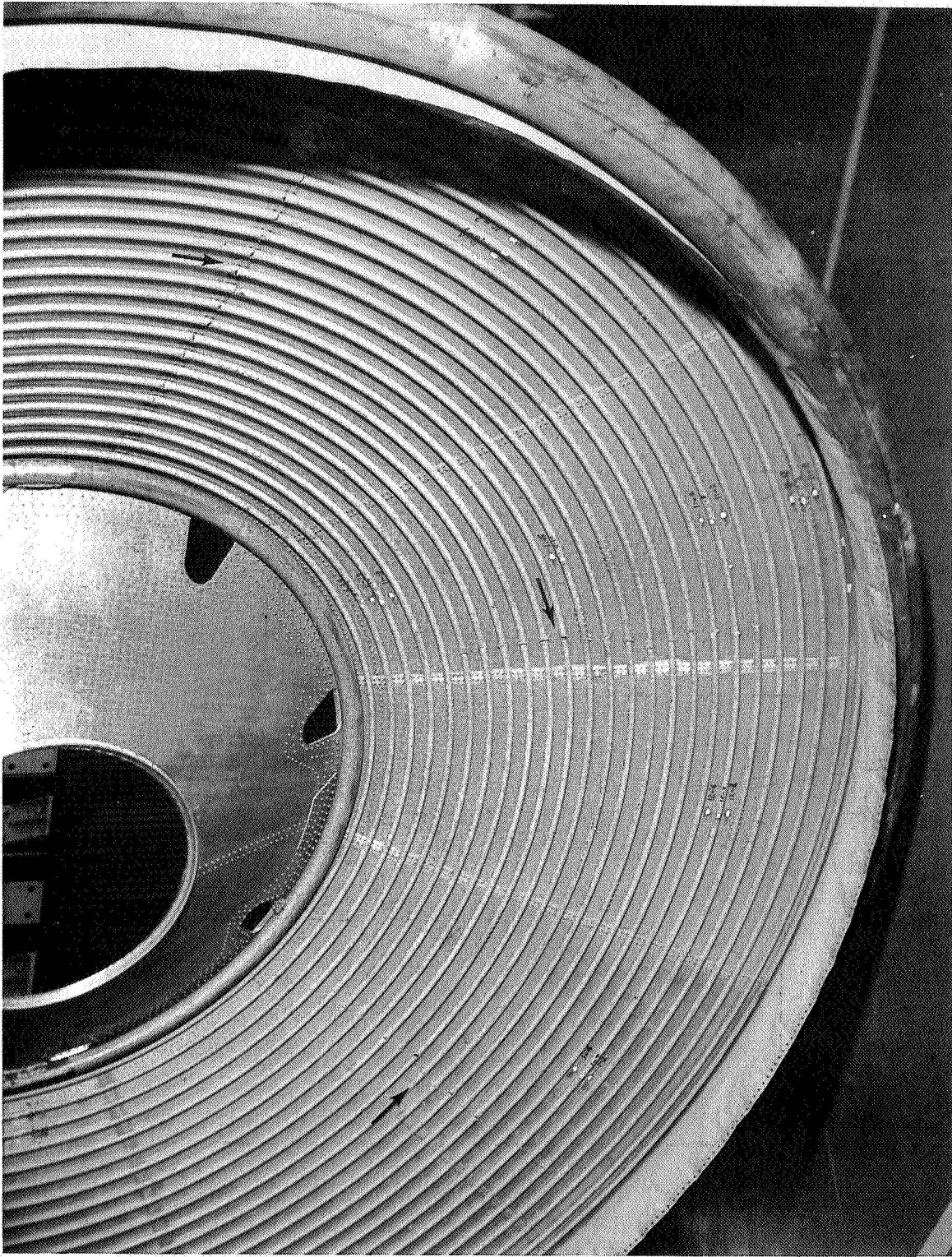
Figure 12.- Outside surface of cone 2 after buckling and while still under pressure loading.



L-69-4619

(a) Overall view after removal from test setup.

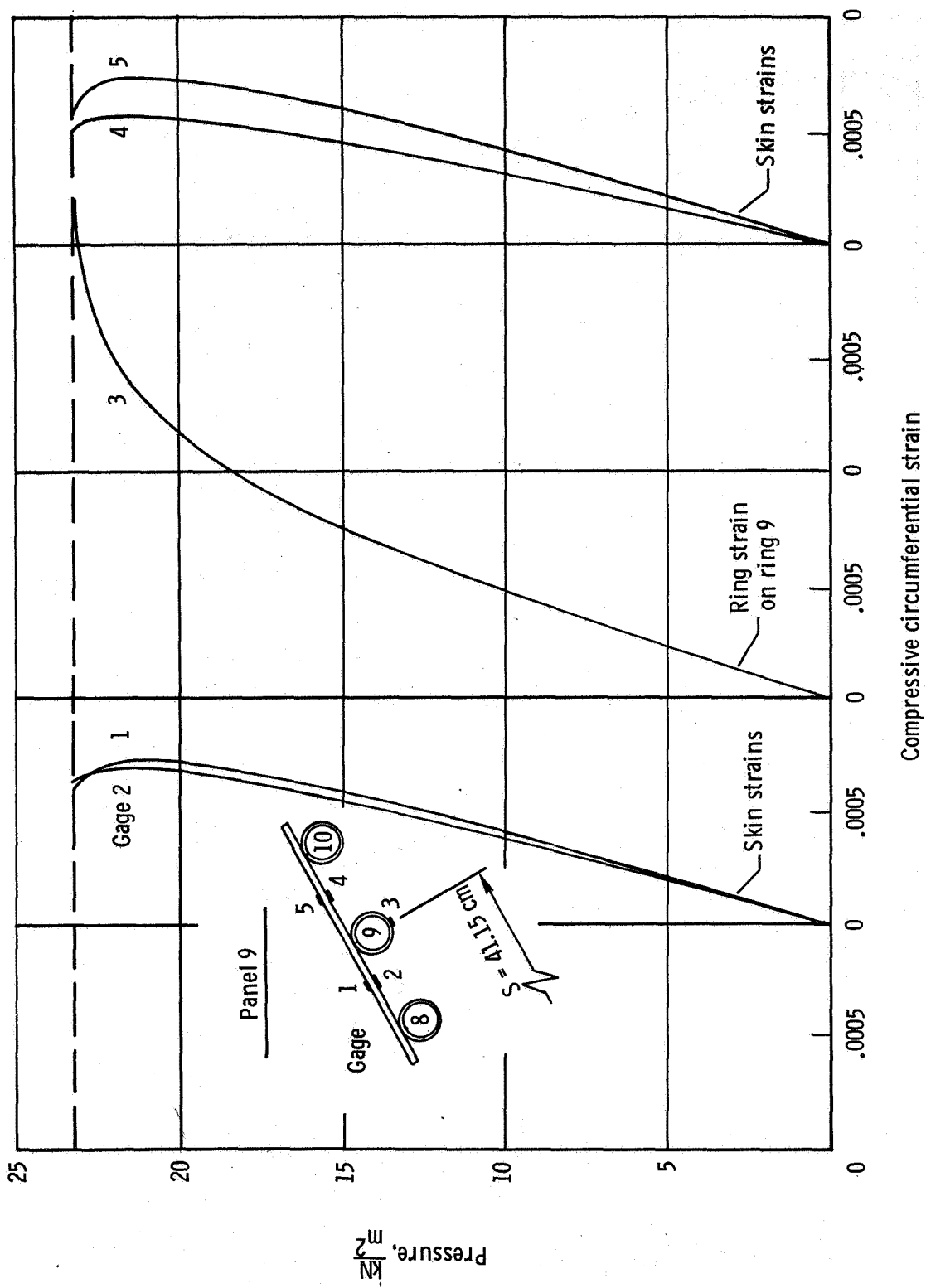
Figure 13.- Views of inside surface of cone 2.



L-69-4620

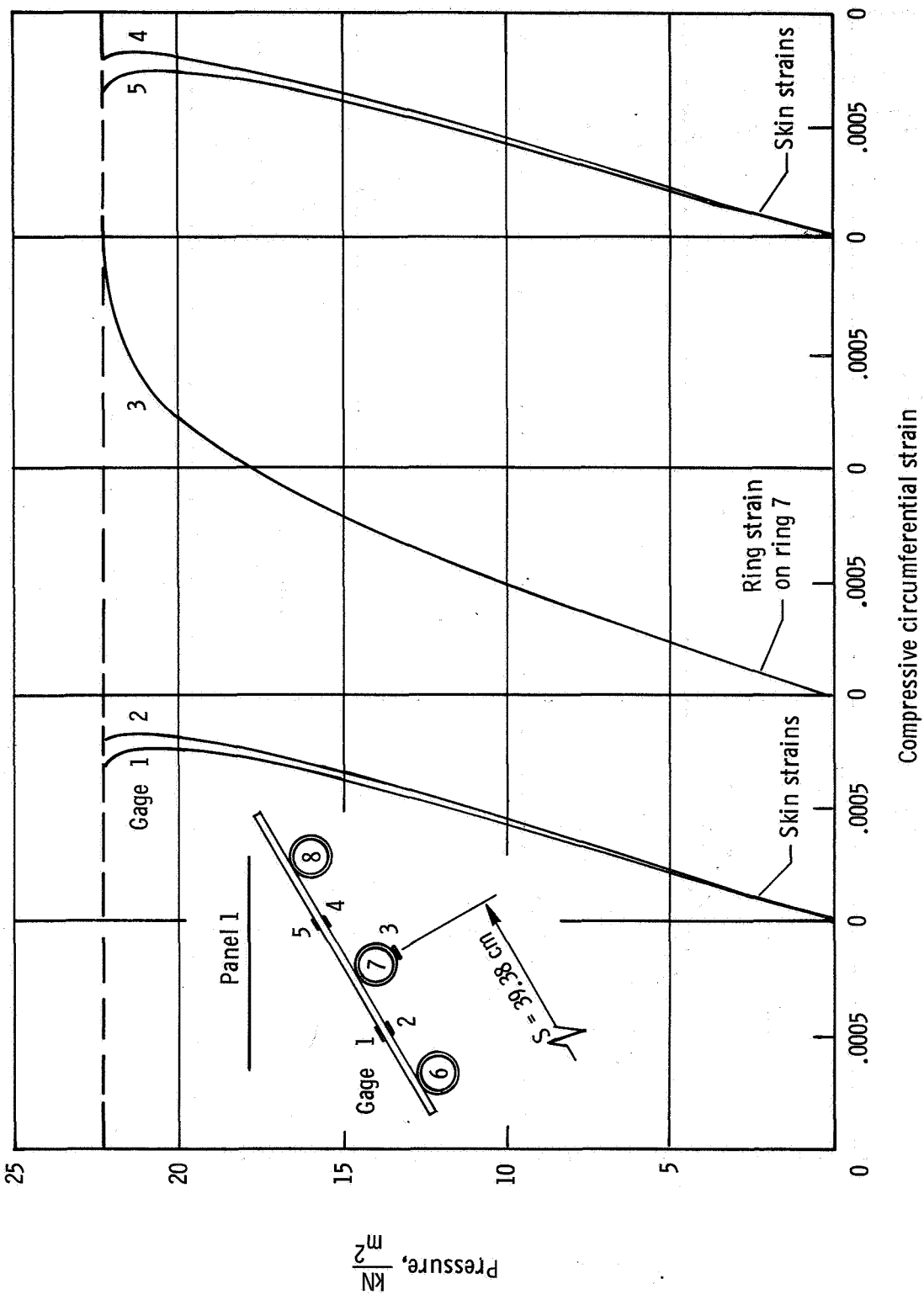
(b) Closeup view showing crippled shell stiffening rings.

Figure 13.- Concluded.



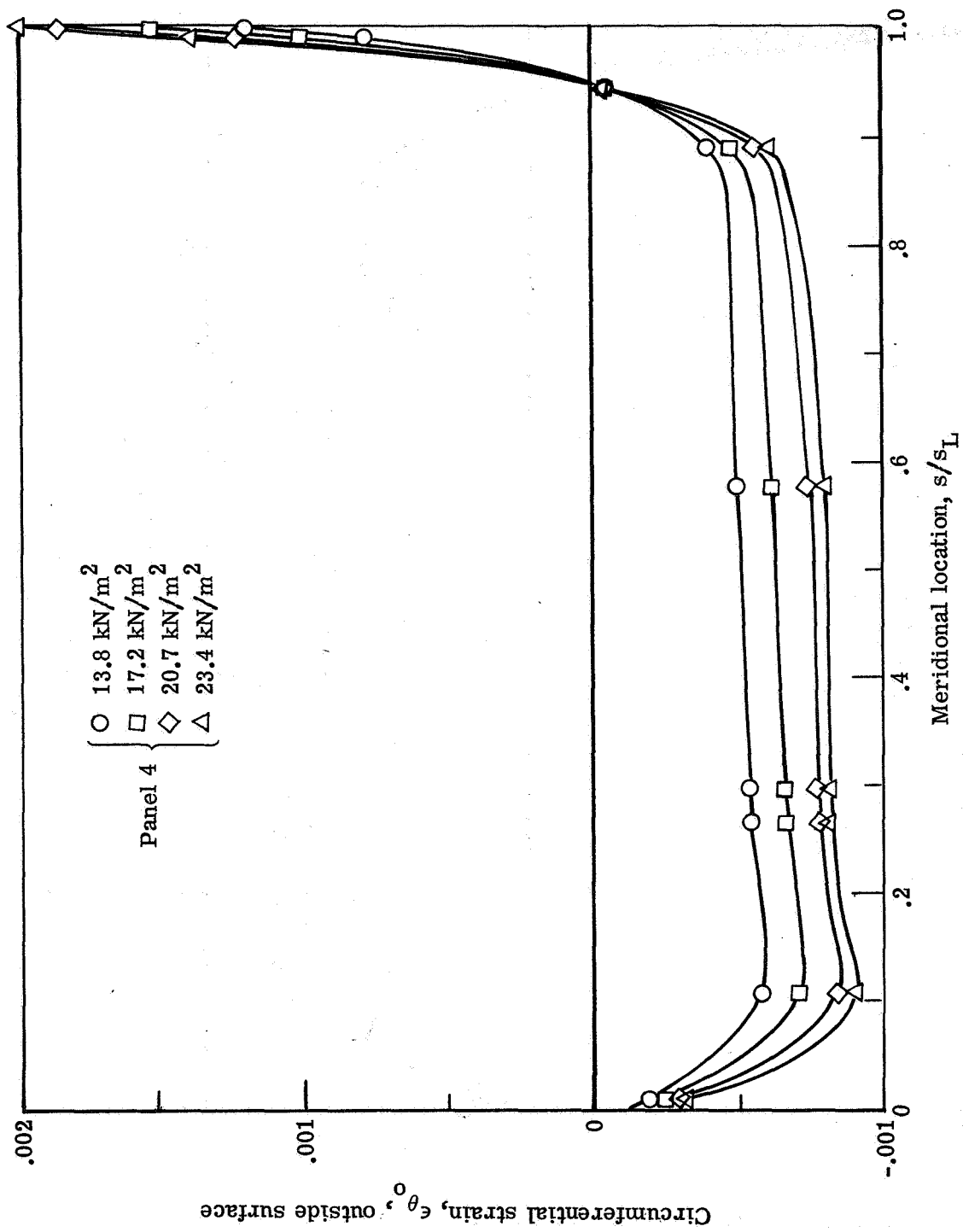
(a) Cone 1.

Figure 14.- Pressure-strain relationship at center of panel exhibiting most shell wall bending.



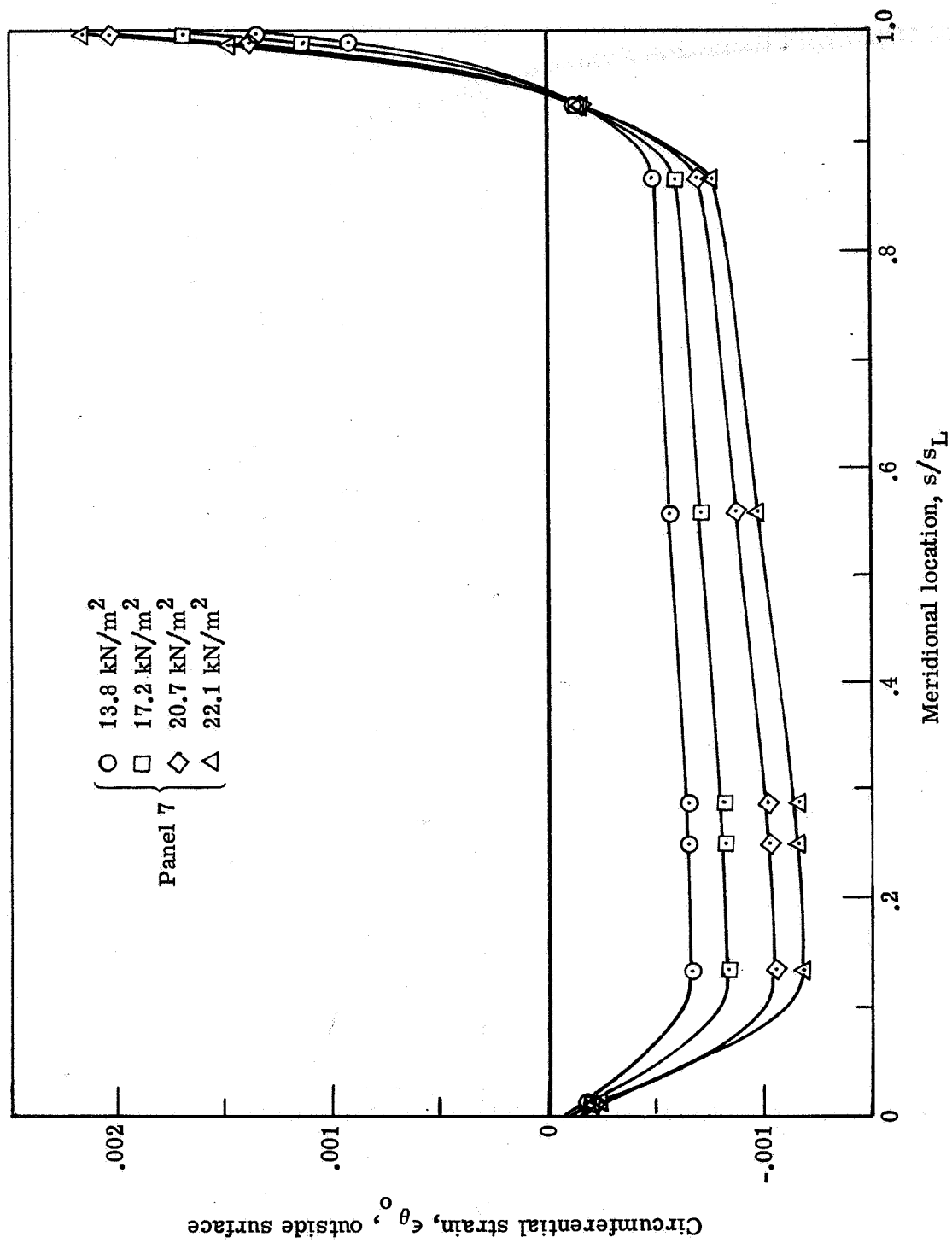
(b) Cone 2.

Figure 14.- Concluded.



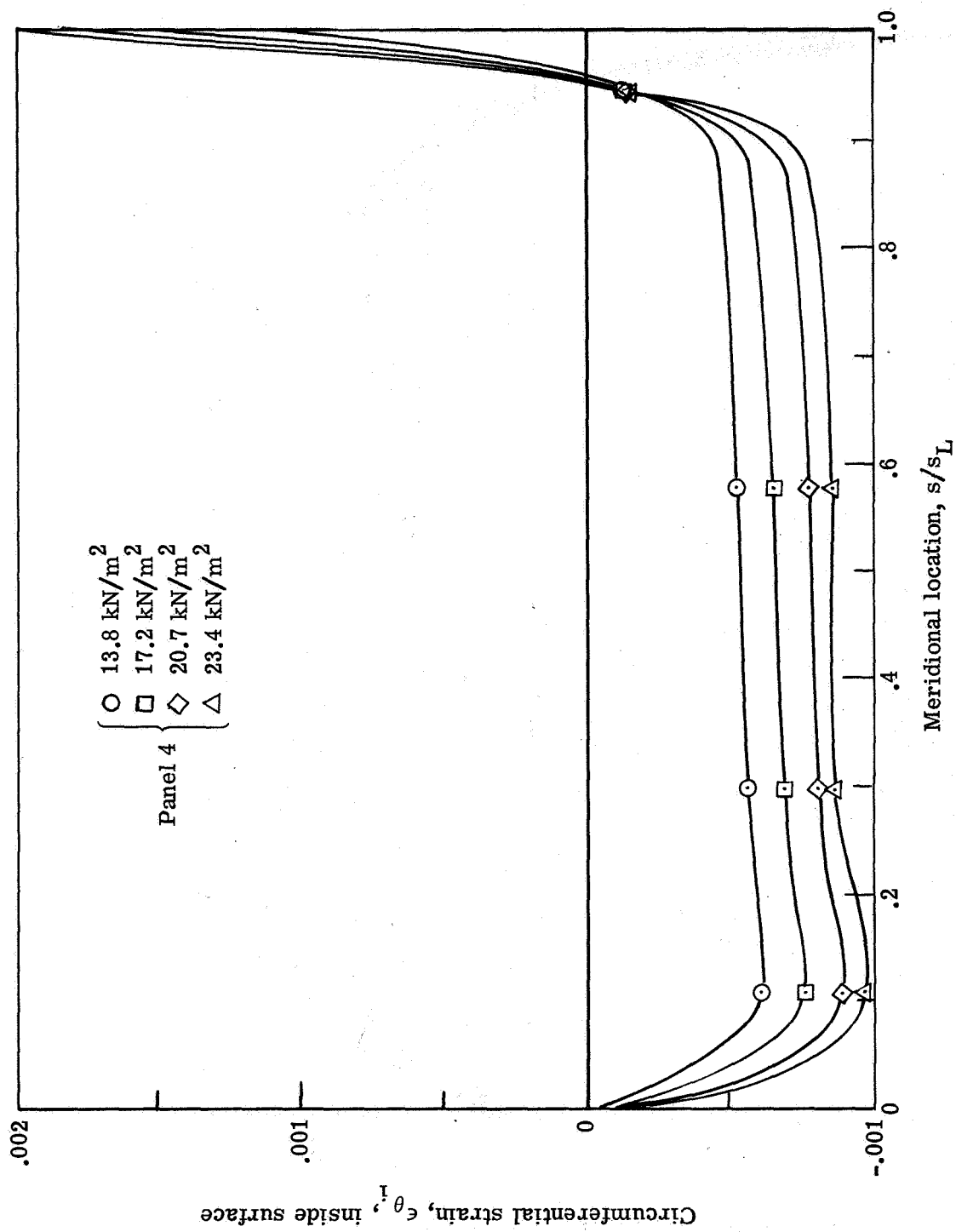
(a) Cone 1.

Figure 15.- Profiles of outside surface circumferential strains during the buckling test.



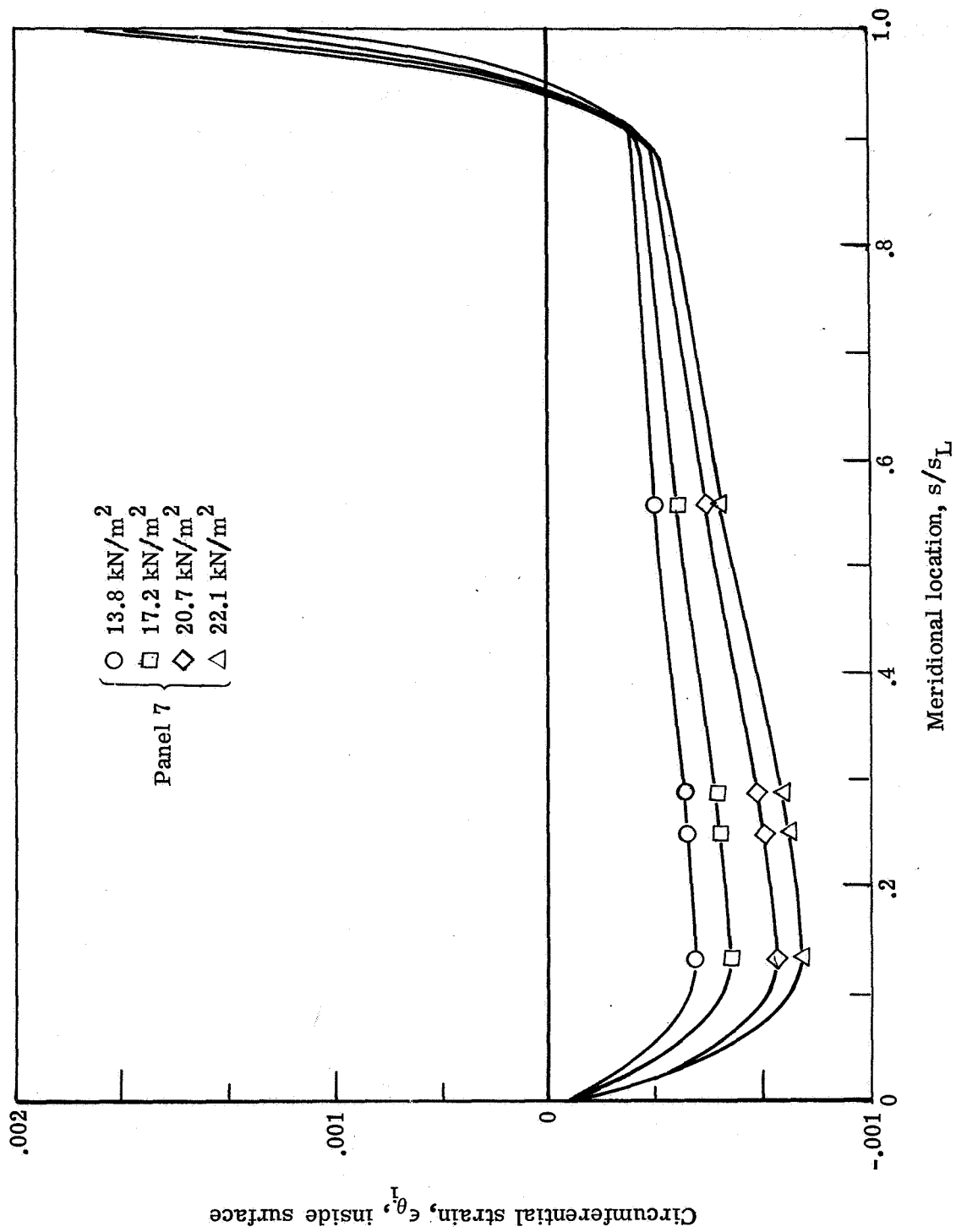
(b) Cone 2.

Figure 15.- Concluded.



(a) Cone 1.

Figure 16.- Profiles of inside surface circumferential strains during the buckling test.



(b) Cone 2.

Figure 16.- Concluded.

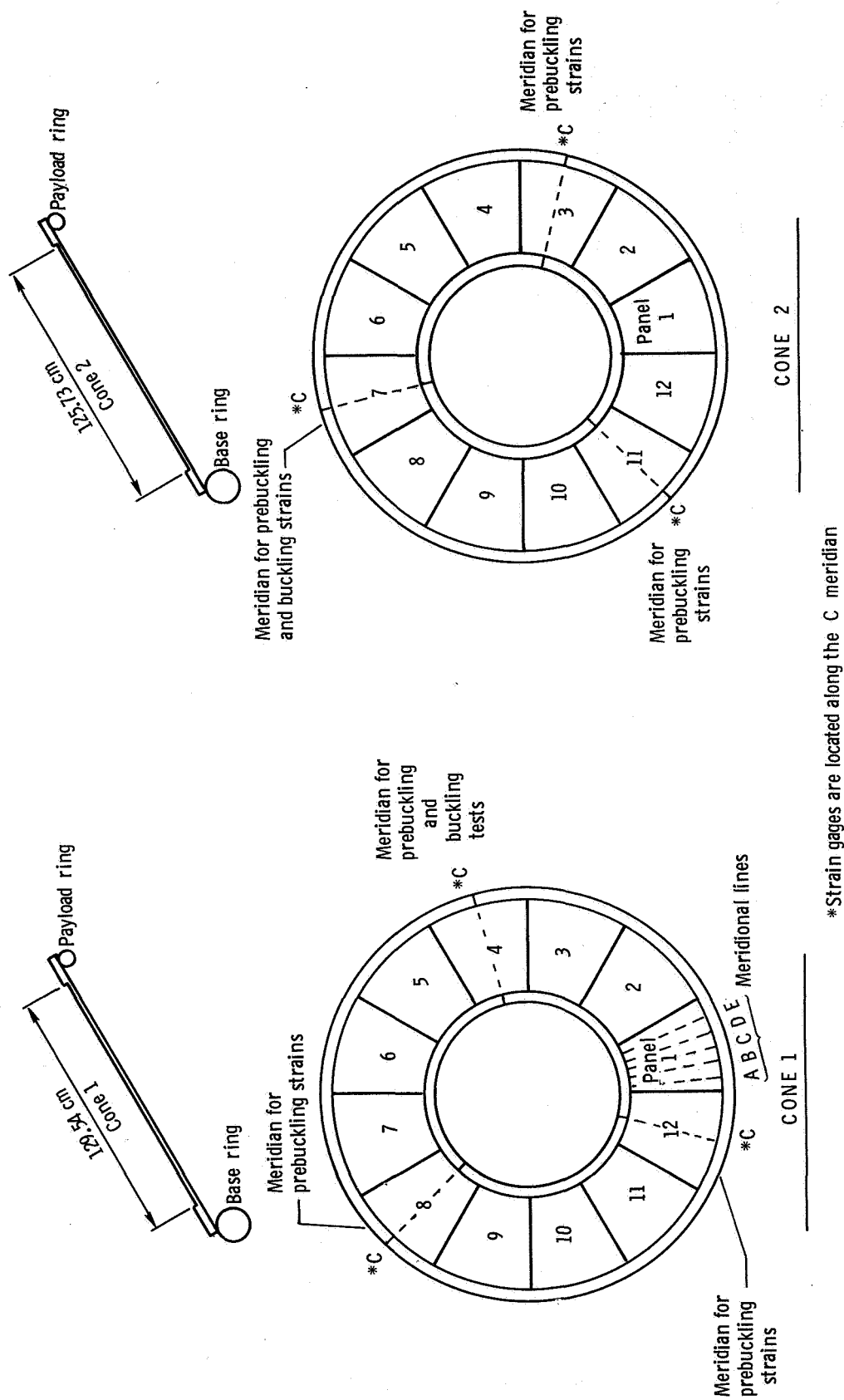
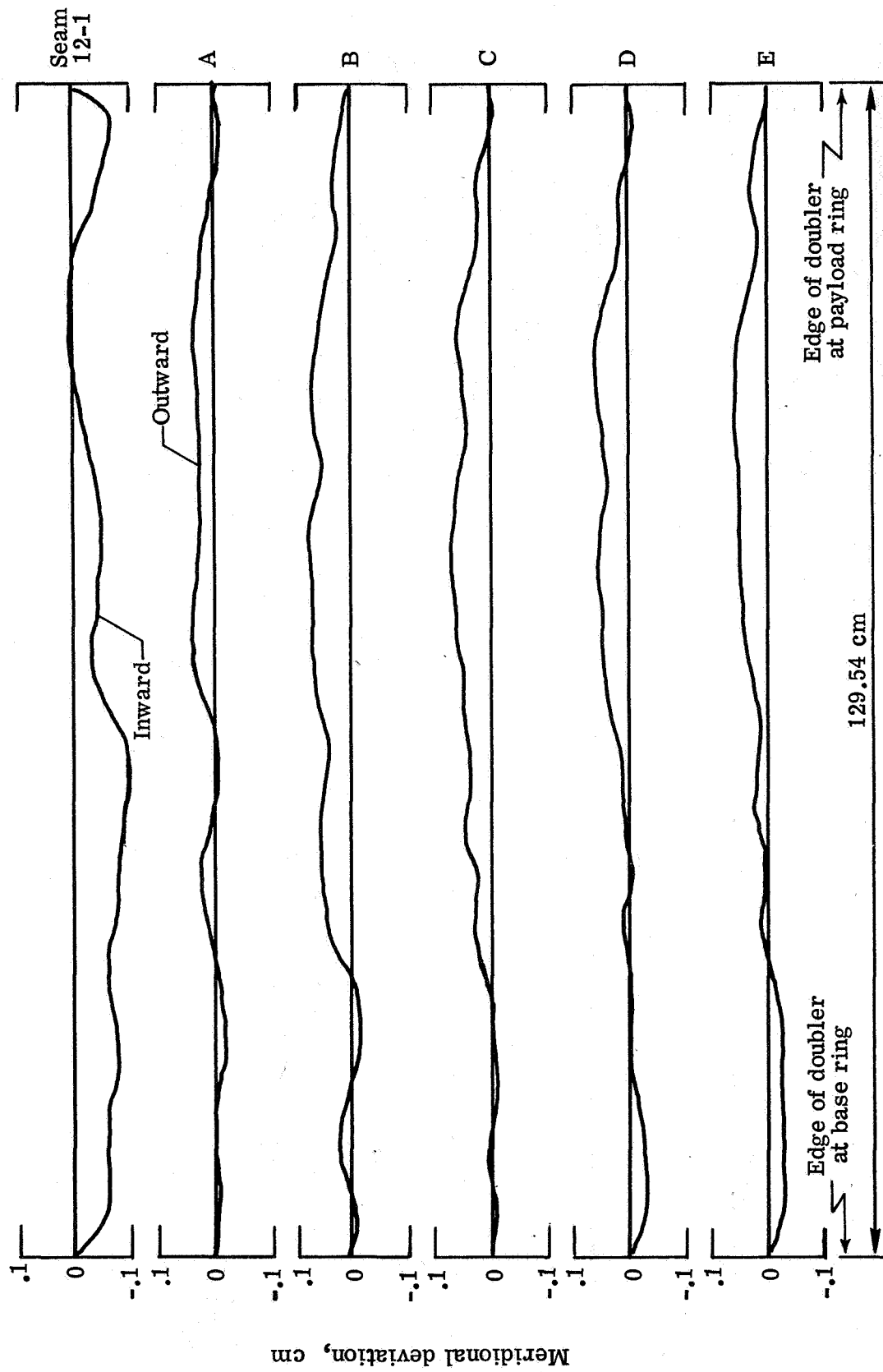
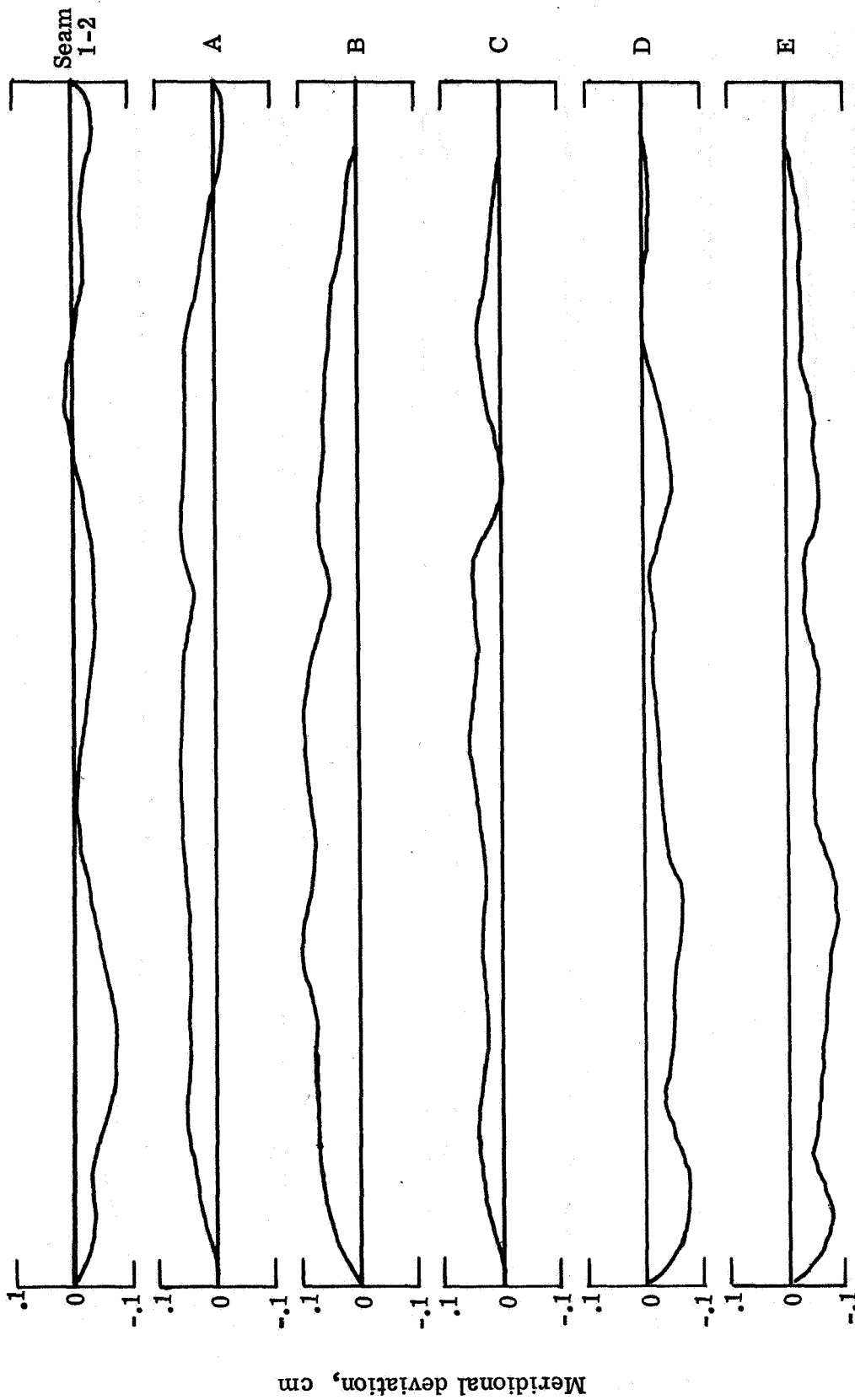


Figure 17.- Panel orientation and imperfection measuring details for cones 1 and 2 (inverted inner cone not shown).



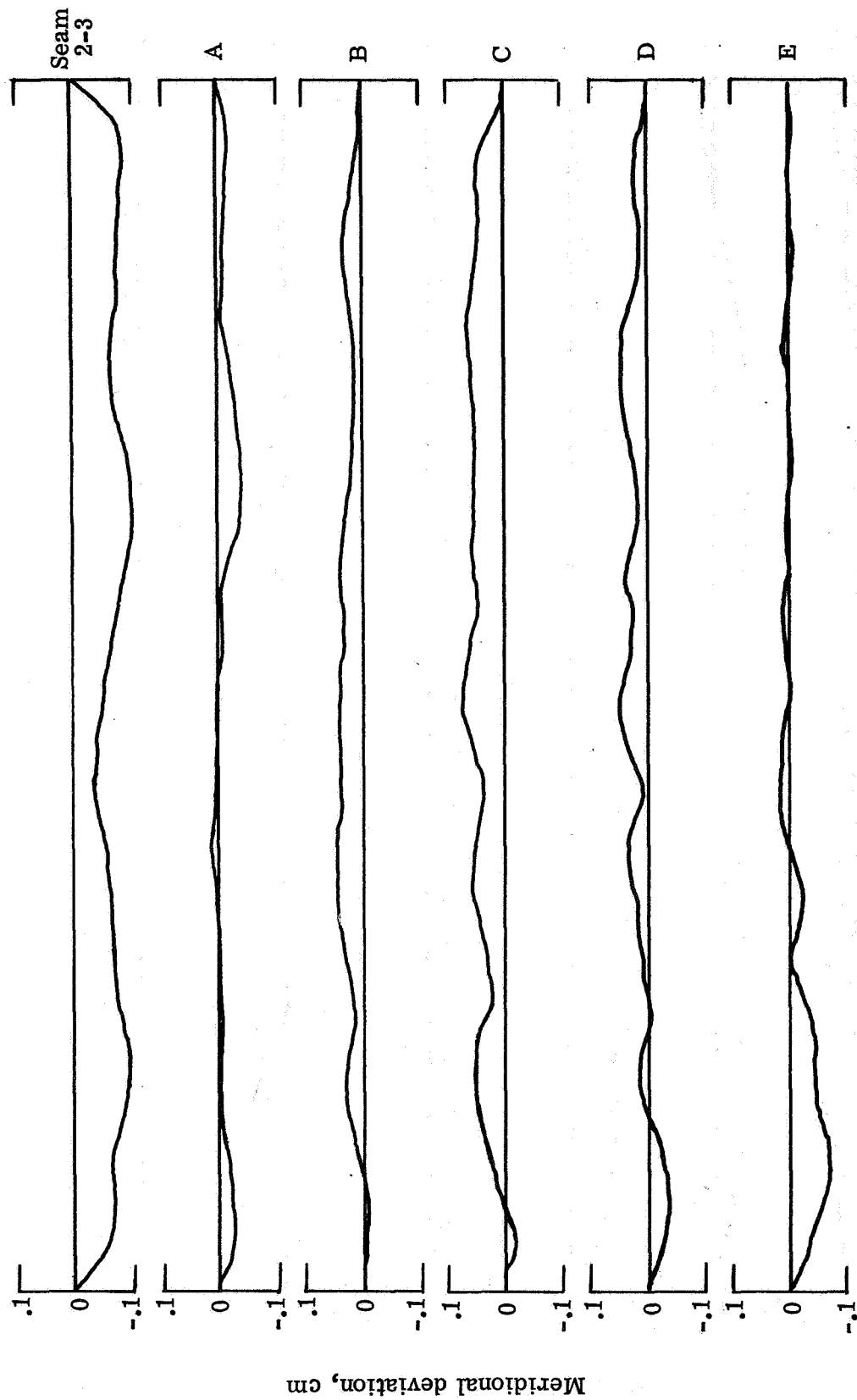
(a) Panel 1.

Figure 18.- Imperfection measurements of cone 1.



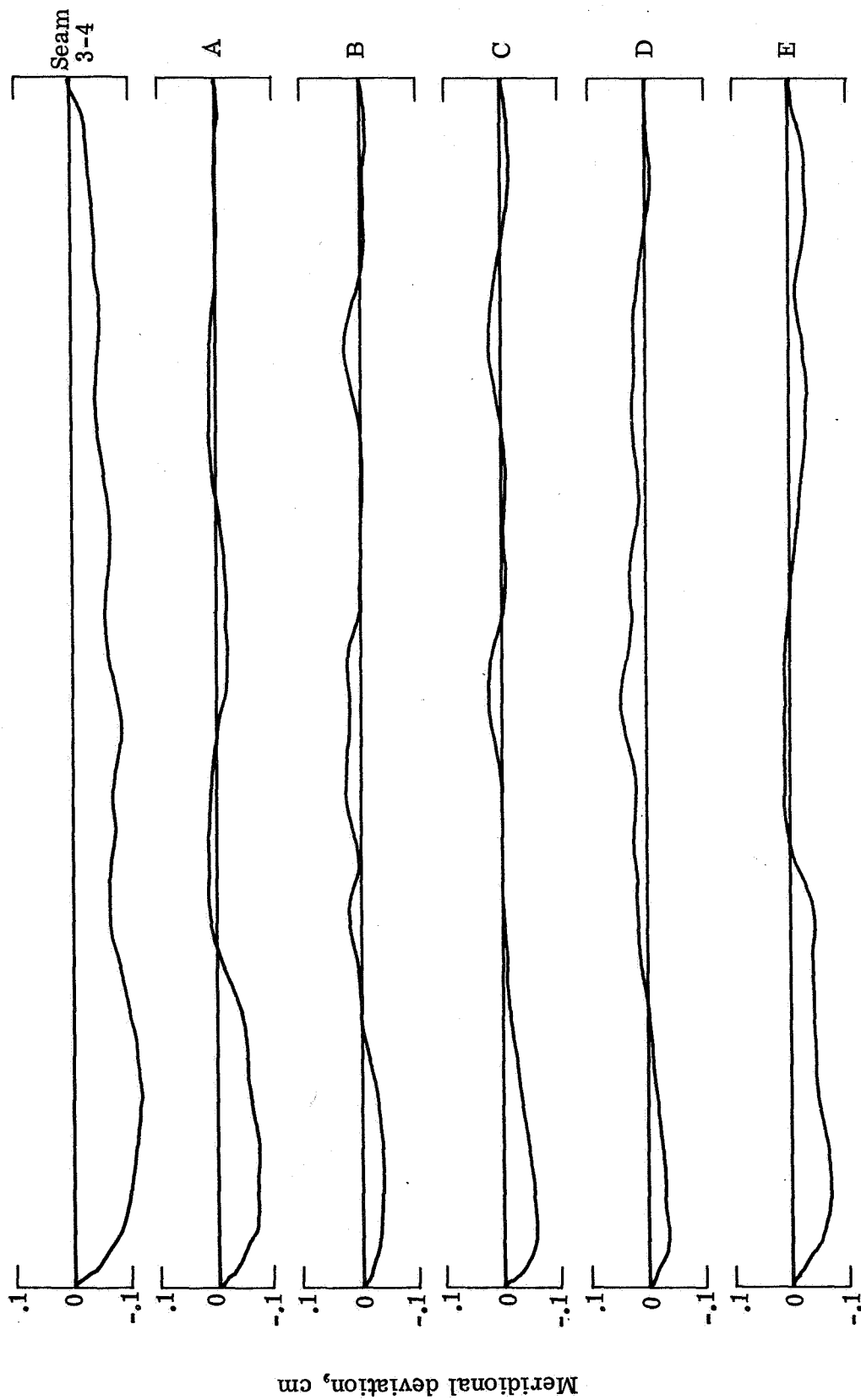
(b) Panel 2.

Figure 18.- Continued.



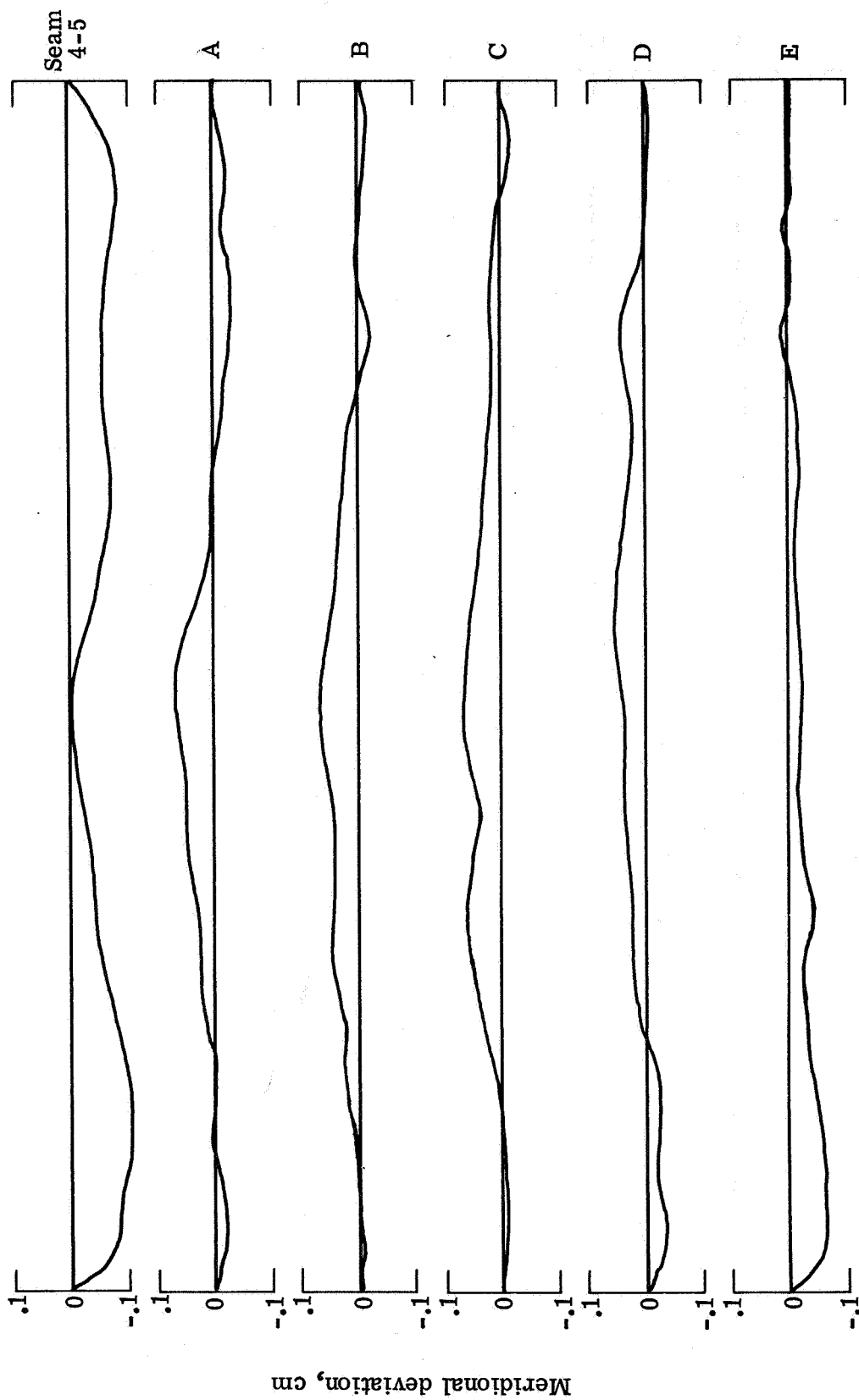
(c) Panel 3.

Figure 18.- Continued.



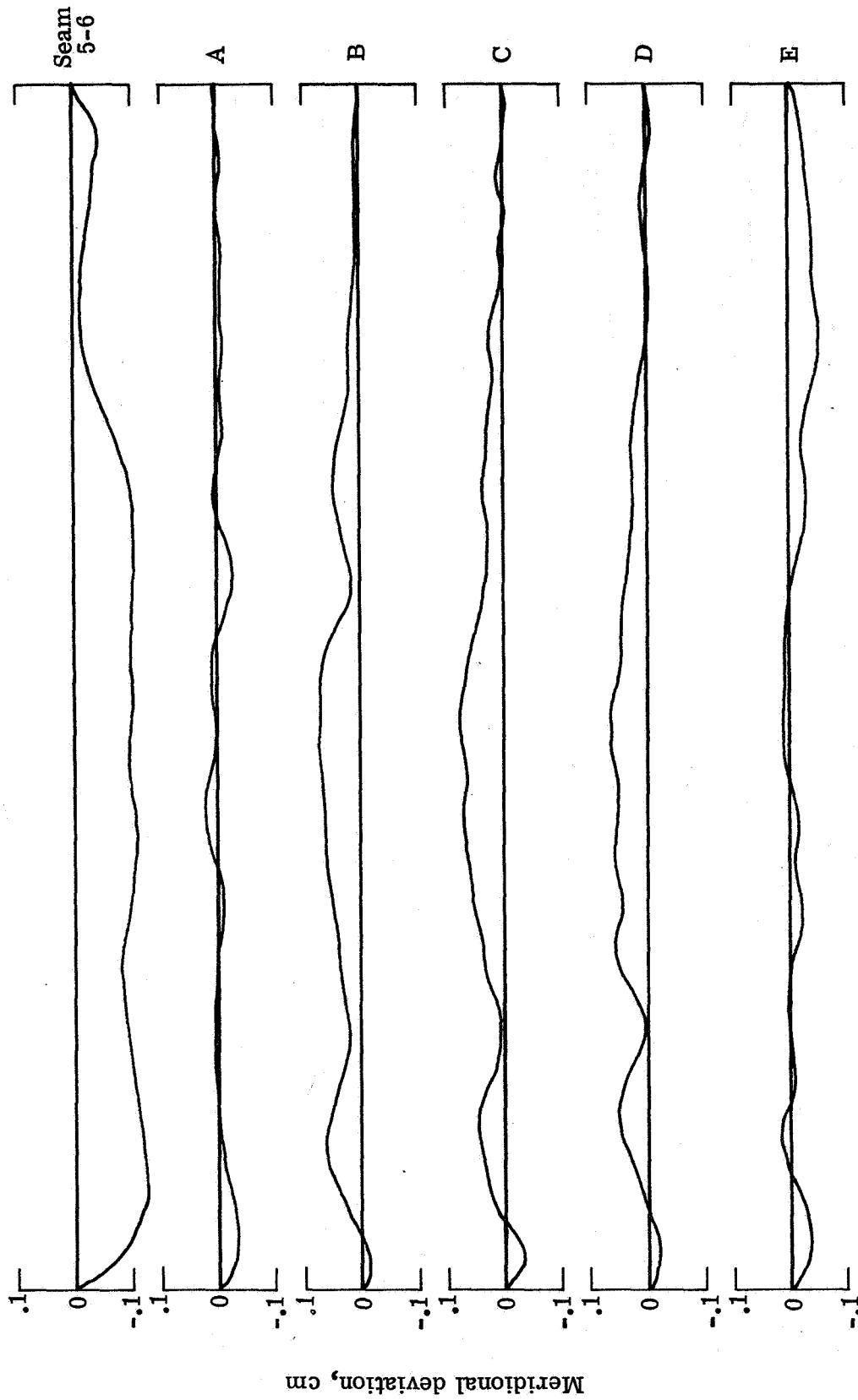
(d) Panel 4.

Figure 18.- Continued.



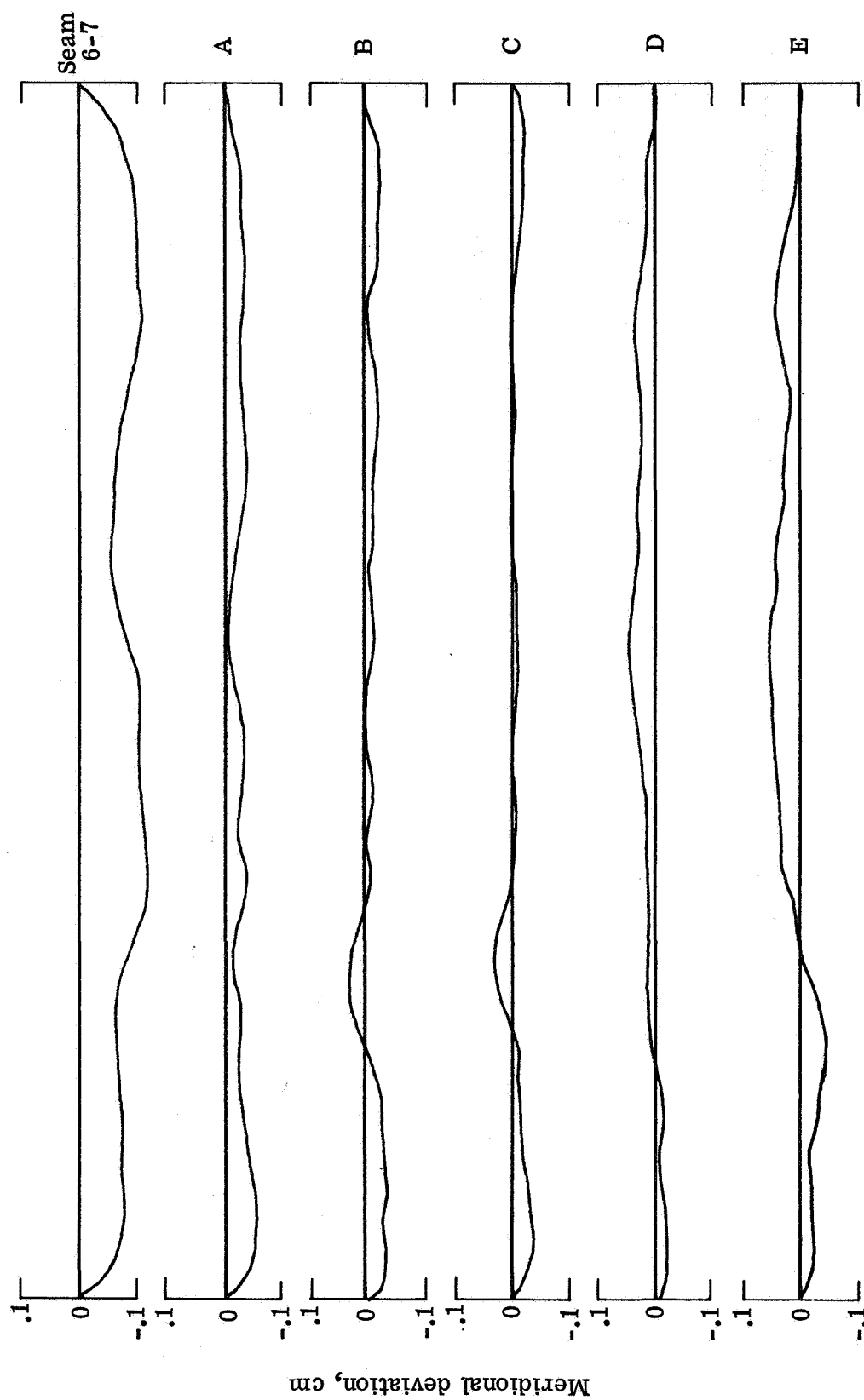
(e) Panel 5.

Figure 18.- Continued.

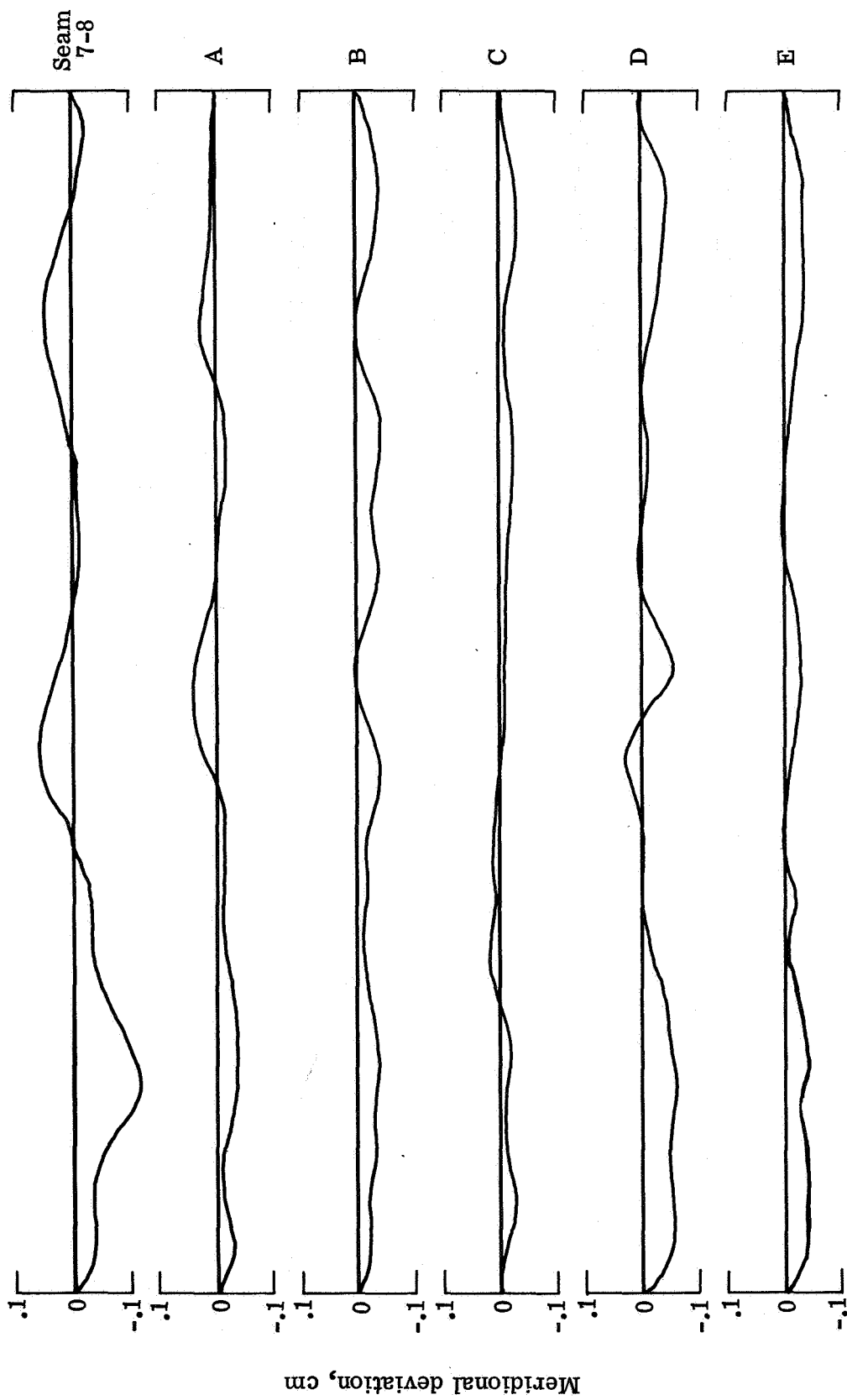


(f) Panel 6.

Figure 18.- Continued.

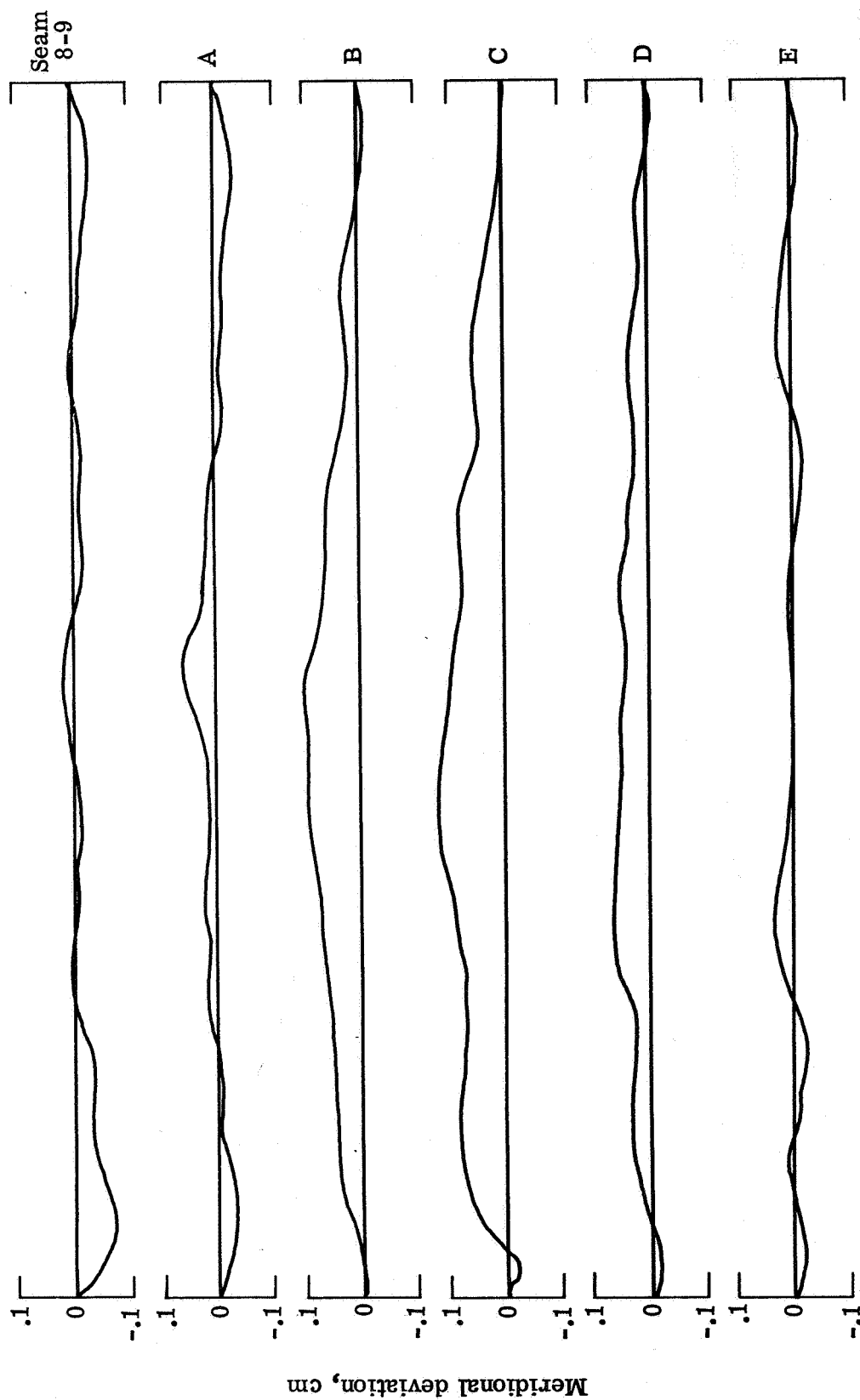


(g) Panel 7.
Figure 18.- Continued.



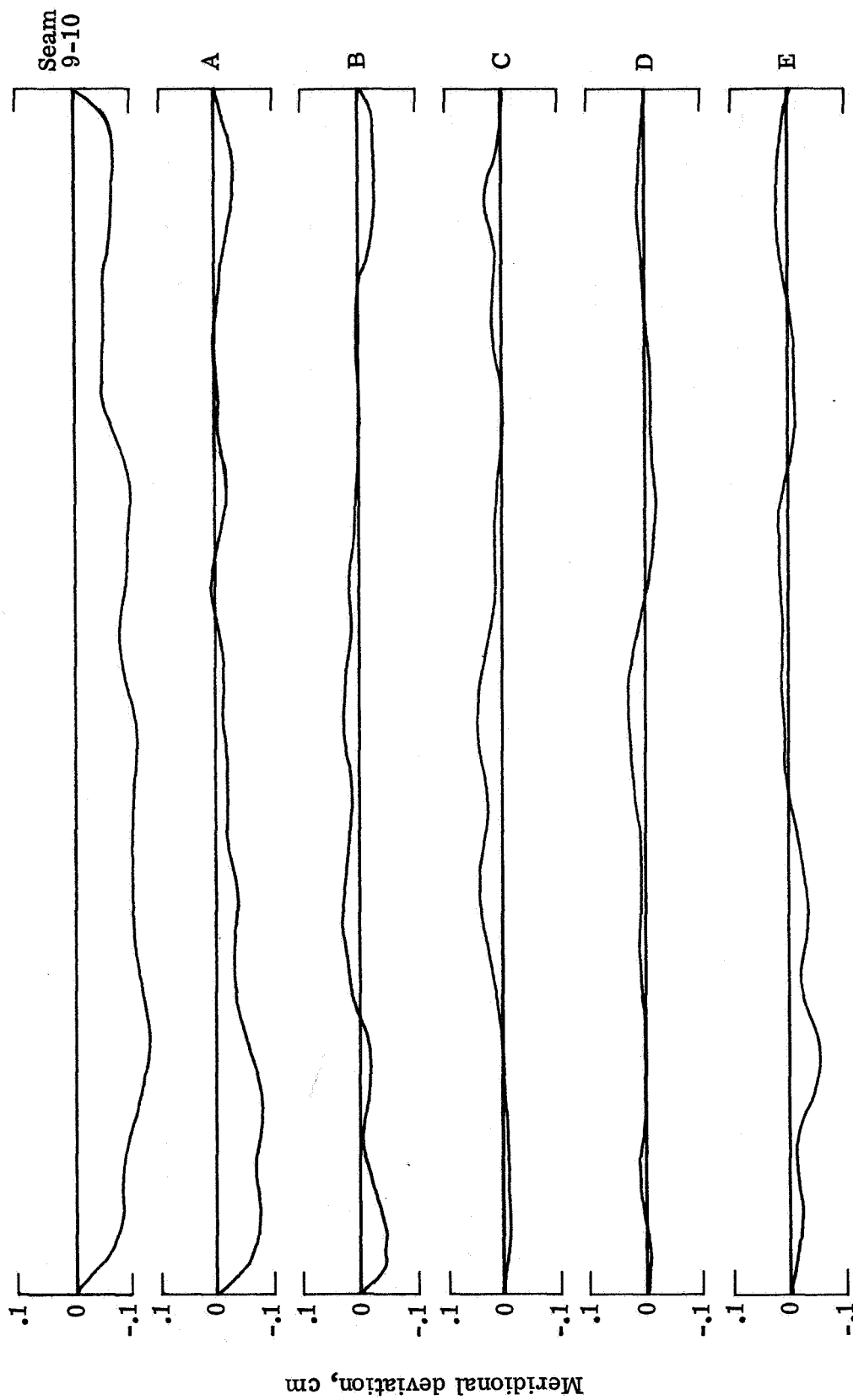
(h) Panel 8.

Figure 18.- Continued.



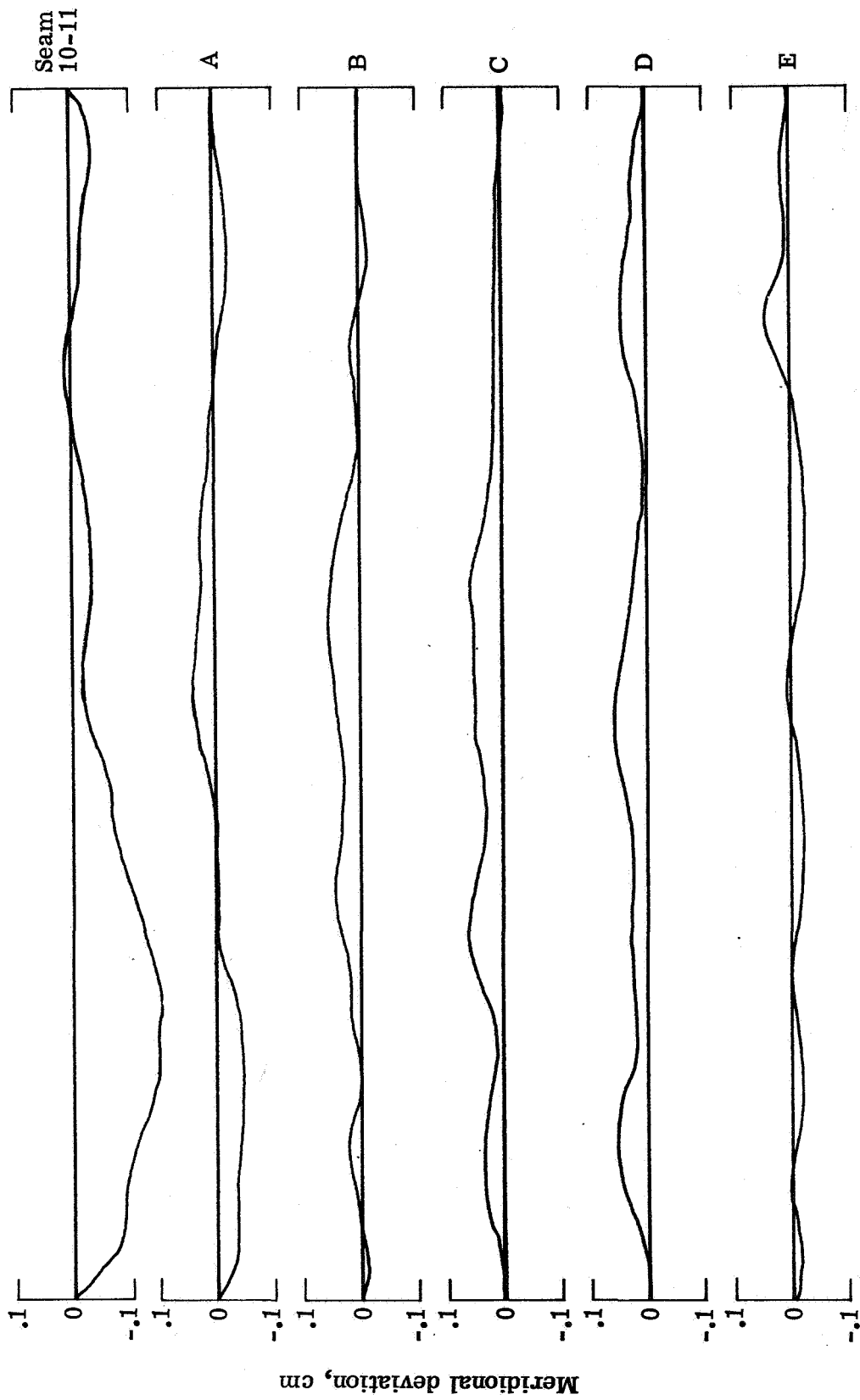
(i) Panel 9.

Figure 18.- Continued.

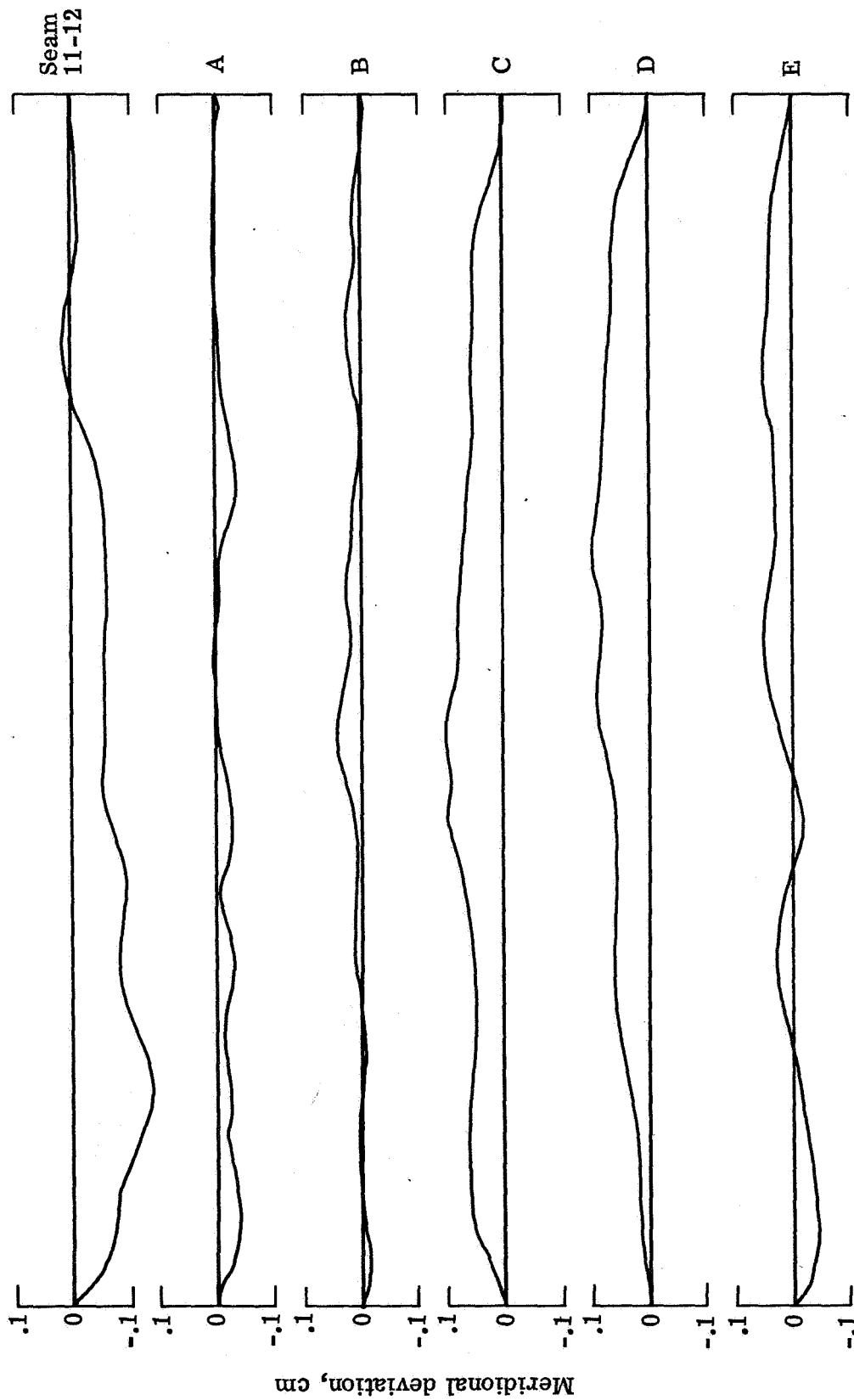


(i) Panel 10.

Figure 18.- Continued.

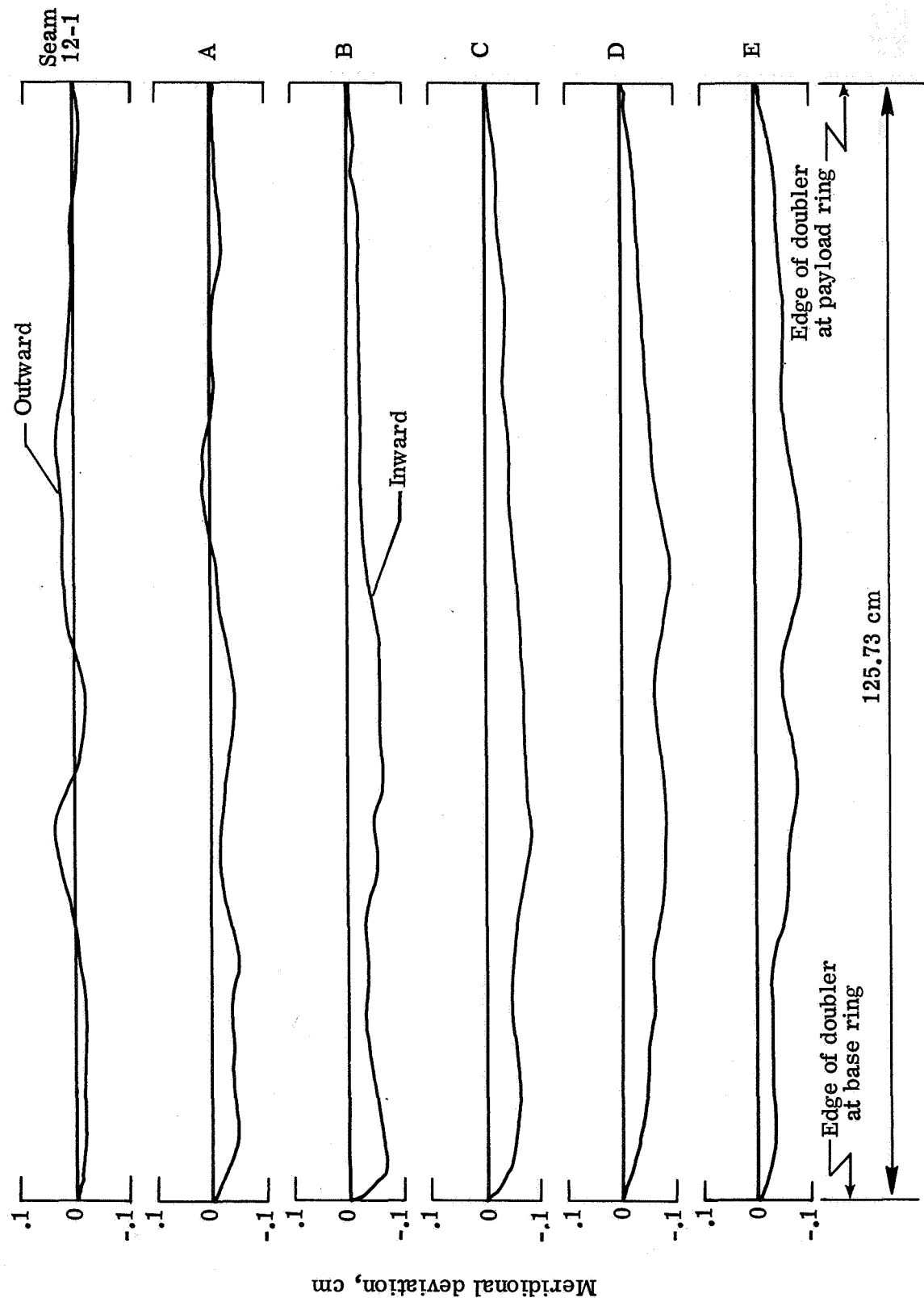


(k) Panel 11.
Figure 18.- Continued.



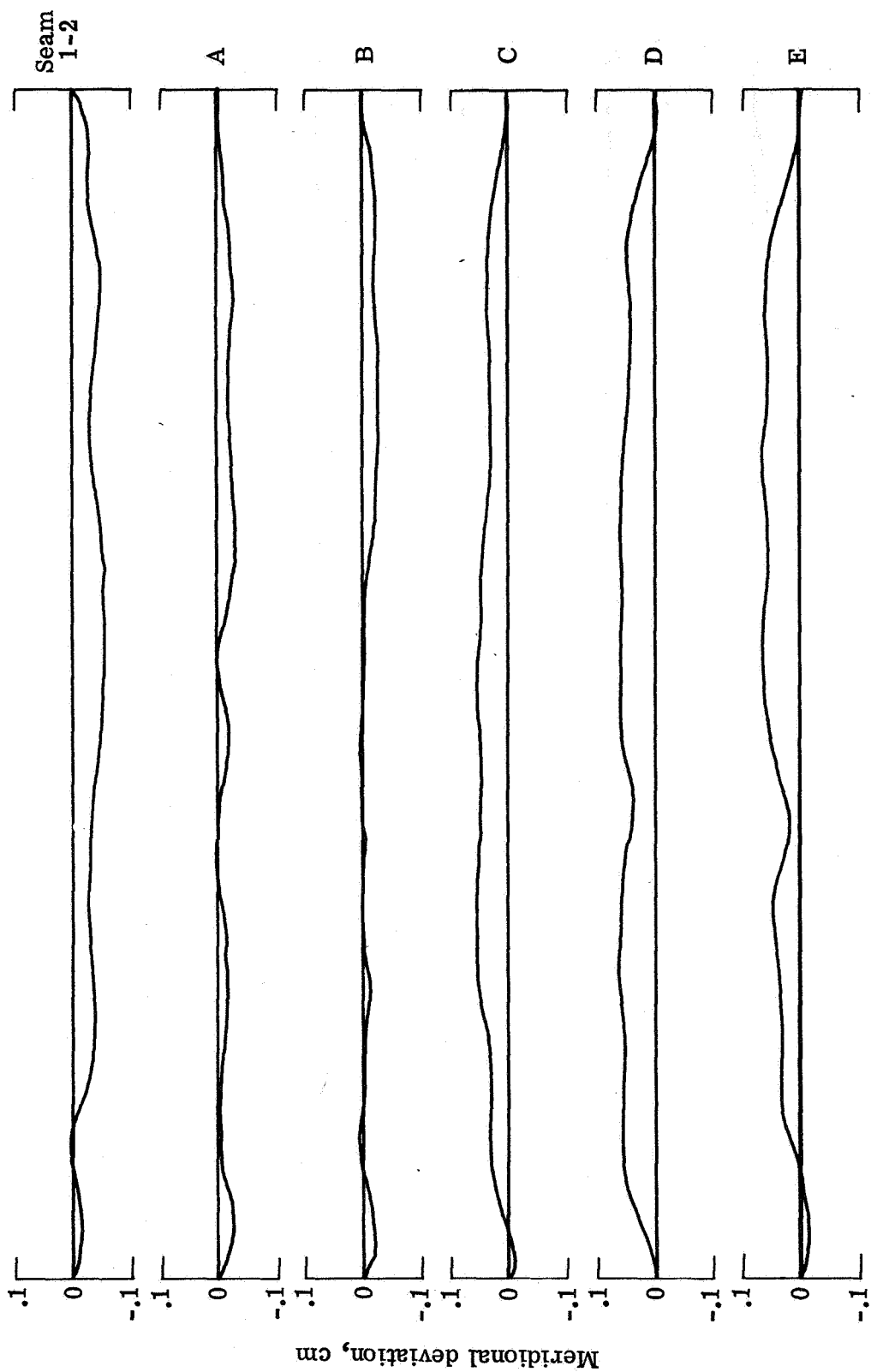
(1) Panel 12.

Figure 18.- Concluded.



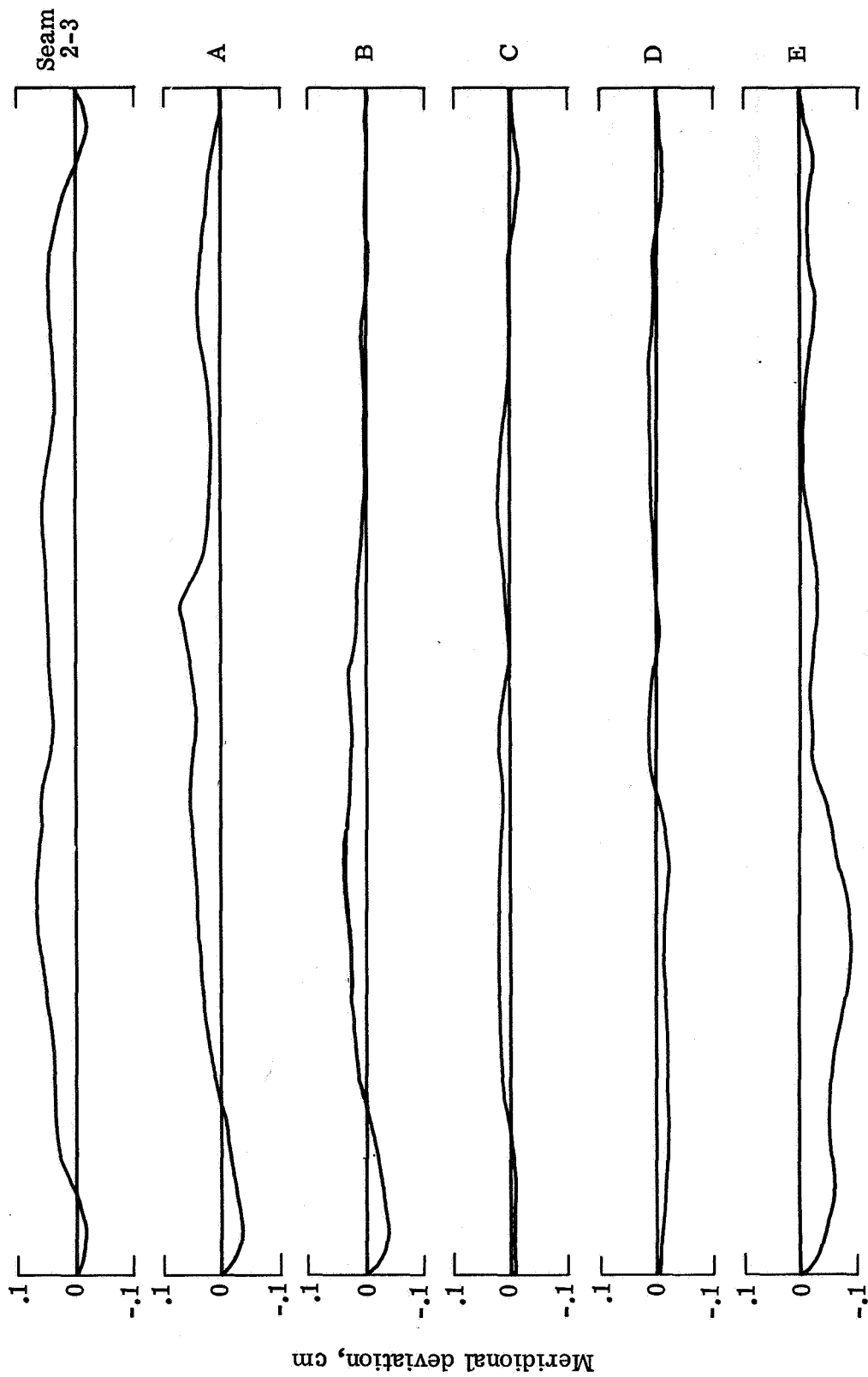
(a) Panel 1.

Figure 19.- Imperfection measurements of cone 2.



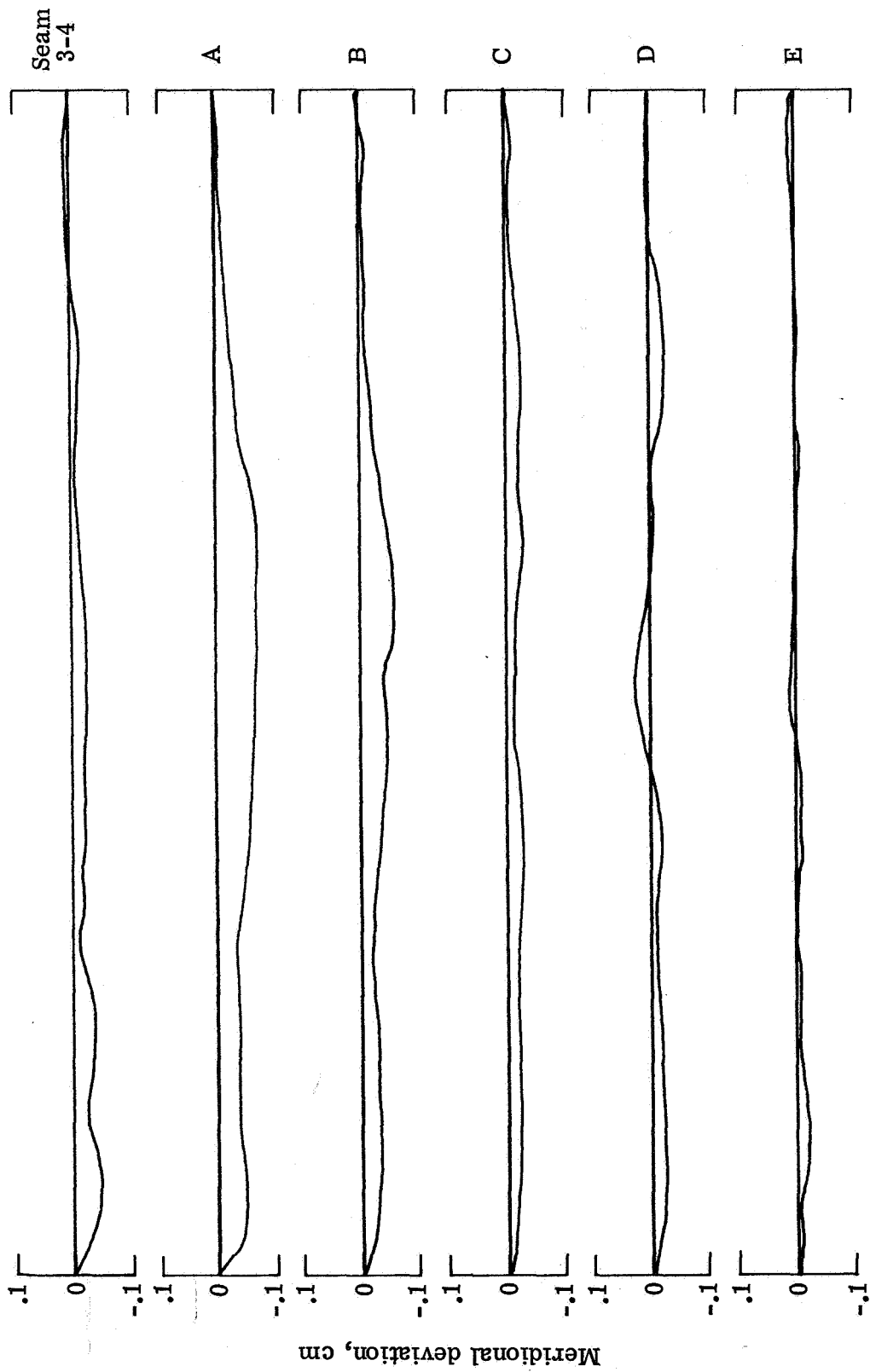
(b) Panel 2.

Figure 19.- Continued.



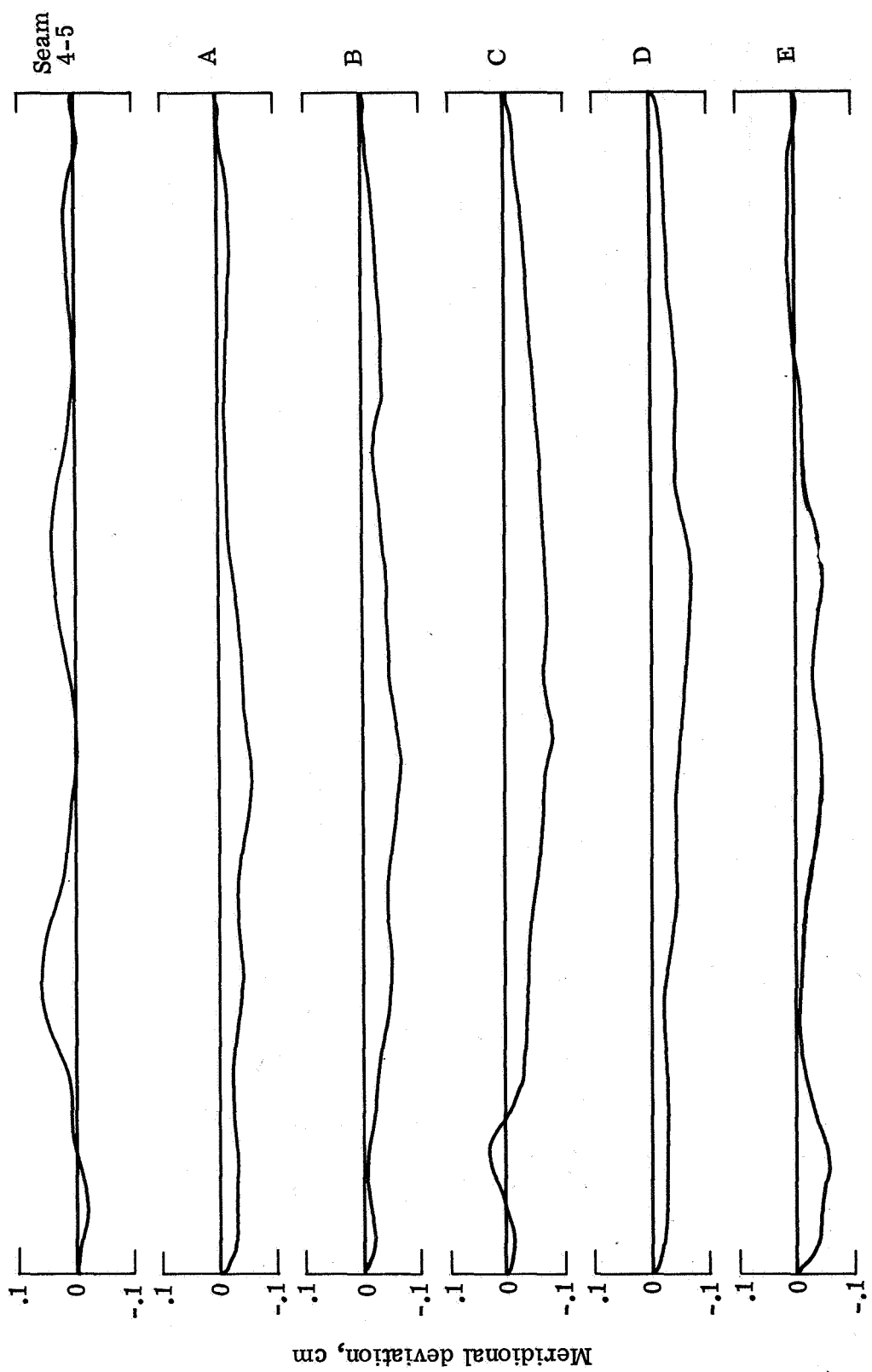
(c) Panel 3.

Figure 19.- Continued.



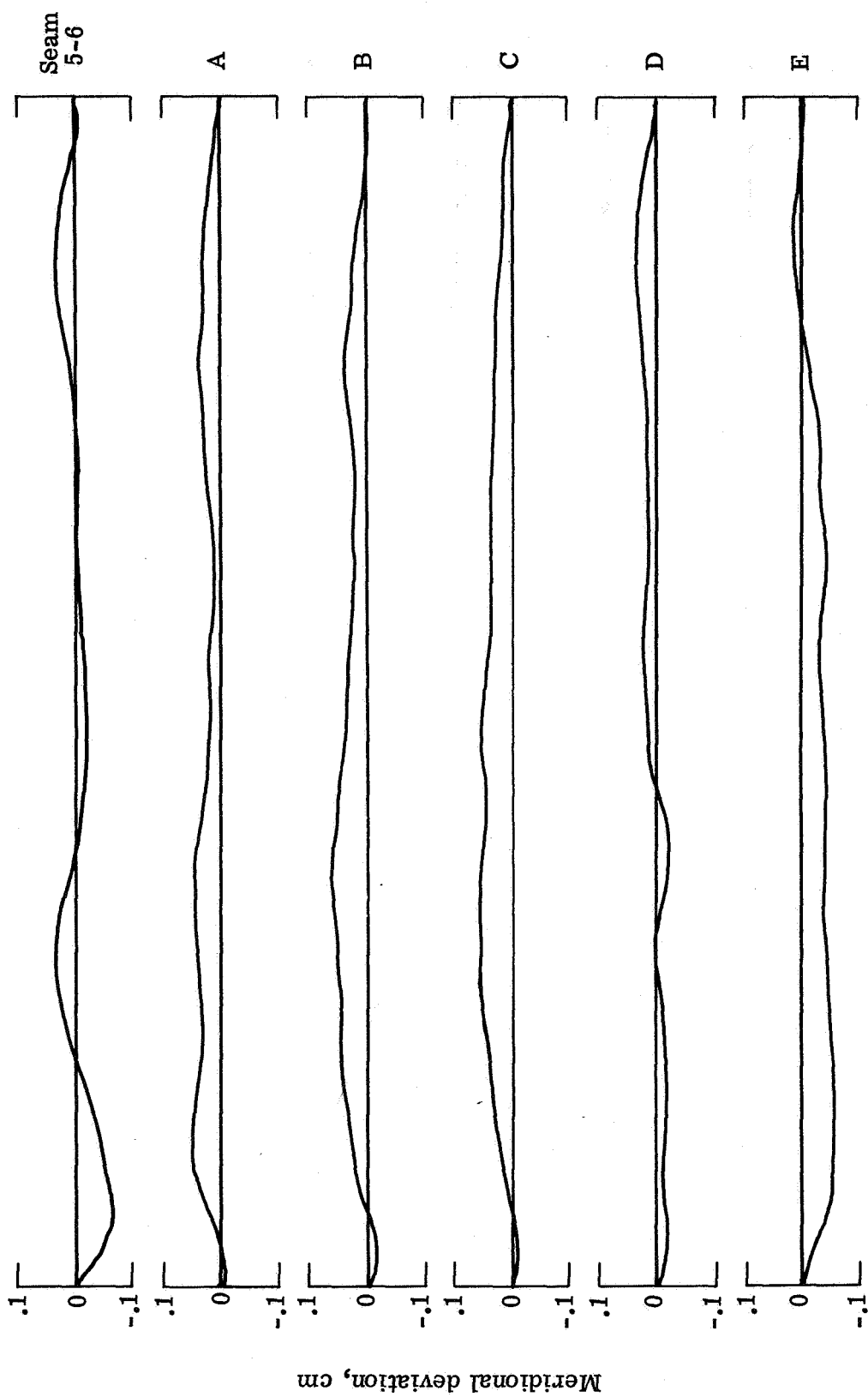
(d) Panel 4.

Figure 19.- Continued.



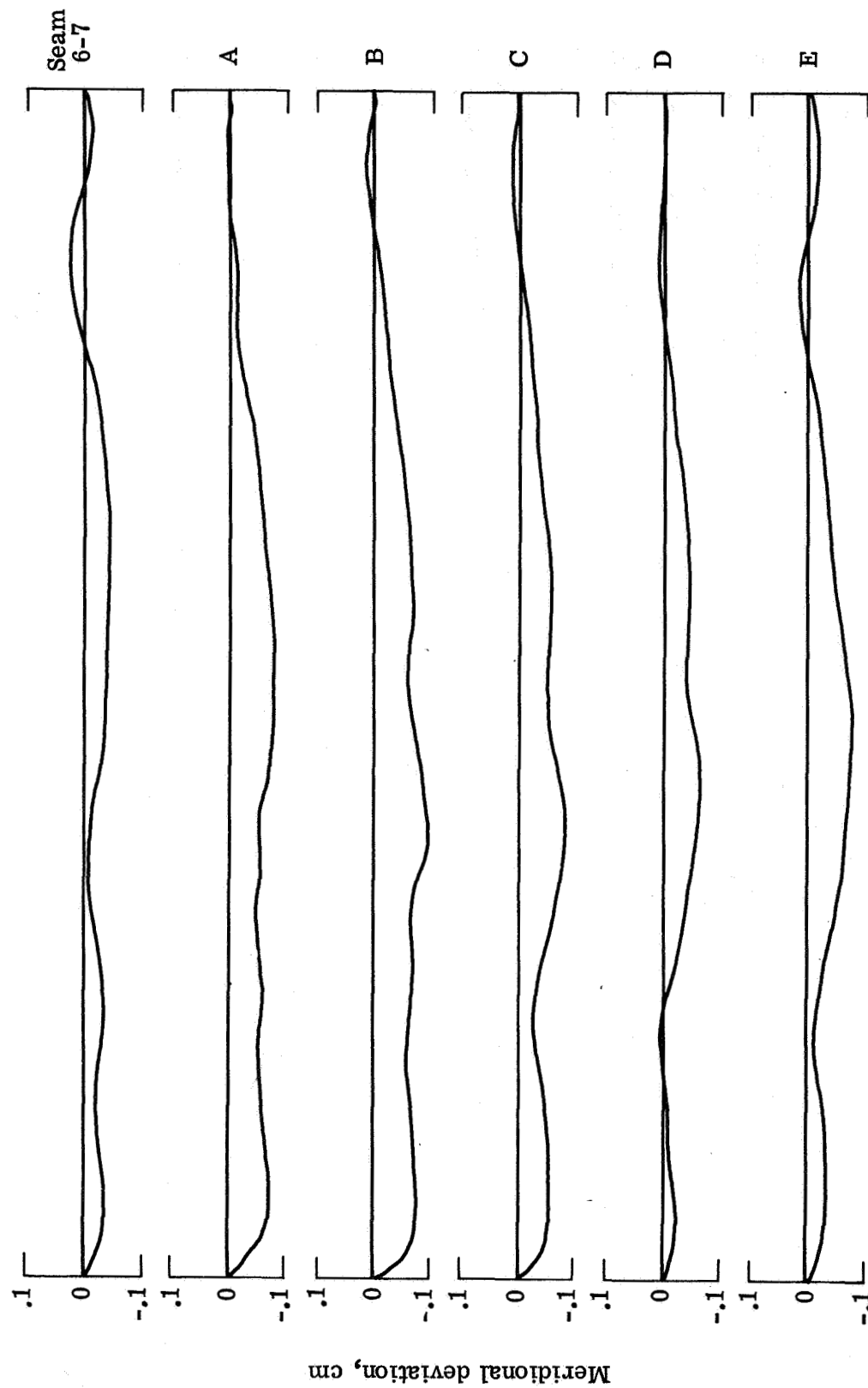
(e) Panel 5.

Figure 19.- Continued.



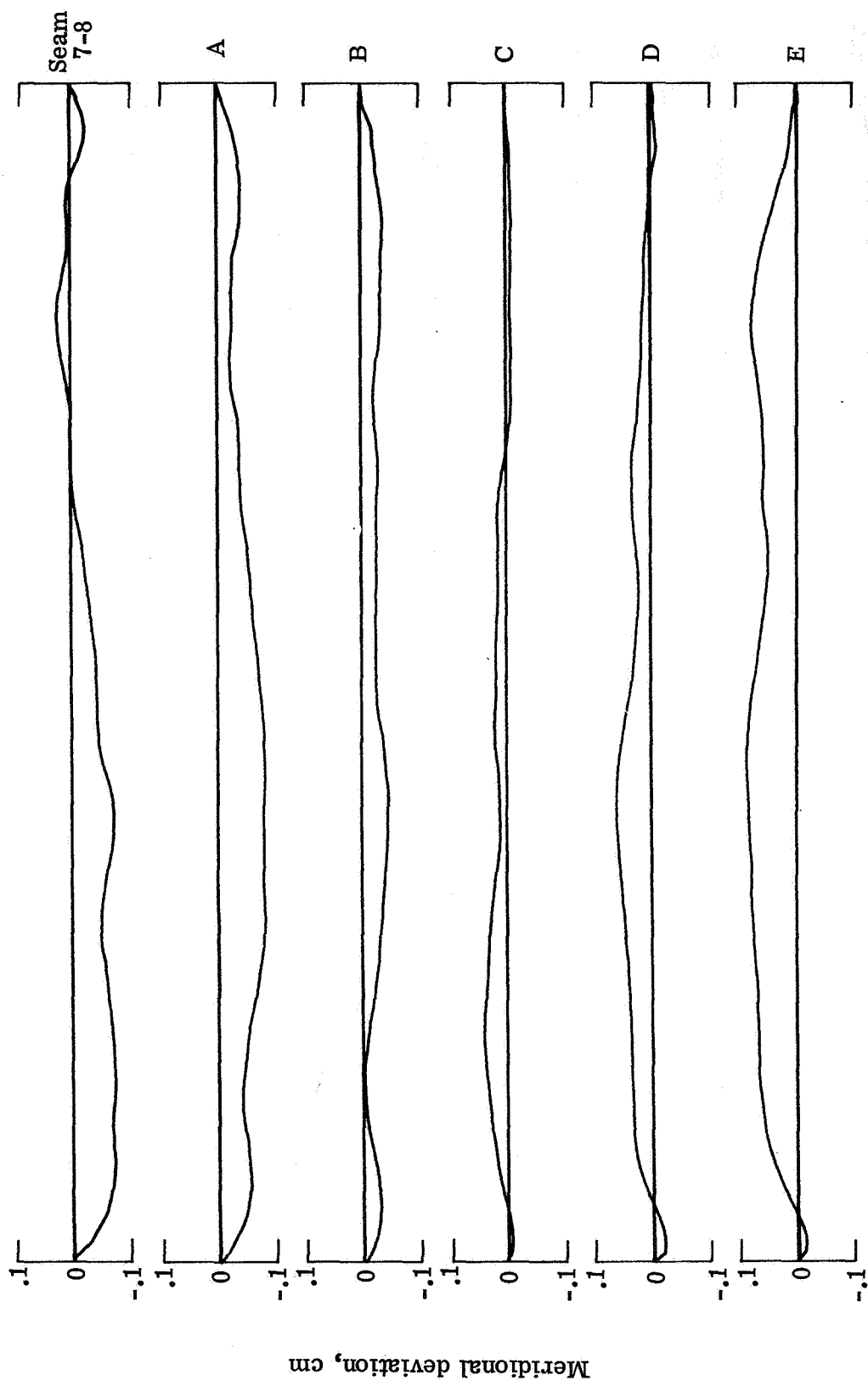
(f) Panel 6.

Figure 19.- Continued.



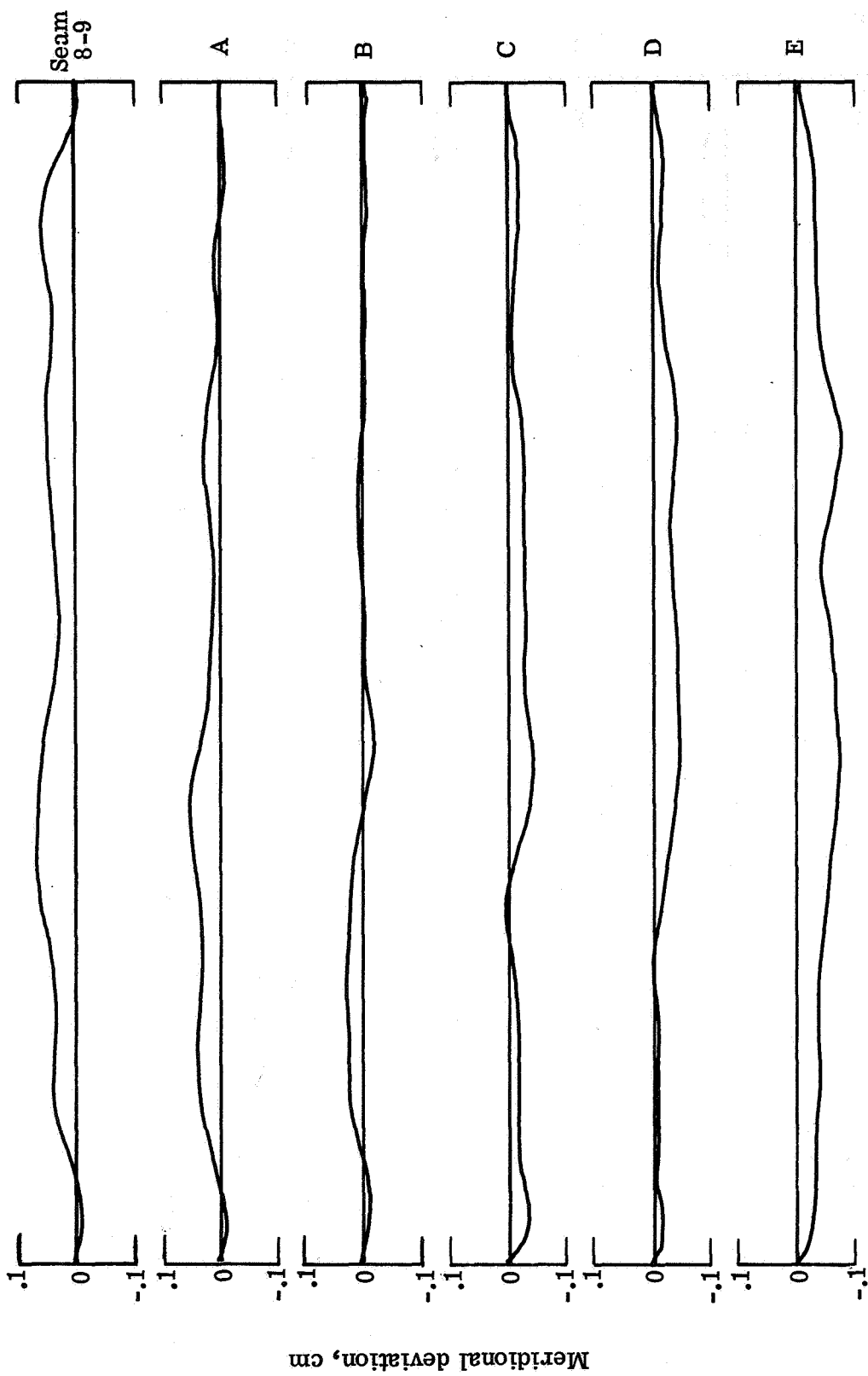
(g) Panel 7.

Figure 19.- Continued.



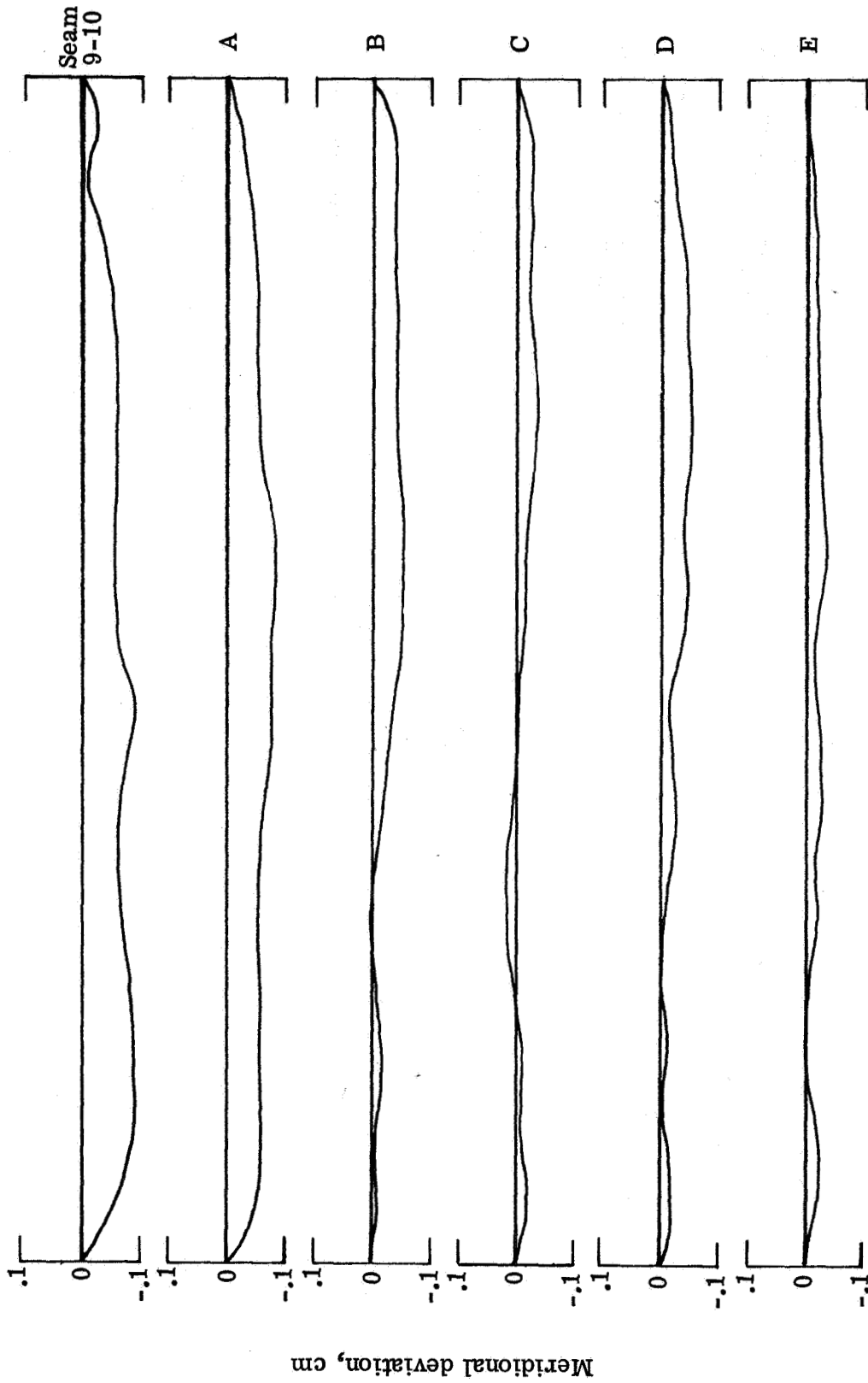
(h) Panel 8.

Figure 19.- Continued.



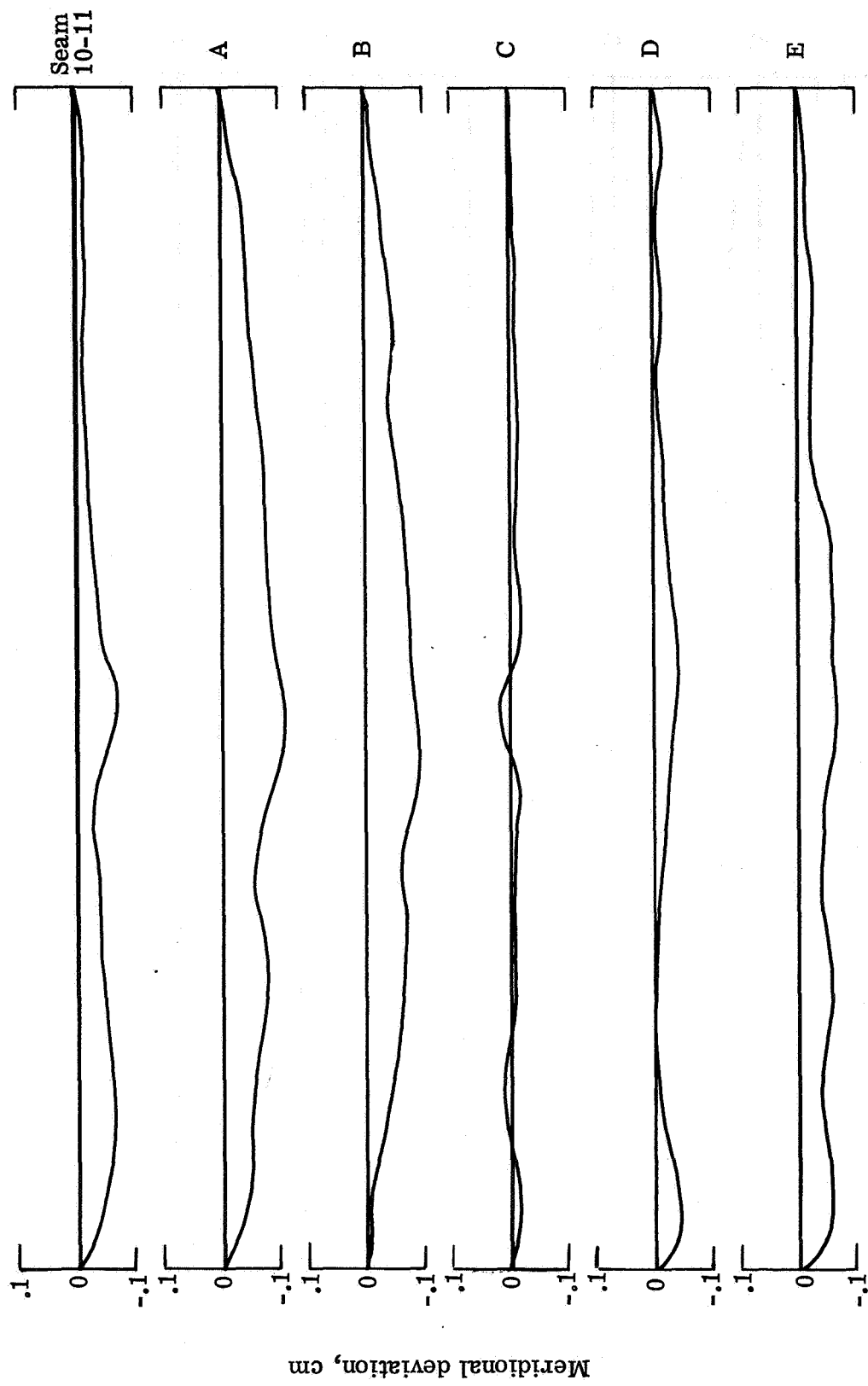
(i) Panel 9.

Figure 19.- Continued.

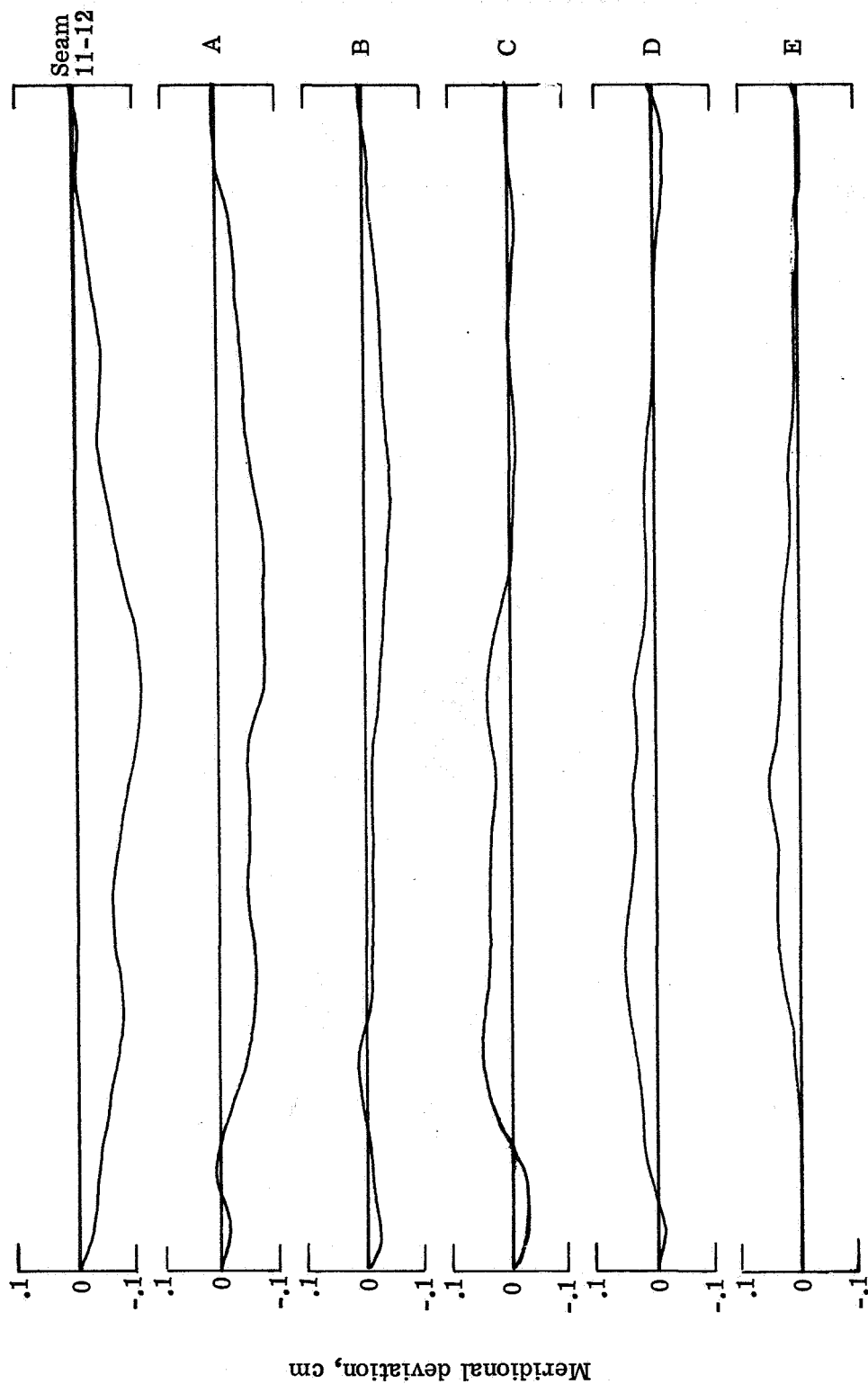


(j) Panel 10.

Figure 19.- Continued.

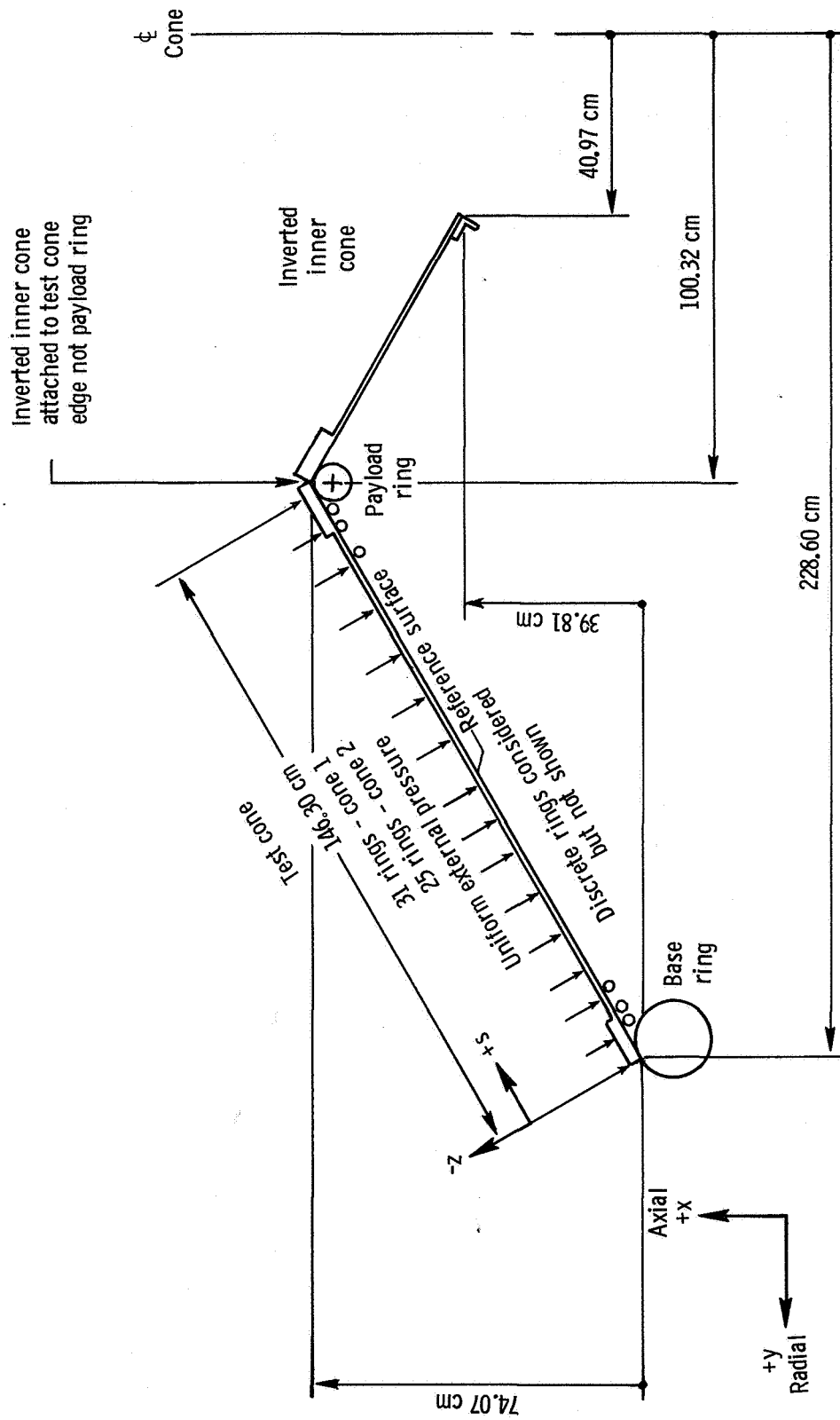


(k) Panel 11.
Figure 19.- Continued.



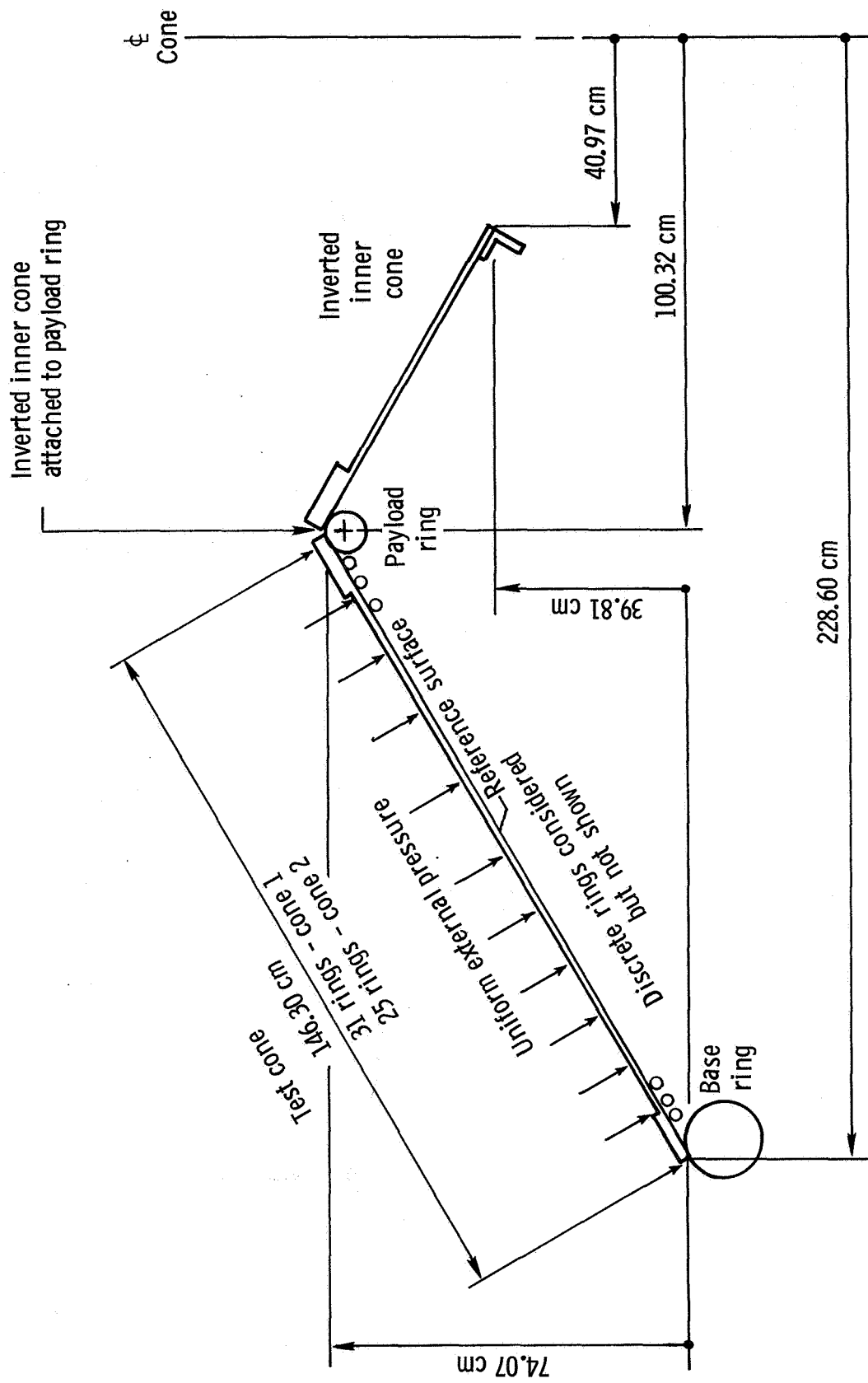
(1) Panel 12.

Figure 19.- Concluded.



(a) Model for SALORS program.

Figure 20.- Analytical models for program analyses.



(b) Model for BOSOR 2 program.

Figure 20.- Concluded.

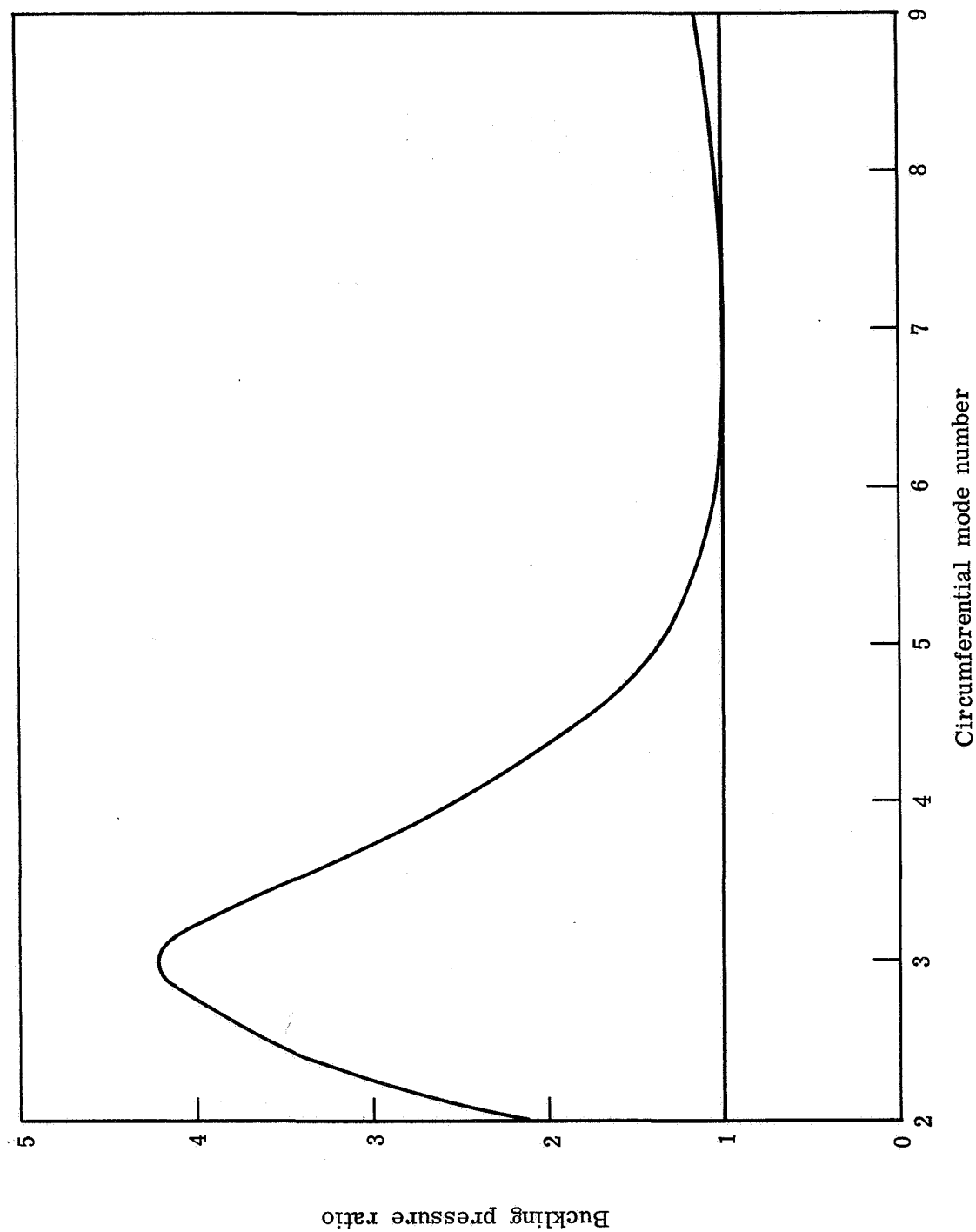


Figure 21.- Buckling pressure as a function of buckling mode number, as computed by BOSOR 2.



POSTMASTER: If Undeliverable (Section 158
Postal Manual) Do Not Return

"The aeronautical and space activities of the United States shall be conducted so as to contribute . . . to the expansion of human knowledge of phenomena in the atmosphere and space. The Administration shall provide for the widest practicable and appropriate dissemination of information concerning its activities and the results thereof."

—NATIONAL AERONAUTICS AND SPACE ACT OF 1958

NASA SCIENTIFIC AND TECHNICAL PUBLICATIONS

TECHNICAL REPORTS: Scientific and technical information considered important, complete, and a lasting contribution to existing knowledge.

TECHNICAL NOTES: Information less broad in scope but nevertheless of importance as a contribution to existing knowledge.

TECHNICAL MEMORANDUMS: Information receiving limited distribution because of preliminary data, security classification, or other reasons. Also includes conference proceedings with either limited or unlimited distribution.

CONTRACTOR REPORTS: Scientific and technical information generated under a NASA contract or grant and considered an important contribution to existing knowledge.

TECHNICAL TRANSLATIONS: Information published in a foreign language considered to merit NASA distribution in English.

SPECIAL PUBLICATIONS: Information derived from or of value to NASA activities. Publications include final reports of major projects, monographs, data compilations, handbooks, sourcebooks, and special bibliographies.

TECHNOLOGY UTILIZATION PUBLICATIONS: Information on technology used by NASA that may be of particular interest in commercial and other non-aerospace applications. Publications include Tech Briefs, Technology Utilization Reports and Technology Surveys.

Details on the availability of these publications may be obtained from:

**SCIENTIFIC AND TECHNICAL INFORMATION OFFICE
NATIONAL AERONAUTICS AND SPACE ADMINISTRATION
Washington, D.C. 20546**